Photoluminescence Spectroscopy on Microtube Bottle Resonators formed by Rolled-Up Semiconductor Bilayers

Dissertation
zur Erlangung des Doktorgrades
des Fachbereichs Physik
der Universität Hamburg

vorgelegt von
Christian Strelow
aus Pinneberg

Hamburg
2009

Gutachter der Dissertation:	Professor Dr. Detlef Heitmann Professor Dr. Ulrich Merkt Professor Dr. Jonathan J. Finley
Gutachter der Disputation:	Professor Dr. Detlef Heitmann Professor Dr. Wolfgang Hansen
Datum der Disputation:	10. 12. 2009
Vorsitzender des Prüfungsausschusses:	Dr. Tobias Kipp
Vorsitzender des Promotionsausschusses:	Professor Dr. Robert Klanner
Dekan der Fakultät für Mathematik, Informatik und Naturwissenschaften:	Professor Dr. Heinrich H. Graener

Abstract

In this work we investigate optical microcavities that are formed by the self-rolling meachnism of thin strained semiconductor bilayers. We demonstrate the fabrication of rolled-up microtube resonators, as well as experiments on their optical eigenmodes. We performed micro photoluminescence spectroscopy on semiconductor emitters that were either embedded inside the microtube wall during the bilayer growth by molecular beam epitaxy (MBE) or inserted by fluid filling insight the hollow core of the microtube. In addition we developed a theoretical model that describes the three-dimensional light confinement in rolled-up microtube resonators in an accurate and intuitive way.

Total internal reflection leads to light confinement in the thin walls of the microtube and to the formation of ring modes by constructive interference after a round-trip. The spiral-shaped cross section with its inside and outside rolling edge has the strongest impact on the optical eigenmodes. We demonstrate that the rolling edges can be functionalized as strongly directive output couplers, as well as for a controlled axial light confinement. A specific modulation of the outside rolling edge allows us even to tailor the mode energies and the axial field distributions. Furthermore, we introduce other structurings of the geometry along the microtube axis that all lead to a controlled axial light confinement. The axial light confinement is explained in a model based on the adiabatic separation of circular and axial mode propagation. The measured axial intensity distributions and mode energies are reproduced by solutions of a quasi-Schrödinger equation in which the circular propagation is introduced as a quasi-potential. The quasi-potential can easily be determined from the microtube geometry along the axis. The controlled axial light confinement strongly improves the quality of the eigenmode spectrum and makes further interesting experiments possible. A special axial structuring allows us to observe and to explain a well pronounced splitting by the broken rotational symmetry that has not been observed so clearly for other microtubes up to now. Due to the growth by MBE microtubes can have very thin walls. The observation of eigenmodes excited by evanescent-field-coupled nanocrystals demonstrates that, because of their long ranging evanescent fields, microtubes are good candidates for possible applications as sensors in lab-on-a-chip devices or as laser resonators for a huge amount of gain materials that cannot be integrated easily into other types of microcavties. Finally, we succeeded in the realization of a rolled-up microtube laser. We present time-resolved photoluminescence measurements that give insight into the photoluminescence dynamics in active microtube resonators during the lasing interaction.

Inhaltsangabe

In dieser Arbeit werden optische Mikroresonatoren untersucht, die durch den Selbstaufrollmechanimus verspannter Halbleiterschichten entstehen. Wir zeigen die Herstellung aufgerollter Mikroröllchenresonatoren und Experimente an den optischen Eigenmoden. Die Untersuchung erfolgt mittels Mikrophotolumineszenzspektroskopie an Halbleiteremittern die entweder während des Wachstums mit Molekularstrahlepitaxie in die Miroröllchenwand eingebettet oder in Lösung in das hole Innere des Mikroröllchens gefüllt werden. Außerdem haben wir ein theoretisches Modell entwickelt, das den dreidimensionalen Einschluss von Licht in Mikroröllchen präzise und intuitiv beschreibt.

Totalreflexion führt zu einem Lichteinschluss in der dünnen Röllchenwand und zur Ausbildung von Ringmoden durch konstruktive Interferenz nach einem Umlauf. Der spiralförmige Querschnitt mit seiner inneren und äußeren Aufrollkante hat den stärksten Einfluss auf die optischen Eigenmoden. Wir zeigen, dass die Aufrollkanten sowohl für eine stark gerichtete Lichtauskopplung, als auch für einen kontrollierten axialen Lichteinschluss funktionalisiert werden können. Eine spezielle Modulation der äußeren Aufrollkante ermöglicht es, die Modenenergien und die axialen Feldverteilungen sogar maßzuschneidern. Wir stellen verschiedene Strukturierungen der axialen Röllchengeometrie vor, die alle zu einem kontrollierten Lichteinschluss führen. Der axiale Lichteinschluss wird in einem theoretischen Modell erklärt, das auf adiabatischer Separation von zirkularer und axialer Lichtausbreitung basiert. Die gemessenen axialen Intensitätsverteilungen und Modenenergien werden durch Lösungen einer Quasi-Schrödinger-Gleichung wiedergegeben, in die die zirkulare Lichtausbreitung als ein Quasi-Potential eingeht. Das Quasi-Potential kann leicht aus der axialen Röllchengeometrie bestimmt werden. Der kontrollierte axiale Lichteinschluss führt zu scharfen, wohldefinierten Moden und ermöglicht weitere interessante Experimente. Ein spezieller axialer Einschluss erlaubt, eine starke Aufspaltung durch gebrochene Rotationssymmetrie zu beobachten und zu erklären, die bisher an anderen Mikroröllchen nicht so klar beobachtet wurde. Durch Wachstum mittels Molekularstrahlepitaxie können Mikroröllchen sehr dünne Wände aufweisen. Die Beobachtung von Eigenmoden, die über an das evaneszente Feld ankoppelnde Nanokristalle angeregt werden, zeigen, dass Mikroröllchen aufgrund ihrer weit reichenden evaneszeneten Felder gute Kandidaten für mögliche Anwendungen als Sensoren in "Lab-On-A-Chip" Bauteilen sind. Sie könnten auch als Laserresonatoren für eine große Anzahl von Verstärkungsmaterialien dienen, die schwer in andere Typen von Mikroresonatoren eingebracht werden können. Schließlich konnten wir einen Mikroröllchenlaser realisieren. Wir zeigen zeitaufgelöste Photolumineszenzmessungen, die Einsicht in die Photolumineszenzdynamik von aktiven Mikroröllchenresonatoren während der Laserwechselwirkung geben.

Contents

Introduction

The research on optical microcavities is a very important and frequently discussed field. On the one hand technologies for information processing and telecommunication have to be fast and require high bandwidths so often optical components are applied, which can operate with the speed of light. Here, microcavities can be used in fast, compact and efficient light sources, for example in laser diodes, or they allow to fabricate novel kind of light sources like single photon sources for quantum cryptography. Semiconductor microcavities play an important role in this context since in these structures emitters can easily be integrated during the fabrication. This allows directly to industrially fabricate devices like laser diodes that could be used for example in commercial compact disk players. On the other hand microcavities can be used for the fundamental research on light-mater interaction, since they confine and influence light on the size of its own wavelength. The large amount of control on semiconductor emitters makes it also possible to study fundamental light-matter interaction, known from atomic physics, in a solid state system. The small size of microcavities enables one also to use them as very sensitive sensors, since very small amounts of material are sufficient to change the properties of the light confined in the cavity.

A couple of geometries has been realized to fabricate optical microcavities that all have different advantages and disadvantages. Presently, a lot of research is conducted to improve the properties of the existing microcavities, but also new concepts are developed. A novel kind of microcavity is a rolled-up microtube resonator. Such microtubes are fabricated by the self-rolling mechanism of thin strained semiconductor bilayers. This mechanism was invented in 2000 by Prinz *et al.* [Pri00]. In 2006 we succeeded in the first demonstration of an optical microtube resonator [Kip06] utilizing the important technological step of controlled lifting of the microtube from the substrate. The light is confined inside the thin walls of the microtube by total internal reflection. After a round trip constructive interference leads to the formation of ring modes. But although the circular cross section of the microtube has the strongest impact on the optical modes the axial light confinement is also important in these structures. Even in nominally axially unstructured microtubes small

inhomogeneities lead to an axial confinement resulting in further modes with small energy spacings that tend to broaden all modes on their high energy side.

The further development and improvement of this type of microcavity is the topic of the present doctoral thesis. I will show that rolled-up microtubes have a couple of very useful properties that arise from the fabrication by the self-rolling mechanism. The optical modes are studied by micro photoluminescence spectroscopy on semiconductor emitters that are either embedded into the microtube wall during the growth or filled into the microtube after fabrication.

Due to their spiral-shaped cross section rolled-up microtubes has typical rolling edges that have strong impact on the microtube modes. These rolling edges can be functionalized and can lead to directional light emission as well as to a controlled axial light confinement. Specific modulations of the rolling edges along the axis can even tailor the mode energies. This is understood in an accurate and intuitive model. The three-dimensional light confinement modifies the modes in microtubes strongly and results in further interesting observations. Other structurings along the microtube axis allow a well-pronounced mode splitting due to the broken rotational symmetry that is not observed for a modulated rolling edge. This phenomenon is discussed in the framework of finite-difference time-domain simulations. The self-rolling mechanism enables us to fabricate hollow microtubes with very thin walls. We show that chemically synthesized nanocrystals, that are filled into the microtubes, can couple excellently to the long-ranging evanescent fields of the microtube modes. Emitters that are embedded inside the microtube wall exhibit a nearly perfect spatial overlap between the optical mode and the emitter. Furthermore we present the realization of a rolled-up microtube laser and results of time-resolved photoluminescence spectroscopy.

This work is organized as follows: The first chapter gives an introduction into the field of microcavities. The key properties of microcavities are presented and the mostly studied geometries are introduced. In the second chapter the fabrication of optical microtube resonators, as well as the design of the underlying layer systems is demonstrated. The experimental setups are introduced in chapter three. In this work optical microtube resonators were studied experimentally, as well as theoretically and both treatments are strongly related to each other. All experimental and theoretical results are demonstrated in chapter four together in one chapter. In the first and in the second section experiments on axially unstructured microtubes are shown. On these microtubes already axial light confinement on accidental inhomogeneities and directional emission could be demonstrated. In section three experiments on microtubes with a controlled axial light confinement are presented. Here, also a detailed theoretical description of three-dimensional light confinement is given. We present different mechanisms of axial light confinement that allow us to tailor

the eigenmodes or the observation of a pronounced splitting by the broken rotational symmetry. In section four and five microtubes with a controlled three-dimensional confinement are used for further experiments. Section four demonstrates that the modes in microtubes can also be excited by emitters that are filled into the hollow core and couple to the evanescent field of the microtube modes. Section five shows the realization of a microtube laser and presents measurements and calculations on the dynamics of the photons and charge carriers in the microtube laser.

Chapter 1

Microcavities

In this part of my thesis I want to give an introduction into the field of optical microcavities. I will show why optical microcavities bear interesting properties and present the mostly studied geometries of optical microcavities in a comparative way.

The key property of optical microcavities is that they confine light on the scale of its wavelength. This offers some unique properties in contrast to macroscopic cavities. This can, for example, be observed in lasers. In macroscopic lasers, due to their large size, usually many modes take part in the lasing interaction. Because of the competition between these modes and also because of the size of the optical active material more gain has to be provided and, thus, more excitation power is required to exceed the threshold power. Consequently, for microcavity lasers the threshold power is much lower and also single-mode lasing can be achieved. Very small cavities that additionally exhibit long life times of the photons inside the cavity provide the observation of quantum electrodynamical effects by interaction of the photons with emitters embedded into the micro cavity. In this context two quantities are important to characterize a microcavity, the quality factor and the mode volume. The quality factor is defined by $Q = E/\Delta E$, where E is the mode energy and ΔE the spectral width of the mode. ΔE is directly related to the losses of the microcavity by $\Delta E = \hbar\Gamma$, where Γ is the loss rate of the cavity. Thus, high Q values are desired. The mode volume is defined as

$$V_{\text{eff}} = \frac{1}{n^2} \int\int\int_V n(\vec{r})^2 \left|\vec{f}(\vec{r})\right| \mathrm{d}^3\vec{r}, \tag{1.1}$$

where n is the refractive index of the material and $\vec{f}(\vec{r})$ is the field distribution inside the cavity normalized with respect to its maximum [Gér99]. The spontaneous emission of emitters is induced by vacuum fluctuations of the electromagnetic field. Since light can be described as a harmonic oscillator the ground state of the electro-

magnetic field (the vacuum) has a non zero energy [Lou01]. The mean value of the intensity vanishes in contrast to the mean value of the electric field. This stimulates excited emitters to decay with their natural lifetime. In microcavities the dielectric environment is modified which can lead to a decrease or to an increase of the spontaneous emission rate [Pur46]. A figure of merit to quantify the modification of the spontaneous decay rate is the Purcell factor:

$$F_p = \frac{3Q(\lambda_c/n)^3}{4\pi^2 V_{\text{eff}}}. \tag{1.2}$$

Here, c is the vacuum velocity of light, n the refractive index of the cavity material and λ the vacuum wavelength. The Purcell factor is defined for emitters that are situated inside the field maximum of the microcavity with their dipole moment aligned parallel to the electric field and emitting at the wavelength of the cavity mode. If the Purcell factor is larger than 1, the spontaneous emission rate is enhanced, if not, the emitter decays with its natural lifetime. Consequently, small values of V_{eff} and large values of Q are desired to achieve a high Purcell factor. The Purcell effect leads not only to an enhancement of the spontaneous emission rate but also to an enhanced decay into the cavity mode, similar to stimulated emission. The difference is, that the photons decay spontaneously, and, thus, have all different phases. For very small microcavities with high Q factors even thresholdless lasing is possible since the Purcell effect leads already to the direction of almost all spontaneous photons into the cavity mode before the system lases and stimulated emission is the dominant process. For those lasers a smooth transition from spontaneous emission to lasing is observed. The Purcell effect can also be used for improving single photon sources. In general, for those devices only a single quantum emitter, e.g., a single quantum dot, is needed. But in this case the photons are emitted statistically with a typical life time and isotropically in all dimensions. Here, a strong Purcell effect helps to enhance the emission rate and to direct most of the photons in the cavity mode.

In systems of cavities and emitters, where the lifetime of the photons in the cavity is larger than the lifetime of the emitter and the emitters have a large dipole moment, the so called Vacuum-Rabi-Splitting can be observed [Khi06]. Here, a periodic change between emitting a photon into the cavity and reabsorbing it from the cavity leads to a splitting of the emission line of a single emitter in resonance with the cavity mode into two resonances. This is called strong coupling whereas the enhanced emission rate by the Purcell effect is called weak coupling.

In the following, some typical geometries of optical microcavities are shown and I explain how the light is confined in these structures. The different cavities are compared in terms of their typical quality factors, their size, the directionality of light emission and the possibility to integrate emitters into the microcavity. Figure 1.1 depicts images of microcavities. Figure 1.1(a) shows a microdisk [Gay99] formed

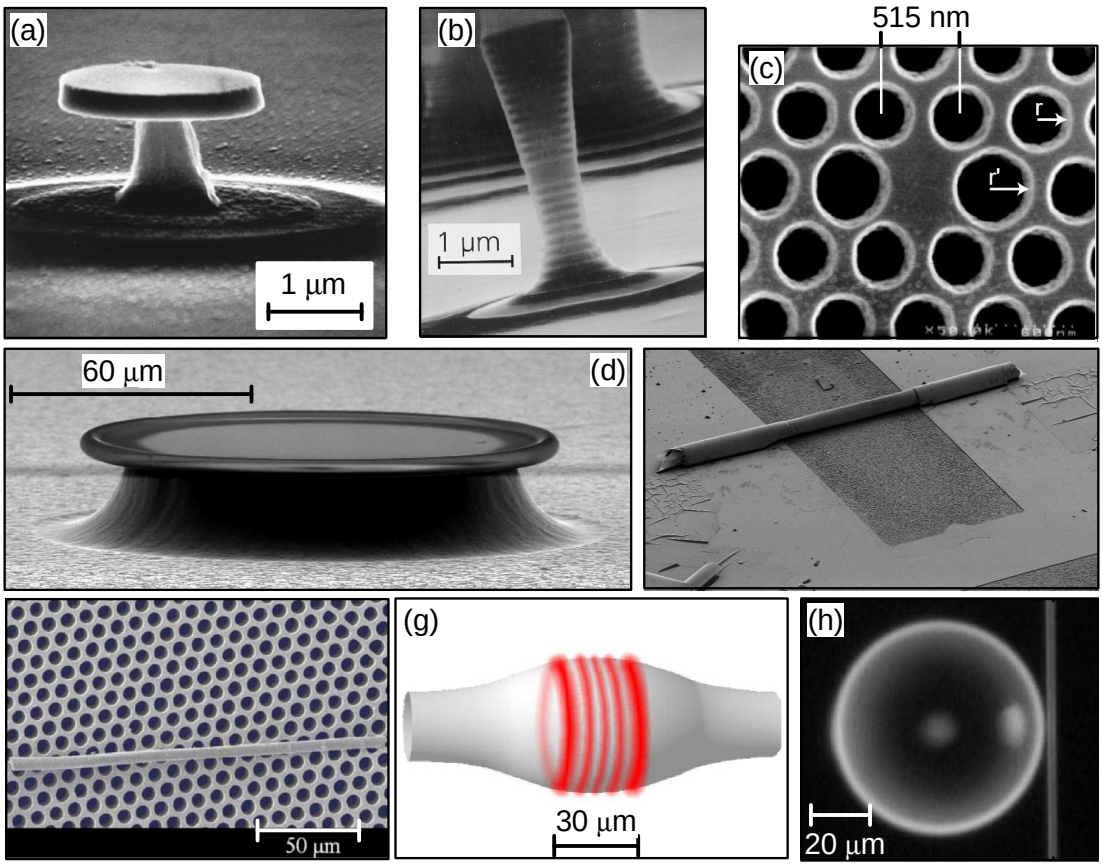

Figure 1.1: Pictures of different optical microcavities. (a)-(f) Scanning electron micrographs of (a) a microdisk [Gay99], (b) a micropillar [Gér96], (c) a two-dimensional photonic crystal cavity [Pai99], (d) a microtoroid [Arm03], (e) a rolled-up microtube bottle resonator and (f) an aluminosilicate microtube on top of its fabrication membrane[Bal06]. (g) Sketch of a bottle resonator formed by a tapered glass fiber [Pöl09]. (h) Image of a glass microsphere coupled to a fiber [Spi02].

by a disk of semiconductor material on top of a pedestal. The light is confined by total internal reflection inside the disk of high refractive index. In vertical direction light is confined like in a waveguide while in plane it is forced to form ring-like, so called whispering gallery modes (WGMs) undergoing multiple internal reflections at the disk edge. Since the mode distribution of most modes is localized at the edge of the disk the losses into the pedestal are very small. Microdisks can be quite small and have high quality factors typically up to 5×10^5 [Bor04], but have the disadvantage to emit nondirectionally in lateral direction. Due to their fabrication of semiconductor material emitters like quantum dots or quantum wells can be embedded into the structures. Microtoroids [Fig. 1.1 (b)] are very similar to microdisks. During the

fabrication first microdisks of SiO_2 on a Si pedestal are prepared. But afterwards, by heating the disk with a CO_2 laser, the edges of the disk melt and form a toroid-like structure [Arm03]. Those cavities have ultra high quality factors around 10^8 due to the very smooth surfaces. They have the disadvantages of being typically considerably large, emitting nondirectionally in lateral direction and can not be fabricated of semiconductor material due to the fabrication by the melting process. Consequently, it is difficult to embed emitters into the structure. Figure 1.1(c) depicts a micropillar [Gér99]. Here, in vertical direction the light is confined in a $\lambda_n/2$ thick region between two distributed Bragg reflectors formed by alternating layers of $\lambda_n/4$ thickness with different refractive indices, where λ_n is the wavelength in the material. In lateral direction the light confinement is also achieved by total internal reflection. The quality factors reach typically up to 12000 [Rei04] and the light is emitted in vertical direction. Those cavities are used to fabricate vertical cavity surface emitting lasers (VCSELs). The disadvantage is that a very accurate periodicity has to be kept, to achieve high quality factors. Emitters can easily be introduced inside the structure during the growth. Figure 1.1(d) shows a two-dimensional photonic-crystal cavity. Such structures are fabricated by etching a periodic grid of holes into a free-standing membrane. While in vertical direction total internal reflection confines the light, in lateral direction photonic bandgaps are formed. The light is confined in a defect of the periodic grid. These cavities reach the smallest mode volumes and can have high quality factors of up to 10^6 [Th07]. Thus very high Purcell factors up to 165 [Eng05] can be achieved. The light is predominantly emitted in vertical direction. Photonic crystal microcavities have great potential, since they can easily be introduced into photonic integrated circuits. Microdisks, micropillars and photonic cystals are the mostly studied microcavities since here, semiconductor emitters can easily be embedded into the structures. This leads to the possibility of realizing optically and electrically pumped lasers and single-photon sources. Rolled-up microtubes, as shown in Fig. 1.1(e), represent a novel type of semiconductor microcavity. These tubes are fabricated by the self-rolling mechanism of very thin strained semiconductor bilayers [Pri00]. Here, the light is confined in ring modes that are guided inside the thin microtube wall by total internal reflection at the outer and the inner interface and interfere constructively after a round trip [Kip06]. In order to suppress loses into the substrate, microtubes are fabricated as free-standing bridges. The study of these rolled-up microtube resonators is the topic of the present doctoral thesis. We will show that in these cylindrical microcavities a controlled axial light confinement is possible. The light is generally emitted isotropically into the plain perpendicular to the rolling axis, but we will demonstrate that the rolled-up geometry can lead also to directional emission. Up to now the quality factors reach typically up to 3500. During the growth by molecular beam epitaxy emitters can by embedded inside the microtube wall. Due to the thin walls emitters can also be coupled very efficiently to the long

ranging evanescent fields of the modes. Hollow cylindrical microcavities can also be fabricated by aluminosilicate tubes formed by vacuum assisted filtration of a glass matrix [Bal06], as shown in Fig. 1.1(f). Here, a controlled axial light confinement is not possible. In addition the wall thickness of some microns is much larger than in rolled-up microtubes (down to 42 nm in this work). The light is emitted non-directionally in the plane perpendicular to cylinder axis. As internal emitters Si nano crystals can be formed by annealing the structure. Tapered glass fibers can also be used as micro cavities, as schematically shown in Fig. 1.1(g). The eigenmodes are WGMs propagating around the cylinder axis. Very recently also a controlled axial light confinement could be demonstrated [Pöl09]. A modulated radius leads to a back reflection of the light to larger radii. The field distribution is very similar to a charged particle in a magnetic bottle and, consequently, the cavity is called bottle resonator. Such field distributions are also observed for the microtubes in this work. Thus, we adopt this term also for rolled-up microtubes. The quality factors of bottle resonators in tapered glass fibers can reach about 10^8 [Pöl09]. Typically for cylindrical micro cavities, the light is emitted nondirectionally into the plane perpendicular to the axis. Well-defined emitters can not be embedded into the structure. Fig. 1.1(h) shows a glass microsphere. In microspheres light is confined, similarly to bottle resonators in Fig.1.1(g), in lateral direction as WGMs and in the perpendicular direction by the changing radius. Microspheres exhibit ultra high quality factors in the range of 10^8 [Spi02]. Like for tapered glass fibers emitters can hardly be embedded into the cavities. As shown above the highest quality factors are achieved for cavities fabricated of glass since here, the smoothest surfaces can be prepared. However, the integration of internal emitters is difficult. For the study of such passive resonators evanescent-field coupling is very important. As shown in Fig. 1.1(h), light can be coupled in and out by a fiber via the evanescent fields. Long-ranging evanescent fields are an advantage of rolled-up microtubes, since their very thin walls confine the light in radial direction on a scale below its wavelength. In this work we will present that external emitters can excite the modes in microtube resonators in an excellent way just by filling them into the core of the microtube.

Chapter 2

Fabrication and Sample Design

In this chapter the fabrication of rolled-up microtube resonators is demonstrated starting from the design of the underlying layer system that is grown by molecular beam epitaxy and ending in the complete sample containing the microtubes. The first part gives an overview over the fabrication of the two types of microtubes that were mostly studied in this work: microtubes with lobes in the rolling edge and microtubes with etched rings in the microtube wall. The second part gives a more detailed insight into the wafer design and presents the wafer layout of the strained layer systems used in this work.

2.1 Fabrication of Rolled-Up Microtube Bottle Resonators

The possibility to fabricate three-dimensional micro and nano objects by the self-rolling mechanism of thin strained semiconductor bilayers was invented by Prinz *et al.* [Pri00]. The mechanism bases on the pseudomorphically strained growth of a bilayer consisting of InGaAs and GaAs on top of a GaAs substrate and an AlAs sacrificial layer. By selectively etching the AlAs layer the bilayer is lifted off from the substrate, bends up, and forms multi-walled microtubes. The fabrication of rolled-up microtubes in Hamburg was established by Stefan Mendach during his doctoral thesis [Men05]. Besides the realization of such structures the thesis focussed on the study of curved two-dimensional electron systems in magnetic fields. The fabrication of rolled-up microtubes acting as optical microcavities was first demonstrated here in Hamburg by Tobias Kipp [Kip06]. Since then these optical microtube resonators were extensively studied in Hamburg starting with my diploma thesis [Str06] and followed by the theses of the diploma students Hagen Rehberg and Christoph M.

Schultz [Reh07], Kay Dietrich [Die08] and Michael Sauer [Sau09] in collaboration with me. Here, I briefly present the cycle of the sample fabrication. Detailed process parameters like etching times and acid compositions can be found in the works above. First, I demonstrate the fabrication of microtubes with lobes, afterwards the rather similar fabrication of microtubes with etched rings. Finally, I show some improvements that were developed in the framework of this thesis.

Figure 2.1(a) shows the starting point of the fabrication which is the unstructured layer system with the GaAs part of the bilayer on top (blue). For simplicity the fabrication is demonstrated on hand of a bilayer of GaAs and InGaAs. Here, the InGaAs layer (yellow) stands exemplarily for the pseudomorphically strained layer while the GaAs layer stands exemplarily for the layer that is grown nearly unstrained. All lithography steps are performed with shadow masks and a mask aligner. The shadow masks were fabricated by us using e-beam lithography on chrome blanks. In the first step the rolling-direction and the total length of the microtube in axial direction are defined. Typical for crystals with zincblende structure, the most strain is relaxed when the microtube rolls in $\langle 100 \rangle$ direction, but naturally in perpendicular direction the same amount of strain can be relaxed. Thus, a preferred direction must be generated during the fabrication. As shown in Fig. 2.1(b), after optical lithography flat stripes are etched into the surface leaving a few nanometer thick InGaAs layer on top of the sacrificial layer. This layer protects the sacrificial layer and does not roll up. In a second lithography step the specific structure of the microtube like the winding number in form of the length of the U-shaped mesa, the shape of the lobe and the starting edge are defined. This mesa is etched about 500 nm deep into the substrate [shown dark blue in Fig. 2.1(c)]. In this step one has to be careful: on the one hand, the depression has to be deep enough to ensure a sufficient distance between substrate and the free-standing microtube, on the other hand, deep etching leads to a mutation of the lobe shape [Reh07]. Before selectively etching the sacrificial layer (red), in a third lithography step, the depression is protected by photoresist to avoid that the U-shaped mesa rolls up perpendicular to the desired rolling direction [Fig. 2.1(d)]. During the selective-etching step with HF solution the strained bilayer is undercut by etching the sacrificial layer (red), the bilayer bends up and rolls up until the photoresist is reached [as depicted in Fig. 2.1(e)]. In the last step the photoresist is removed and the free-standing microtube bridge is formed over the depression.

The fabrication process of microtubes with etched rings is very similar to the process for microtubes with lobes, but here an additional lithography and etching step is required. Fig. 2.2 depicts the fabrication cycle of those microtubes. The additional step is depicted in Fig. 2.2(b). Here, we etch two slits of about 4 nm depth into the GaAs part of the bilayer. After rolling-up, these slits result in two rings with a thinner wall and one ring with a thicker wall between them. This structure is

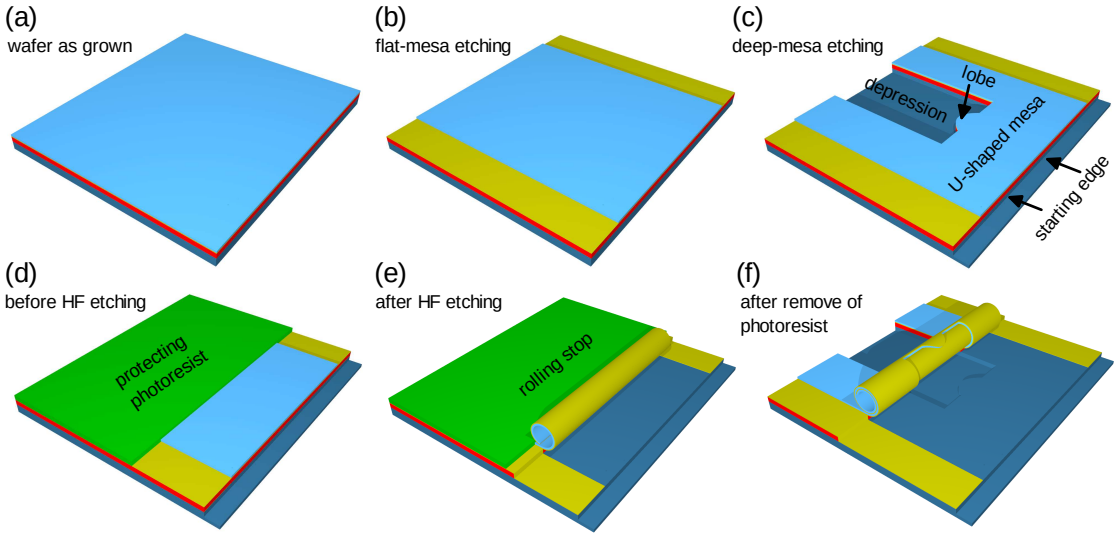

Figure 2.1: Sketch of the fabrication cycle of microtubes with lobes in the rolling edge: (a) Starting point. (b) Sample after flat-mesa etching leaving a thin InGaAs layer (yellow) on top of the sacrificial layer. (c) Sample after etching a deep mesa into the substrate (dark blue). The specific structure of the lobe, a depression and the starting edge is formed. (d)-(f) Sample before (d) and after (e) selective etching, as well as (f) the complete sample after removal of the protecting photoresist.

similar to planar ridge waveguides, but in our case the structure is rolled-up.

The self-rolling mechanism allows us to define most of the properties of the three-dimensional microtube by standard two-dimensional lithography on the bilayer before rolling-up. In general, all investigated microtubes in this work are very similar and differences occur only in a small region of the free-standing part of the microtube. Thus, it is useful to develop a standard process for the fabrication of the shadow masks. We redesigned our existing masks for the purpose of obtaining more microtubes on the same area and to automatically generate and vary the parameters over the mask area. Our redesigned shadow mask enables us to fabricate 750 microtubes on a typical e-beam writing field of 2 mm×2 mm in contrast to 74 microtubes on the old masks. This large number of microtubes allows us, on the one hand, to vary different parameters very smoothly or to prepare different designs in one fabrication cycle and, on the other hand, to have more statistics to prepare entire microtubes. Figure 2.3(a) shows a scanning electron micrograph of an array of 750 possible microtubes and (b) an enlarged view of a part of the array. The parameters for each individual microtube on the shadow mask are defined by coordinates in a rectangular region, as marked by the white rectangle. The coordinates of the individual microtube masks in the array are calculated automatically by a computer

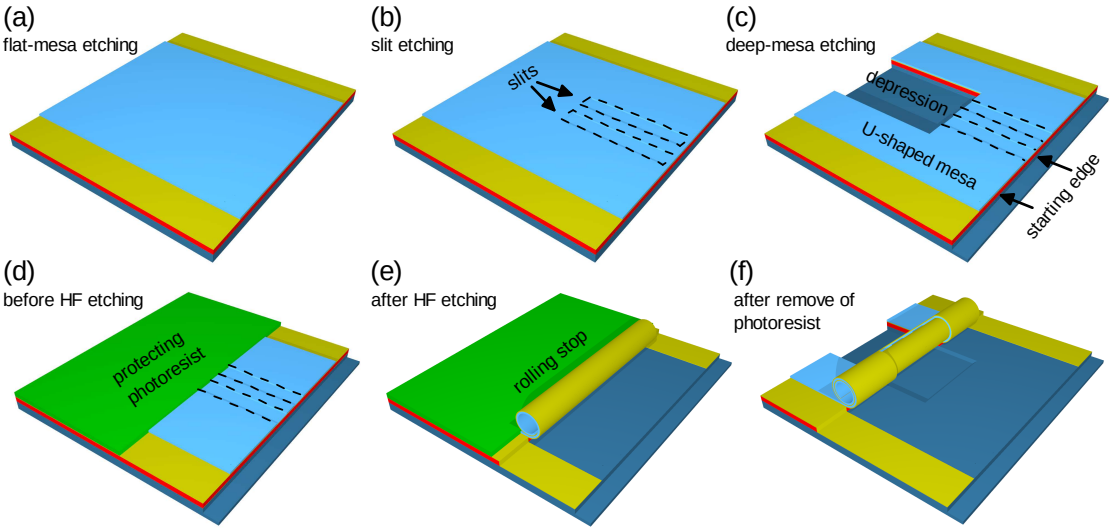

Figure 2.2: Sketch of the fabrication cycle of microtubes with etched rings in the wall: (a) Sample after flat-mesa etching leaving a thin InGaAs layer (yellow) on top of the sacrificial layer. (b) Sample after definition of two very shallow slits. (c) Sample after etching a deep mesa into the substrate (dark blue) forming a depression and the starting edge. (d)-(f) Sample before (d) and after (e) selective etching, as well as the complete sample (f) after removal of the protecting photoresist.

program. In this way a shadow mask with a large number of automatically generated microtube designs but individual properties can be fabricated.

It turned out that microtubes very often persist at the rolling-stop position depicted in Fig. 2.2(e) or get damaged during the removal of the photoresist instead of rolling to the final position. In the case of the particular layer system used in Fig. 2.3 (wafer F, as shown in the next section) we developed a slight modification of the fabrication process, which leads to a higher yield of entire microtubes. This is shown in Fig. 2.3(c) and (d). In contrast to Fig. 2.2(d), we did not completely protect the depression with photoresist. However, the microtubes rolled to their final position without rolling perpendicular to the desired rolling direction starting from the depression. In addition we left the photoresist on top of the complete sample after the selective-etching step. To avoid losses into the photoresist we prepared an outcut in the photoresist. This procedure has a big advantage: As shown in Fig. 2.3(b), most of the microtubes stopped at the same final rolling position defined by the photoresist. Contrarily, in other samples the individual microtubes stopped at different final rolling positions. By leaving photoresist on top of the sample we are able to predefine how the rolling edges are situated in the final rolling position. As will be shown later the rolling edges can lead to directional light

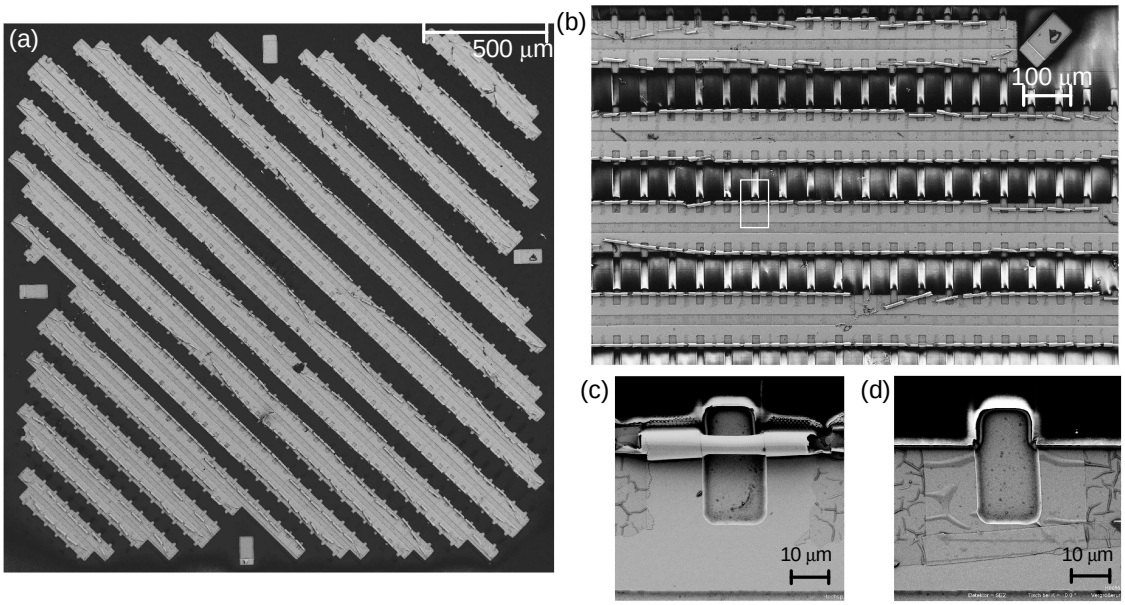

Figure 2.3: Scanning electron micrographs of microtubes on a sample. (a) 2mm×2mm array of microtubes on the sample. (b) Zoom into the array shown in (a). (c)-(d) Individual places of microtubes in the array, (c) an entire microtube, (d) a non rolled-up mesa. For these microtubes the photo resists (black) remains on the sample. A cutout is prepared into the photoresist to avoid losses.

emission. Unfortunately, this procedure worked only for microtubes fabricated of wafer F. For other samples we observed a rolling of the U-shaped mesa perpendicular to the desired rolling-direction starting from the depression. Nevertheless, for this sample the procedure led to a higher yield. We believe that the rather thin bilayers in this case, compared to our other samples, exhibit too small strain to start rolling from the depression. In addition, these microtubes had only small winding numbers (1-2 revolutions). It might be possible to use this procedure also for other samples with thin bilayers, but that could not be proven within this work.

2.2 Design of Strained Layer Systems with Tailored Mechanical and Optoelectronical Properties

The layer systems described in the previous part consisted of InGaAs and GaAs. However in general, the self-rolling mechanism works also for bilayers of AlGaAs and InAlGaAs, as mostly used in this work. The diameter of the microtubes can be defined by the thicknesses of the two layers and the In concentration [Den02, Men05]. A rule of thumb is, the smaller the thickness of the bilayer and the higher the In concentration, the smaller is the radius of the microtube. But to plan the wafer structure for the growth by molecular beam epitaxy (MBE) one can also calculate the desired rolling radius in dependence on the layer thicknesses and layer compositions. To determine the mechanical properties of our microtubes we used the model developed by Grundmann [Gru03]. In this model the rolling diameter is found by minimizing the total strain energy as function of the radius and the lattice constant at the inner wall. Besides the mechanical properties we also have to consider the optoelectronical properties, here understood as the band structure of the semiconductor layers. Since we investigate the optical eigenmodes of the microtube resonators by photoluminescence spectroscopy, internal emitters have to be embedded inside the microtube wall or emitters have to be placed very close to the tube wall to couple to the modes by their evanescent fields. In both cases the band gaps of the microtube walls have to be designed in a way that they are transparent for the wavelength of the emitters. This can easily be done by adding Al to the layer compositions. Due to the large energy separation of the valence and the conduction band at the Γ point Al strongly enlarges the band gaps of the layers. An upper limit for the Al concentration is about 40% since above this value the layers are etched during the selective etching step. In the following, we want to briefly introduce the wafer structures used in this work. All wafers were grown in the research group of Prof. Dr. Wolfgang Hansen and Dr. Christian Heyn. Figure 2.4(a) sketches wafer A of which the first microtube resonators were fabricated [Kip06]. One layer of self-assembled InAs quantum dots was embedded in the center part of the GaAs layer. The emission from the *s-s* transition of the quantum dots is observed at about 1.17 eV at 4 K. The radius of the rolled-up microtubes is about 2.6 µm. Wafer B in Fig. 2.4(b) is very similar to the one in (a), but here we added Al to the composition of the In-containing layer. The idea was that charge carriers excited in the InGaAs layer of wafer A cannot relax into the quantum dots since the GaAs band gap acts as a barrier. In wafer B the band gap of the InAlGaAs layer is larger, thus more charge carriers can relax into the quantum dots. Further on, we used the In flush technique [Was99] to blueshift the emission energy of the quantum

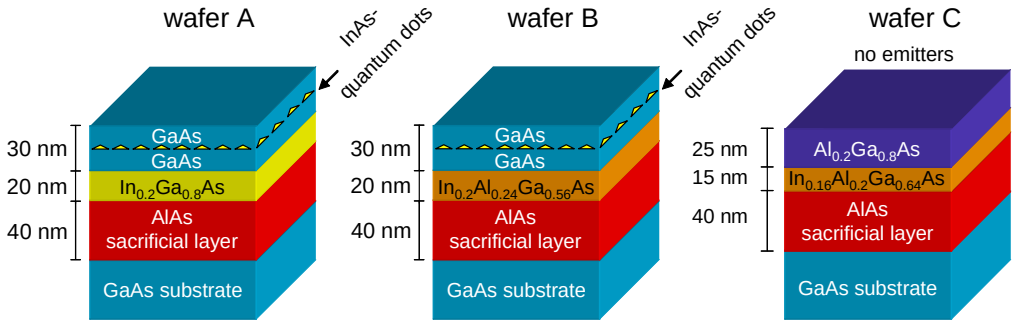

Figure 2.4: Wafer structures of different strained layer systems for the fabrication of rolled-up microtubes with quantum dots as internal emitters or no internal emitters. Wafer A is wafer ♯1653, wafer B is wafer ♯1984 and wafer C is wafer ♯2067 in the notation of the MBE Hamburg.

dots more into the sensitive range of our detector. The emission of the *s*-*s* transition is observed at about 1.25 eV at 4 K. Indeed, this wafer exhibits a two-times larger signal [Reh07] compared to wafer A, but it is not unambiguously clear, if this effect is caused by the enlarged band gap of the InAlGaAs layer or by the higher detector sensitivity at 1.25 eV compared to 1.17 eV. The radius of the tubes of wafer B is typical 2.7 µm. Wafer C, sketched in Fig. 2.4(c), does not contain any internal emitters. This wafer was designed to fabricate microtubes that can be excited by chemically synthesized nanocrystals coupling to the evanescent field of the modes. Since many types of these nanocrystals emit at rather high energies compared to the band gaps of GaAs and InGaAs we added Al to both layers of the strained bilayer. Due to the strain inside the microtube wall and the complex composition of the InAlGaAs layer we cannot exactly determine the size of the band gaps. But, as will be shown later, we could observe optical modes up to 1.41 eV at 4 K that were excited by PbS nanocrystals filled into the microtube. From this observation we can conclude that the band gap is larger than 1.41 eV. It would be desirable to couple also highly luminescent nanocrystals like CdSe/ZnSe to the microtube modes, but these emitters have quite large emission energies. Thus, more Al should be added to the bilayer composition to make the bilayer transparent at these energies. However, the Al composition must not exceed 40% since otherwise the microtube will be etched by the HF in the selective-etching step. Figure 2.5 sketches further wafer structures for the fabrication of microtubes. Here, quantum wells were embedded as internal emitters. For these wafers the InAlGaAs layer also has to act as a barrier for the electrons and holes inside the quantum well in addition to its function as strained layer for the self-rolling process. Wafer D was used for the fabrication of microtubes in which optical modes in microtubes containing quantum wells were observed for

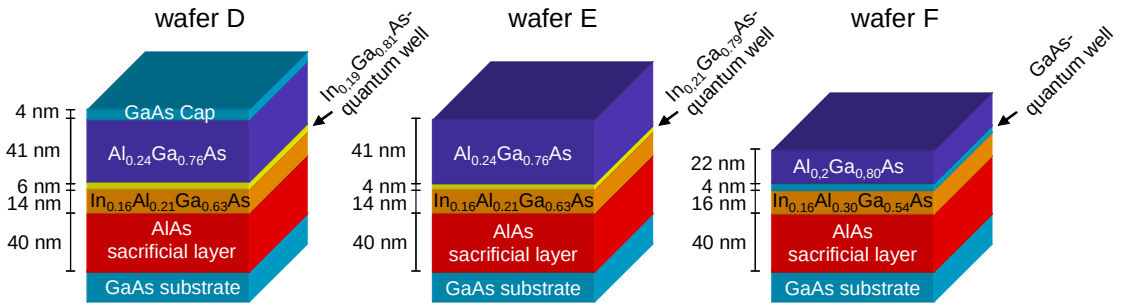

Figure 2.5: Wafer structures of different strained layer systems for the fabrication of rolled-up microtubes with quantum wells as internal emitters. Wafer D is wafer ♯1784, wafer E is wafer ♯1783 and wafer F is wafer ♯2245 in the notation of the MBE Hamburg.

the first time [Str07]. The quantum well emits around 1.33 eV at 4 K. The typical rolling radius of the microtubes is 3.2 µm. Wafer E is very similar to wafer D. Here, a 4 nm quantum well emits at about 1.38 eV at 4 K. The rolling radius of the corresponding microtubes is considerably small (approximately 1.8 µm). For wafer F the Al content was enlarged to 30% to act even as a barrier for a GaAs quantum well. The quantum well emits around 1.56 eV. The microtubes have typical radii of 2.4 µm. Besides the higher emission energy compared to InAs quantum dots and thus an emission energy in the range of higher detector sensitivity, quantum wells are good candidates for possible laser gain. Quantum wells can provide a much higher exciton density than quantum dots and the excitons exhibit larger dipole moments. The high emission energy of the GaAs quantum well allowed us to perform time-resolved photoluminescence spectroscopy with the streak camera of the research group of Prof. Dr. Christian Schüller in Regensburg which is only sensitive for energies higher than about 1.46 eV.

Chapter 3

Experimental Setups

This section gives a short introduction into the experimental setups on which the photoluminescence measurements were performed. Most of the experiments were done on the setup in Hamburg on which only time-integrated experiments are possible. This setup is demonstrated in the first section. The time-resolved measurements were carried out on the setup in the research group of Prof. Dr. Christian Schüller in Regensburg that is equipped with a streak camera.

3.1 Time-Integrated Photoluminescence Spectroscopy

Figure 3.1 sketches the micro photoluminescence setup in Hamburg. Main part of the setup is the confocal microscope and the cryostat. The sample is investigated in an optical continuous flow He cryostat. Inside the cryostat the sample is mounted on a stepper motor stage (step size 25 nm) that can be moved in x-y direction either by a joystick or computer-controlled. In the microscope a moveable mirror allows us either to observe the sample directly through an ocular or to couple the signal out of the microscope to the spectrometer. As an excitation source we used a continuous wave Ti:sapphire laser tunable between 700 nm and 810 nm that is pumped by a frequency-doubled Nd:YAG laser. The laser is stabilized by a noise eater and can be attenuated computer-controlled by an arrangement of a $\lambda/2$-plate between two linear polarizers. As an alternative excitation source a He-Ne laser emitting at 633 nm can be used. The beam is coupled into the microscope by a pellicle beam splitter and focussed onto the sample by a 50× microscope objective (NA=0.5). The signal is collected by the same objective and imaged by a $f = 600$ mm lens onto the entrance slit of the spectrometer. The large focal length of the lens in front of

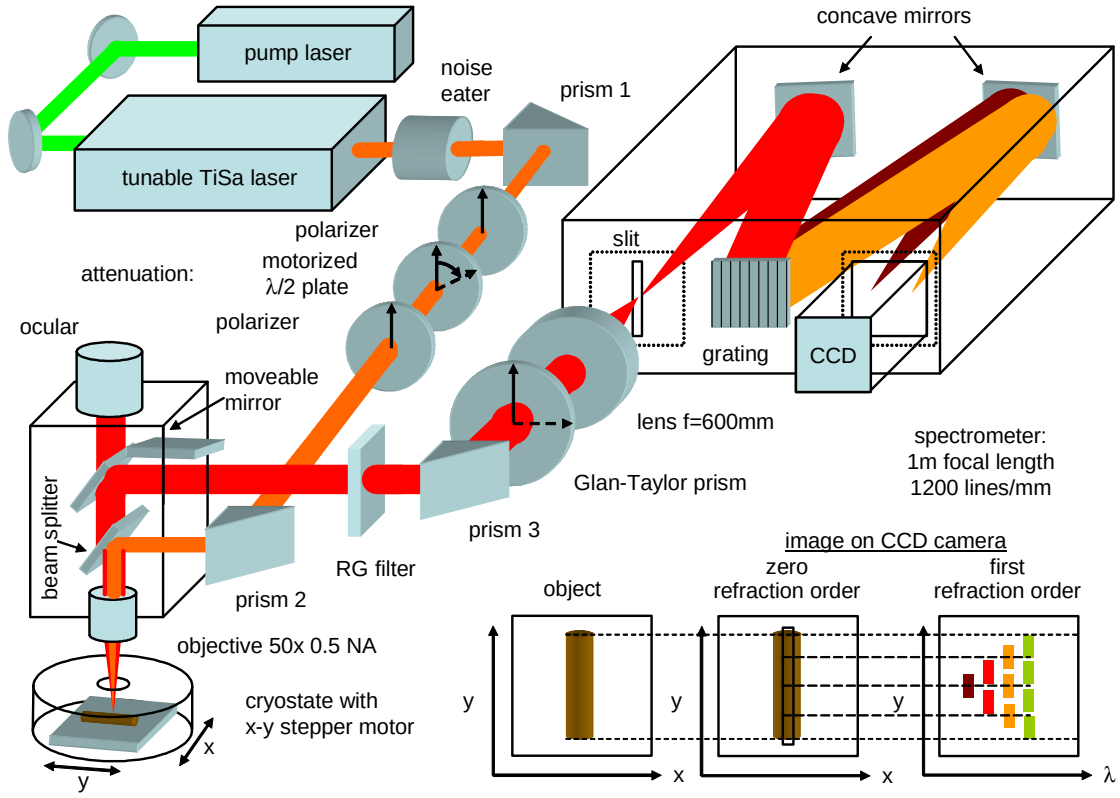

Figure 3.1: Setup for spatially resolved micro photoluminescence spectroscopy in Hamburg. The inset elucidates how the spatial resolution on the CCD in vertical direction is kept in the first refraction order.

the spectrometer enables a large spatial resolution. The arrangement of the setup allows us to observe images of the sample in every focal plane, i.e., in the plane of the slit and on the chip of the cooled Si charge coupled device (CCD) camera. We used the spectrometer not only with the grating in the first refraction order but also in the zeroth refraction order. By cutting-off the laser light with long pass filters we can directly image the PL emission from the microtube in the zero-order mode. But also in the dispersive mode in the first refraction order we still have spatial resolution in vertical direction of the CCD camera chip. This is elucidated in the inset of Fig. 3.1. When the microtube is aligned in a way, that its image in the focal plane of the entrance slit lies parallel to the slit, the spatial resolution along the microtube axis (in vertical direction) is kept. Thus, as depicted in the inset of Fig. 3.1, light from the center part of the microtube appears vertically centered on the CCD camera image and light from the upper part of the microtube is detected in the upper part of the CCD camera image.

3.2 Time-Resolved Photoluminescence Spectroscopy

Figure 3.2(a) sketches the micro-photoluminescence setup for time-resolved spectroscopy in Regensburg. In general, the setup is very similar to the one in Hamburg. But here, the laser can operate in pulsed mode. The tunable Ti:sapphire laser emits pulses of 600 fs length with a repetition rate of 81 MHz. For the experiments in this work the laser wavelength was fixed at 750 nm. The laser was focussed on the sample mounted in a continuous flow cryostat. Here, the cryostat was mounted on a manual x-y stage. The step size of the stage of 1 µm was rather large, thus we could use no objectives with magnifications larger than 40× to measure sufficiently stable signals. Instead of a microscope with an ocular, in Regensburg the sample is imaged with an additional camera that can also be used during the data acquisition. The light dispersed by the spectrometer can either be analyzed by a Si-CCD camera to measure time-integrated spectra or by a streak camera to achieve time resolution. The spectrometer can also be used in the zeroth refraction order to image the microtube emission with spatial resolution in horizontal and vertical direction. In the first refraction order of the grating the CCD image exhibits spatial resolution in vertical direction, as demonstrated for the setup in Hamburg. If the

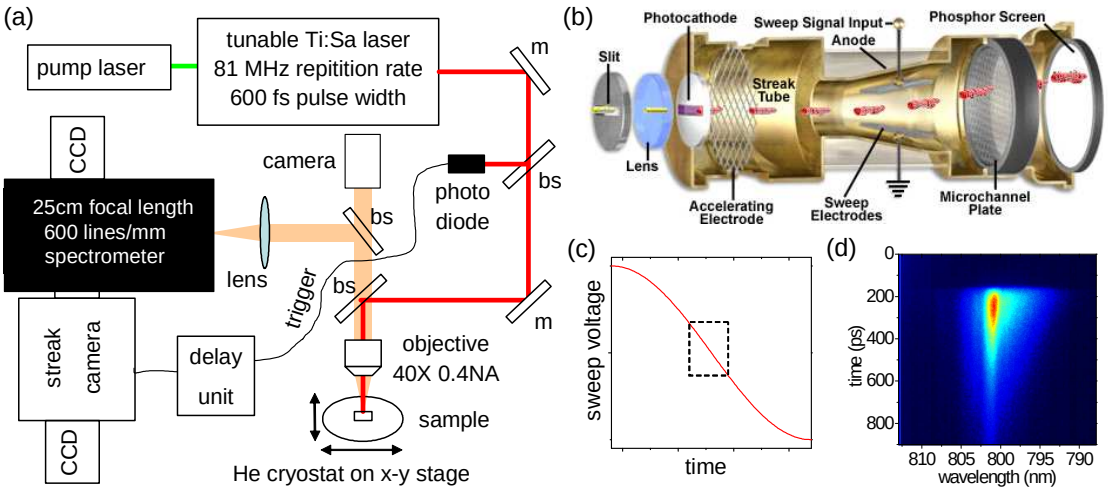

Figure 3.2: Setup for time-resolved photoluminescence spectroscopy in Regensburg. Beam splitters are marked with "bs" and mirrors with "m". (b) Cross section of the streak camera [Ham]. (c) Time dependence of the voltage applied on the sweep electrodes deflecting the photo electrons. The dashed rectangle marks the nearly linear part of the sinusoidal sweep voltage. (d) Image taken from the phosphor screen of the streak camera. Behind a spectrometer the image has wavelength resolution in horizontal direction.

acquisition is switched to the streak camera by a mirror inside the spectrometer, this spatial resolution is lost. Instead, the images taken by the streak camera exhibit time resolution in vertical direction. A sketch of the streak camera is shown in Fig. 3.2(b). After the photons are dispersed by the spectrometer in horizontal direction they have to pass a horizontal slit. Here, the spatial resolution in vertical direction gets lost. We had to be very careful during our measurements in Regensburg that light from the correct position of the tube passed the horizontal slit of the streak camera. After passing a lens the photons generate photo electrons on a photocathode that are accelerated by an electrode and pass a vertical electric field. This field is swept time-dependently with a sinusoidal voltage. The sweep is triggered by the laser pulses and retarded by a delay unit in that way that the arriving photo electrons pass the electric field during its zero point with nearly linear time-dependence [see Fig. 3.2(c)]. By this procedure early electrons (generated by early photons on the photocathode) are deflected in positive vertical direction and late photons in negative vertical direction. Thus, we achieve time resolution in vertical direction. After passing a microchannel plate the electrons are reconverted into photons on a phosphor screen that is imaged by a CCD camera. Such an image is exemplarily shown in Fig. 3.2(d). Here, we observe emission from a microtube containing a GaAs quantum well that emits around 800 nm. At about 801 nm, we find an optical mode.

Chapter 4

Experimental and Theoretical Results

4.1 Axial Light Confinement in Unstructured Microtube Resonators

The following Publication 1 is my first publication which was prepared during the time of my doctoral thesis. It deals with results that were obtained both during my diploma thesis and some important additional measurements that were performed during the first months of my doctoral thesis.

Interestingly, from the point of view at the end of my doctoral thesis this work contains a couple of key observations that are important for most parts of the present doctoral thesis. With the described sample we succeed in the first observation of optical modes in microtubes containing quantum wells as internal emitters. The wafer structure (wafer D) was only slightly modified for the sample on which we observed lasing (wafer F) in Publication 6. Furthermore, these microtubes showed for the first time an axial light confinement that can be understood on the hand of the underlying microtube geometry. The axial localization of the modes at kinks in the rolling edge that happened unintentionally during the fabrication process is the key mechanism for the controlled axial light confinement in Publication 3. The observed energetical shifting and spatial pinning of the modes along the microtube axis can be understood by a waveguide model. It turned out later that this waveguide model, slightly modified, can take into account all geometrical properties of a microtube like radius, wall thickness and winding number and acts even as the most important ingredient for the full three-dimensional description of microtube modes in Publication 3 and Manuscript 4. As a last important finding we observed pre-

ferential emission from the inside edge of the microtube. The line shaped emission from the inside edge enables one to perform photoluminescence spectroscopy with spatial resolution along the microtube axis by a single shot of the CCD camera. By aligning the microtube in the cryostat in a special way the CCD image keeps the spatial information along the microtube axis in vertical direction. Thus in a single shot the information of the whole microtube can be obtained. From that time on this procedure was the standard acquisition mode for all experiments and helped a lot to understand the recorded spectra.

The fabrication of the sample, most of the experiments and all calculations were performed by me and I created parts of the figures. Some experiments were done in collaboration with the diploma students Christoph M. Schultz and Hagen Rehberg. The paper was written by Tobias Kipp.

Publication 1

Three dimensionally confined optical modes in quantum-well microtube ring resonators

Ch. Strelow, C. M. Schultz, H. Rehberg, H. Welsch, Ch. Heyn, D. Heitmann, and T. Kipp

Physical Review B **76**, 045303 (2007)

PHYSICAL REVIEW B **76**, 045303 (2007)

Three dimensionally confined optical modes in quantum-well microtube ring resonators

Ch. Strelow, C. M. Schultz, H. Rehberg, H. Welsch, Ch. Heyn, D. Heitmann, and T. Kipp*
Institut für Angewandte Physik und Zentrum für Mikrostrukturforschung, Universität Hamburg, Jungiusstraße 11, 20355 Hamburg, Germany

(Received 15 February 2007; revised manuscript received 2 May 2007; published 5 July 2007)

We report on microtube ring resonators with quantum wells embedded as an optically active material. Optical modes are observed over a broad energy range. Their properties strongly depend on the exact geometry of the microtube along its axis. In particular, we observe (i) preferential emission of light on the inside edge of the microtube and (ii) confinement of light also in the direction of the tube axis by an axially varying geometry, which is explained in an expanded waveguide model.

DOI: 10.1103/PhysRevB.76.045303 PACS number(s): 78.66.Fd, 78.67.De, 42.82.Cr, 42.55.Sa

Semiconductor microcavities confining light on the scale of its wavelength have gained considerable interest in the past years, both for possible applications in integrated optoelectronics and for basic research on light-matter interaction, the latter especially in cavity quantum electrodynamic experiments.[1,2] Another growing field in the past years is the research on semiconductor micro- and nanostructures fabricated by use of strain relaxation of pseudomorphically grown bilayers, which are lifted off the substrate.[3–8]

We have recently shown that, by combining both research fields, it is possible to fabricate rolled-up microtubes which act as optical ring resonators.[7] In this paper, we report on a microtube ring resonator design with embedded quantum wells (QWs) as optically active material instead of self-assembled quantum dots as in our previous work. We observe optical modes over a broad energy range expanding from a little above the QW center emission energy to its low-energy side. The quality factor of the modes and its mode spacing are affected by reabsorption of light by the QW. We study the mode structure of our microtubes by scanning photoluminescence spectroscopy along the tube axis. The interesting aspect of our investigation is that we clearly observe (i) preferential emission of light at the axial edges and (ii) confinement of optical modes also along the tube axis. The latter is caused by spatially varying revolution numbers. Taking into account the exact geometric dimensions which we derive from scanning electron microscope (SEM) investigations, the spatial dependency of the mode energies along the tube axis can be nicely calculated.

The starting point of the fabrication of our QW microtube ring resonator is a molecular beam epitaxy grown layer system. On a GaAs substrate and a GaAs buffer layer, 40 nm AlAs will serve as a sacrificial layer in the later processing. The strained layer system which will by lifted off the substrate consists of 14 nm $In_{0.15}Al_{0.21}Ga_{0.64}As$, 6 nm $In_{0.19}Ga_{0.81}As$, 41 nm $Al_{0.24}Ga_{0.76}As$, and 4 nm GaAs. Both In-containing layers are pseudomorphically strained grown. The InGaAs layer forms a QW sandwiched between higher band gap barriers. The actual preparation process of self-supporting microtube bridges by using optical lithography and wet etching processes starts with the definition of a U-shaped strained mesa followed by the definition of a starting edge. The details can be found in Ref. 7. Here, we further improved our preparation technique by etching deeply into the AlAs layer in the region between the legs of the U-shaped mesa (see SEM picture in Fig. 1). During the following selective etching step, this region is protected by photoresist. This process leads to a larger and more controllable lifting of the central part of the microtube from the substrate. The SEM image in Fig. 1 depicts the specific microtube on which all measurements presented in this paper have been performed. It is slightly more than twofold rolled in its self-supporting part; correspondingly, the wall thickness is mostly 130 nm except for the small region along the tube axis where three strained sheets sum up to a 195 nm thick wall. The self-supporting part has a diameter of about 6.4 μm and a distance to the substrate of about 1 μm. The left inset in Fig. 1 sketches a *nonscaled* cross section of the microtube.

We investigated our microtubes by microphotoluminescence spectroscopy at low temperature $T=7$ K. A He-Ne laser ($\lambda=633$ nm) was focused on the sample by a microscope objective ($50\times$), having a spot diameter of about 1.5 μm.

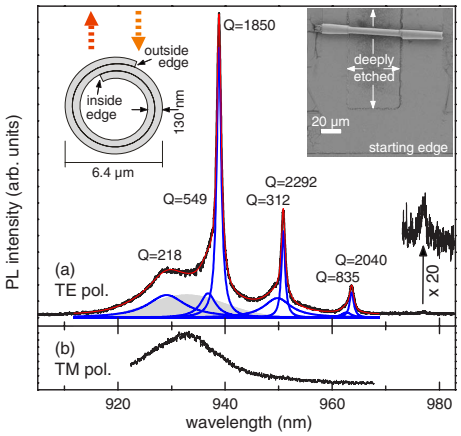

FIG. 1. (Color online) Measured PL spectra (black lines) of the microtube for (a) TE and (b) TM polarizations. The excitation power density was about 4 kW/cm^2. The spectrum in (a) is approximated by the sum of Lorentzian curves for the resonant modes (below the measured spectrum) and a Gaussian curve for the leaky modes (gray shaded). Q factors have been obtained by fitting. The left inset shows a nonscaled cross-sectional sketch of the microtube together with the excitation and collection configuration; the right inset shows a SEM image of the microtube.

The PL light was collected by the same objective, dispersed by a 1 m monochromator and detected by a cooled charge coupled device (CCD) camera.

Figure 1(a) shows a photoluminescence (PL) spectrum of the microtube. The sequence of sharp peaks represents optical modes which are observed here in microtubes containing QWs. Before discussing these modes in more detail, we want to point out the excitation and collection configuration used in this measurement. Here, the positions of excitation and collection of the PL light were the same in the z direction along the microtube axis but could be shifted against each other in the radial direction of the microtube. This situation is illustrated in the schematic inset in Fig. 1 by the two vertical arrows. The exciting laser generates electrons and holes which quickly relax into the QW in the vicinity of the focused laser spot on the microtube. There they form excitons which then radiatively decay. A fraction of the emitted light does not fulfill the condition of total reflection on the tube-wall–air interface and therefore couples to leaky modes. The other fraction does fulfill the condition of total reflection and is therefore guided by the tube wall. Constructive interference leads to the formation of optical resonator modes when, in a rather simple picture, light guided perpendicularly to the tube axis has the same phase after one round trip. Therefore, collecting the light at a different position than exciting the QW suppresses the detection of light out of leaky modes with respect to the cavity mode emission. If we collect the PL light from the excitation position, we can identify the emission into leaky modes around 933 nm with a full width at half maximum (FWHM) of 14 nm (23 meV). This is explicitly shown in Fig. 3(d), which will be discussed later in the text. This signal is not affected by interference inside the ring resonator and represents the emission of a curved QW. It is redshifted by about 20 nm (30 meV) compared to the QW emission of the unstructured sample, which is shown in Fig. 2(a). The shifting is strain induced and has been similarly reported by Hosoda *et al.*[5]

We now want to discuss the resonator modes in more detail. All modes are linearly polarized with the electric field vector parallel to the tube axis [TE polarization, Fig. 1(a)]. We find no modes in perpendicular polarization, as can be seen in Fig. 1(b). The strong peaks at about 939, 951, and 963.5 nm clearly show shoulders on their high-energy side. Their origin is not unambiguously clear. They might arise due to the lifting of the degeneracy of a perfectly symmetric cylindrical resonator by the inner and outer edges of the real structure (see sketch in Fig. 1).[9] Another explanation for the double peak structure might be the existence of axially confined modes of slightly different energy, which spatially overlap or at least cannot be separated by our experimental setup. Such axially localized modes will be thoroughly addressed later in this paper. At about 977 nm, a further mode with low intensity can be seen [marked by an arrow and magnified by a factor of 20 in Fig. 1(a)]. By trying to approximate the spectrum by a superposition of Lorentzians for the resonant modes and their high-energy shoulders together with a homogeneous Gaussian curve at about 933 nm with its above given FWHM for the residual intensity from leaky modes, one can clearly identify a further, rather broad mode on the high-energy side of the QW emission at about 929 nm. This peak can clearly be observed only in the described excitation and detection configuration. Collecting the PL light at the excitation position would strongly overlay this peak by leaky modes.

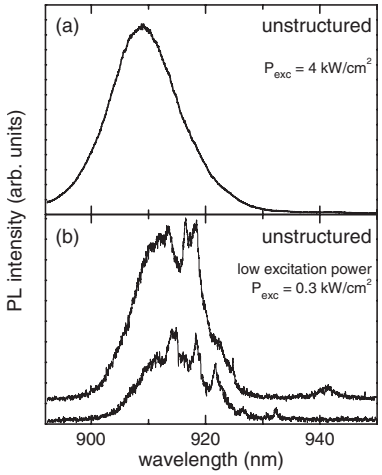

FIG. 2. PL spectra of the unstructured sample obtained with different excitation power densities: (a) 4 kW/cm^2 and (b) 0.3 kW/cm^2. The spectra in (b) (vertically shifted for clarity) were obtained in one and the same measurement for slightly different spatial positions within the area of the laser spot.

Recapitulating, altogether, five linearly polarized optical modes plus some shoulders are observed over an energy range of about 50 nm (70 meV). These modes are reported here in microtube ring resonators containing QWs as the optically active material. The lowest lying mode is separated by about 44 nm (60 meV) from the center QW emission energy. The observation of similar low lying cavity modes has been reported for microdisks containing ternary AlGaAs QWs, and they were attributed to the recombination of electron-hole pairs localized in monolayer and alloy fluctuations.[10] In fact, in measurements with low excitation power density on our unstructured sample, we observe single sharp lines with spatially changing energy positions on the low-energy side of the QW emission, as expected for emission out of such localized states. This can be seen in Fig. 2(b) where the excitation power was decreased by more than a factor of 10 compared to the measurements shown in Fig. 2(a) or in Fig. 1. Both spectra were obtained in one and the same measurement for slightly different spatial positions within the area of the laser spot. Regarding the quality factors $Q=E/\Delta E$, one can deduce a weak trend of slightly decreasing Q factors for increasing mode energies, still below the center QW emission energy if one averages the values of the main modes and its corresponding neighbors. This weak decreasing can be explained with a slight increase of reabsorption of light inside the cavity. Absorption is strongly enhanced for energies above the QW emission center. Consequently, the optical mode above the QW emission energy experiences strong losses resulting in a broadening by a factor of about 10 compared to the sharpest peaks on the low-energy side.

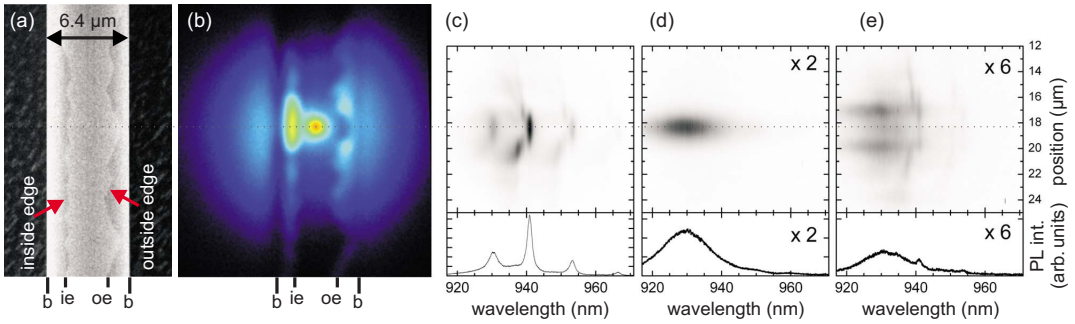

FIG. 3. (Color online) (a) SEM picture of a part of the microtube. Both the inside and outside edges are visible. (b) Undispersed PL image of the sample shown in (a). Both images are equally scaled; the positions of the borders (b), the inside edge (ie), and the outside edge (oe) are marked. [(c)–(e)] Spectrally analyzed PL emission at the (c) inside edge, (d) radial position of the laser spot, and (e) outside edge. In the upper panels, the spatial information along the tube (z) axis is retained. The lower panels show spectra obtained at the z position on the level of the laser spot (marked by the dotted horizontal line). The excitation power density was about 5 kW/cm^2.

Figure 3(a) shows a magnified SEM picture of a part of the investigated self-supporting microtube bridge. As previously mentioned, the tube has rolled up slightly more than two times. For this particular microtube, the small region where the wall consists of three rolled-up strained layers was orientated on top of the tube, just like as that sketched in Fig. 1. Using a rather high acceleration voltage of 20 kV at the SEM, not only the outside edge of the microtube wall but also the inside edge can be resolved. Since the microtube wall in the region between the inside (left) and outside (right) edges consists of three rolled-up layers, it appears slightly brighter in the SEM picture than the material besides this region. We find that applying our preparation technique to the layer system described above, both edges of the microtube tend to randomly fray over some microns instead of forming straight lines. The fraying occurs predominantly along the ⟨110⟩ direction of the crystal, whereas the rolling direction of the microtube is along ⟨100⟩. The spectrum in Fig. 1 proves that optical modes can still develop despite the frayed edges, since it is actually obtained from exactly the microtube shown in Fig. 3(a). By using the grating of the monochromator in zero order as a mirror, we can directly image the microtube on the CCD chip of the detector, as shown in Fig. 3(b). Here, the microtube was excited by the laser, but in the collected signal, the laser stray light was cut off by an edge filter. Therefore, Fig. 3(b) shows an undispersed PL image of the sample. We observe strong emission at the excitation position centrally on the mircotube. We also observe a large corona around this position due to PL emission of the underlying GaAs substrate. The borders of the microtube become apparent by vertical shadows. Furthermore, both the inside and outside edges of the tube are visible in the CCD image. Even though close to the resolution limit, the larger frays especially of the outer edge, which are clearly visible in the SEM picture in (a), can also be identified in (b). Interestingly, we observe a strong enhancement of PL emission near the inside edge of the microtube. Having aligned the microtube axis in the way that its image is parallel to the entrance slit of the spectrometer, we can spectrally analyze the PL light of different radial positions retaining spatial resolution along the tube axis. In Fig. 3(c), the signal along the inside edge is analyzed. The vertical axis gives the spatial position along the tube axis (z direction), the horizontal axis gives the spectral position, the PL intensity is encoded in a gray scale. The lower panel in (c) shows a spectrum obtained at the z position on a level of the laser spot (dotted horizontal line). The sequence of maxima of different wavelengths shows that the light is indeed dominantly emitted out of resonant modes. In Fig. 3(d), the signal emitted underneath the laser spot is analyzed. In contrast to the inner edge, here, only one peak around 930 nm is observed, which is the emission of the QW into leaky modes as already discussed in the context of Fig. 1(a). At last, Fig. 3(e) analyzes the emission at the outside edge. Here, we observe both sequences of resonant modes and leaky modes, but with a much smaller intensity than in (c) or (d). Note that the intensity in (e) is multiplied by a factor of 6 compared to (c). Thus, as a summary of Fig. 3, preferential emission of modes at the inside edge is proven. This result, which is valid for every position along the tube, indicates that the edges of the microtube might be functionalized for a controlled or even directional emission of light.

In order to investigate the influence of the frayed edges on the mode spectrum, we performed micro-PL measurements scanning along the tube (z) axis, which are shown in Fig. 4(b). The graph's horizontal axis gives the wavelength of the detected light, whereas its vertical axis gives the axial position on the microtube which can directly be related to the SEM picture in Fig. 4(a). The PL intensity is encoded in a gray scale where dark means high signal. Note that the gray scale is chosen to be logarithmic in order to better resolve in one and the same graph both intense peaks on a comparatively intense background and small peaks on a weak background. The microtube was scanned in 80 steps over a length of 35 μm [between the two broken horizontal lines in Fig. 4(a)]. In the z direction, the collecting position of the PL light was centered on the excitation spot; in radial direction, we collected over the whole microtube.

For nearly every position on the microtube, we observe three or four optical modes. Their energies are shifting along

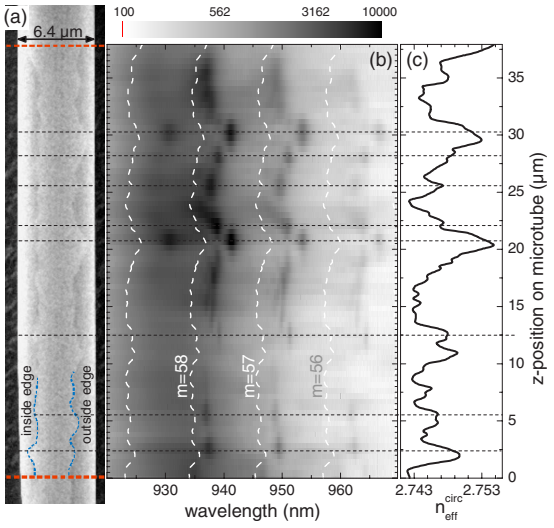

FIG. 4. (Color online) (a) SEM picture of a part of the microtube. Inside and outside edges are marked with broken lines for clarification. The tube wall is thicker between these edges (see sketch in Fig. 1). (b) Scanning micro-PL spectra show three dimensionally confined optical modes (excitation power density of about 4 kW/cm^2). The white broken lines represent calculated mode energies for $m=59$ to 56. (c) Calculated effective refractive index vs position. Horizontal broken lines mark the positions of some pronounced localized modes.

the z direction, but interestingly this shifting is not continuous: The mode energies sometimes seem to be spatially pinned. First, we want to explain the shifting by an expanded model of a closed waveguide. For each position in the z direction, we regard a cross section perpendicular the tube axis as a circular waveguide, having a diameter of $d=6.4$ μm. The waveguide thickness abruptly changes at the edges from 130 to 195 nm. For each region, we translate the thickness in related effective refractive indices $n_{\mathrm{eff}}^{130\ \mathrm{nm}}$ and $n_{\mathrm{eff}}^{195\ \mathrm{nm}}$, respectively.[7] For this calculation, we assumed the average refractive index of the layer system to be $n(E)=0.3225\times E[\mathrm{eV}]+2.982\,32$ by linearly approximating values given in Refs. 11 and 12. From Fig. 4(a), we determine the distance $L^{195\ \mathrm{nm}}(z)$ from the inside to the outside edge on the tube surface by taking into account that the picture is a projection of a curved surface. We can then define an overall effective refractive index for the whole circular waveguide for each z position: $n_{\mathrm{eff}}^{\mathrm{circ}}(z)=n_{\mathrm{eff}}^{195\ \mathrm{nm}}L^{195\ \mathrm{nm}}(z)/(\pi d)+n_{\mathrm{eff}}^{130\ \mathrm{nm}}[1-L^{195\ \mathrm{nm}}(z)/(\pi d)]$. The periodic boundary condition for a resonant mode then reads $n_{\mathrm{eff}}^{\mathrm{circ}}(z)\pi d=m\lambda$, with the vacuum wavelength λ and the azimuthal mode number $m\in\mathbb{N}$. The resonances calculated with this model have azimuthal mode numbers around $m=57$ and are depicted in Fig. 4(b) as bright broken lines. The absolute position of the calculated mth mode strongly depends on the exact dimension of the microtube, whereas the calculated mode spacing fits quite well to the measurements. Deviations can be explained by slightly insufficient approximated refractive index of the layer system, especially because of neglecting absorption inside the QW. As a striking result, the calculation reveals that the overall z dependency of the measured resonant wavelengths is nicely approximated by our model.

In the following, we want to concentrate on the spatially pinned resonances. These resonances can be seen in Fig. 4(b) as isolated dark spots with no significant wavelength shift over 1 μm or more. This implies that these resonances are localized modes, confined also in the z direction along the tube axis. Comparing Figs. 4(a) and 4(b), it seems that some of these localized modes can be attributed to positions on the tube with a broad distance between inside and outside edges. To work out this point in more detail, Fig. 4(c) shows $n_{\mathrm{eff}}^{\mathrm{circ}}(z)$ calculated for $\lambda=940$ nm, which essentially reflects the distance between the edges as a function of the z position. Comparing now (b) and (c), it becomes obvious that optical modes are predominantly localized in regions of local maxima of $n_{\mathrm{eff}}^{\mathrm{circ}}(z)$ representing local maxima of $L^{195\ \mathrm{nm}}(z)$. To better visualize this behavior, all pronounced localized modes are indicated with horizontal lines in Fig. 4(b). Confinement of light along the z direction is achieved by a change of $n_{\mathrm{eff}}^{\mathrm{circ}}(z)$. This important result can be qualitatively explained within the waveguide model. Until now, we implied in our model light having no wave vector component along the tube axis, because, for a perfect infinite microtube, this light would just run away along the tube axis. If we now regard light with a finite but small wave vector component along the axis, this light can experience total internal reflection also in z direction, which leads to a three dimensional confinement. Total internal reflection in this case is quite similar to the situation in a graded-index optical fiber. Our model using an averaged effective refractive index for a circular cross-sectional area of a microtube explains our measured data astonishingly well, despite the fact that this model neglects the abrupt changes of the inside and outside diameters. The experimental data show that it is possible to confine light also along the axis of a microtube ring resonator by a slight change of the wall geometry along the axis. This result opens up new prospects for a controlled three dimensional confinement of light inside a microtube ring resonator by the use of a lithographically controlled variation of the inside and outside edges of the strained layer system before the roll-up process takes place. In this context, we would like to refer to a recent theoretical work by Louyer *et al.* on prolate-shaped dielectric microresonators.[13] We believe that our technique of laterally structuring the edges of a microtube before the roll-up process, which is presented in this paper, might make it possible to fabricate prolate-shaped microtube resonators with similar characteristics as described in Ref. 13.

In summary, we report on a microtube resonator with embedded QWs. We observe optical modes in a quite large energy range, which are partly affected by reabsorption. Scanning micro-PL measurements demonstrate (i) preferential emission of light near the inside edge of the microtube and (ii) confinement of light also in the direction along the tube axis. The confinement is induced by spatial variations of the inside and outside edges of a microtube along its axis and can be approximated in an expanded waveguide model. The

presented results highlight the possibility of both a controlled emission and a controlled three dimensional confinement of light in a microtube by a lithographically controlled definition of the microtube edges.

We gratefully acknowledge financial support of the Deutsche Forschungsgemeinschaft via the SFB 508 "Quantum Materials" and the Graduiertenkolleg 1286 "Functional Metal-Semiconductor Hybrid Systems."

---

*tkipp@physnet.uni-hamburg.de

[1] K. J. Vahala, Nature (London) **424**, 839 (2003).
[2] G. Khitrova, H. M. Gibbs, M. Kiraz, S. W. Koch, and A. Scherer, Nat. Phys. **2**, 81 (2006).
[3] V. Y. Prinz, V. A. Seleznev, A. K. Gutakovsky, A. V. Chehovskiy, V. V. Preobrazhenskii, M. A. Putyato, and T. A. Gavrilova, Physica E (Amsterdam) **6**, 828 (2000).
[4] O. G. Schmidt and K. Eberl, Nature (London) **410**, 168 (2001).
[5] M. Hosoda, Y. Kishimoto, M. Sato, S. Nashima, K. Kubota, S. Saravanan, P. O. Vaccaro, T. Aida, and N. Ohtani, Appl. Phys. Lett. **83**, 1017 (2003).
[6] S. Mendach, T. Kipp, H. Welsch, C. Heyn, and W. Hansen, Semicond. Sci. Technol. **20**, 402 (2005).
[7] T. Kipp, H. Welsch, C. Strelow, C. Heyn, and D. Heitmann, Phys. Rev. Lett. **96**, 077403 (2006).
[8] S. Mendach, R. Songmuang, S. Kiravittaya, A. Rastelli, M. Benyoucef, and O. G. Schmidt, Appl. Phys. Lett. **88**, 111120 (2006).
[9] M. Hosoda and T. Shigaki, Appl. Phys. Lett. **90**, 181107 (2007).
[10] T. Kipp, K. Petter, C. Heyn, D. Heitmann, and C. Schüller, Appl. Phys. Lett. **84**, 1477 (2004).
[11] T. Takagi, Jpn. J. Appl. Phys. **17**, 1813 (1978).
[12] A. N. Pikhtin and A. D. Yas'kov, Sov. Phys. Semicond. **14**, 389 (1980).
[13] Y. Louyer, D. Meschede, and A. Rauschenbeutel, Phys. Rev. A **72**, 031801(R) (2005).

4.2 Preferential and Directional Emission in Microtube Resonators

This Publication 2 arose in the context of my contributed talk on the 13th International Conference on Modulated Semiconductor Structures in Genova in July 2007.

In this work we report on further, more detailed analyses on the emission properties of optical microtube resonators. We performed additional measurements on the microtube also investigated in Publication 1. Here, we focus on the preferential emission of the microtube from the inside rolling edge. By mounting the tube on wedges with different angles, we proved, on the one hand, the preferential emission from the inside edge by positioning it on top of the microtube and, on the other hand, we demonstrated directional emission from the microtube.

Directional emission is important for applications, since the emitted light is coupled out efficiently in a desired direction. For microcavities with rotational symmetry like also microdisks this is a problem since naturally the light is emitted isotropically in the plane perpendicular to the rotational axis. To overcome this the rotational symmetry can be broken. For microdisks there are a couple of works that report on directional emission induced by shape deformations [Lev93, Nöc97, Wie08] or for pierced microdisks [Wie06, Wil09]. Directional emission is also reported for spiral-shaped lasers [Che03, Kne04], but here the quality factors were strongly lowered by the geometrical modification. For all these realizations structures with very special geometries have to be fabricated. This is different in the case of microtubes. By the self-rolling mechanism microtubes naturally exhibit a broken rotational symmetry: the spiral shaped cross section of microtubes is an intrinsic property and directional emission is expected. Indeed, finite-difference time-domain simulations confirm our experimental findings [Hos07].

This work arose out of a close collaboration with the diploma students Christoph M. Schultz and Hagen Rehberg. We performed the experiments together. The publication was mainly written by me.

Publication 2

Spatial emission characteristics of a semiconductor microtube ring resonator

Ch. Strelow, C. M. Schultz, H. Rehberg, H. Welsch, Ch. Heyn, D. Heitmann, and T. Kipp

Physica E **40**, 1836-1839 (2008)

Available online at www.sciencedirect.com
ScienceDirect
Physica E 40 (2008) 1836–1839
PHYSICA E
www.elsevier.com/locate/physe

Spatial emission characteristics of a semiconductor microtube ring resonator

Ch. Strelow*, H. Rehberg, C.M. Schultz, H. Welsch, Ch. Heyn, D. Heitmann, T. Kipp

Institute of Applied Physics, University of Hamburg, Jungiusstraße 11, 20355 Hamburg, Germany

Available online 12 November 2007

Abstract

We demonstrate preferential and directional emission from a rolled up semiconductor microtube ring resonator with a quantum well embedded as an optically active material. The emission of resonant optical modes appears preferentially at the inside edge of the tube with a direction 60° to the tangent of the ring. The emission of leaky modes shows an entirely different behavior. Here, tangential emission seems to be preferred at both the inside and the outside edge.

PACS: 78.66.Fd; 78.67.De; 42.82.Cr; 42.55.Sa

Keywords: Microcavity; Microtube; Directional emission

In the past years there has been a great interest in the development and investigation of new miniaturized and well-defined light sources. In this field semiconductor systems of nano-scaled emitters embedded in micron-scaled cavities are playing a very important role as the latter confine and influence light on a scale of its wavelength. Self-assembling mechanisms, which are extensively used for the fabrication of emitters like InAs quantum dots (QDs), can also be exploited in the precisely controlled fabrication of micron-sized structures. Prinz et al. [1] showed that strained semiconductor bilayers released from the substrate roll up and form microtubes. The diameter of these microtubes can be accurately tuned from some nanometers to several hundred microns by varying the incorporated strain. In a previous work we demonstrated that—combining both fields—microtubes with embedded InAs QDs can be used as optical ring resonators [2]. The photoluminescence (PL) light of the QDs is emitted into a sequence of sharp polarized modes. In a very recent paper we investigated microtube ring resonators containing InGaAs quantum wells (QWs) as optically active material [3]. The most important result was that the typical radial offsets (the edges) of a microtube can be functionalized for a complete three-dimensional confinement of optical modes and for preferential emission. In this paper we continue this investigation focussing on effects of the edges on the emission properties of the microtube. We observe not only preferential but even directional emission of light from the inside edge of a microtube.

Fig. 1 shows a scanning electron microscope (SEM) image of the investigated microtube. Starting point for the preparation of this tube is a molecular beam epitaxy grown layer system. On top of a GaAs substrate 40 nm AlAs will serve as a sacrifical layer in the later lift-off process. On top of this 14 nm $In_{0.15}Al_{0.21}Ga_{0.64}As$, 6 nm $In_{0.19}Ga_{0.81}As$, 41 nm $Al_{0.24}Ga_{0.76}As$, and 4 nm GaAs form the strained layer system (altogether 65 nm), which will bend up after being lifted off the substrate. Here, the 6 nm InGaAs layer is sandwiched between higher bandgap materials and acts as a QW. The geometry of the tube is defined by a U-shaped mesa (see Fig. 1) which is obtained by optical lithography and wet-etching techniques as described in detail in Ref. [3]. In the lift-off process, the mesa rolls up beginning at the starting edge, resulting in a freestanding microtube bridge. Its central part, which is raised about

*Corresponding author.
E-mail address: cstrelow@physnet.uni-hamburg.de (Ch. Strelow).

1386-9477/$ - see front matter © 2007 Elsevier B.V. All rights reserved.
doi:10.1016/j.physe.2007.10.098

1 μm above the substrate, has a diameter of about 6.4 μm. The winding number is slightly larger than two, as sketched in the inset of Fig. 1.

To have a more detailed look at the special geometry of the microtube investigated in this paper a magnified SEM picture of a special part of the tube is shown in Fig. 2(a). A rather high acceleration voltage of 20 kV at the SEM allows the visualization of both the inside edge and the outside edge of the tube due to the contrast between the two-layer and the three-layer part of the tube. One can clearly observe that the edges are not straight. During the etching process the edges tend to fray predominantly along the ⟨1 1 0⟩ direction whereas the rolling direction is along ⟨1 0 0⟩. In particular, often triangle shaped kinks are formed as shown in Fig. 2 on the outside edge.

We probe our microtubes by micro PL spectroscopy at low temperature $T = 7$ K focussing a He–Ne laser ($\lambda = 633$ nm) by a microscope objective (50×) on a spot with a diameter of about 1.5 μm. The emitted PL signal is collected by the same objective and dispersed by a 1 m monochromator. Using the grating in zeroth order as a mirror, one can take images of the investigated microtube and spatially correlate the detected PL signal to its origin very precisely.

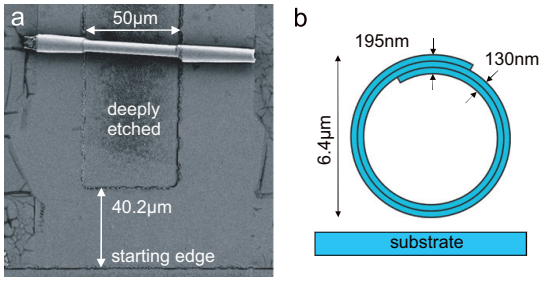

Fig. 1. (a) Scanning electron micrograph of the investigated microtube. (b) Sketch of the cross section of the microtube.

Fig. 2(b) shows an emission image of the microtube part depicted in Fig. 2(a). The laser light is cut off by a long pass filter so that only the emitted PL light is detected. Interestingly, specific parts of the tube exhibit enhanced light emission. The circular shaped emission centrally on the tube originates from the laser spot position. The strong signal on the left side of the laser spot emission is located at the inside edge position. A much weaker signal is located at the outside edge position. The borders of the tube are visible as shadows in the background signal from the GaAs substrate. We spectrally analyzed the PL emission of all three different positions [3]. At the laser position, electron–hole pairs are created inside the tube wall, which quickly relax into the QW. There they form excitons which decay radiatively. When the emitted light hits the tube–wall–air interface it forms two fractions: the first part does not fulfill the condition of total reflection and leaves the resonator without interaction into leaky modes in close vicinity of the exciting laser spot. The spectral analysis delivers a Gaussian lineshape at 933 nm (full-width at half-maximum of 14 nm), which basically represents the decay of the QW excitons. The second part does fulfill the condition and is guided by the tube wall. This light can couple to resonant optical modes when it interferes constructively after one round trip or to leaky modes when it is scattered after a short distance e.g. on the edges of the tube. The light emitted at the inside edge position stems almost totally from resonant modes, while the light emitted at the outside edge position consists predominantly of leaky modes [3]. In summary it becomes obvious that the investigated microtube shows preferential emission of resonant modes from the inside edge of the tube.

In the following we want to focus on the preferential emission of light from resonant modes and investigate the possibility of a directional emission. We therefore

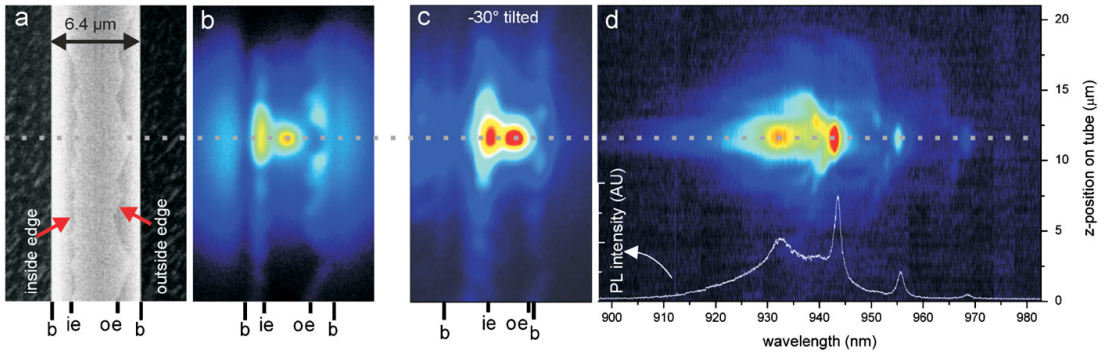

Fig. 2. (a) A magnified scanning electron micrograph taken with a high acceleration voltage of 20 kV resolves both inside edge (ie) and outside edge (oe) of the microtube. (b) PL emission image of the microtube taken with a CCD Camera. Light is emitted especially from the edges and the laser spot position. The borders (*b*) are recognizable as shadows. (c) PL emission image from the microtube tilted about −30°. The borders and the edges of the tube are marked. (d) PL density plot of light collected from the inside edge. Due to the alignment of the monochromator slit parallel to the tube the plot has spatial resolution in vertical direction and spectral resolution in horizontal direction. The dashed line marks the position where the spectrum in (d) is taken.

measured the microtube tilted under different angles with respect to the detection direction. The tilting was realized by mounting the sample on different wedges in the cryostat. Exemplarily, Fig. 2(c) shows an emission image of the same part of the microtube as in Fig. 2(a), but tilted about -30°. Since in this measurement a different longpass filter was used, the borders of the tube are not visible as shadows in the background signal. The positions of the borders are calculated from values from Fig. 2 with respect to the changed projection. Again one can clearly observe strong emission from the inside edge and from the laser spot position. Also signatures of the emission at the outside edge similar to Fig. 2(b) are observed. The tilting leads to a much better differentiation between the inside edge and the left border of the tube. Therefore Fig. 2(c) clearly demonstrates that the strong emission really stems from the inside edge and not from the border of the microtube.

Having aligned the microtube axis in the way that its image is parallel to the entrance slit of the spectrometer, we can spectrally analyze the PL light of a distinct radial position retaining spatial information along the tube axis. In Fig. 2(d) the signal at the inside edge is analyzed. The vertical axis gives the spatial position along the tube axis (z direction), the horizontal axis gives the spectral position, the PL intensity is encoded in a false color scale. We clearly observe a regular sequence of optical modes which are localized at the position of the kink (marked with a horizontal line in Fig. 2). A spectrum taken at this position is shown in Fig. 2(d) as a white curve. The sequence of optical modes is superimposed on a background of leaky modes centered at about 935 nm. In Fig. 2(d), one can also find further sequences which are localized above and below the kink and which are shifted in the wavelength. Due to the frayed edges of the tube the resonance conditions are changing along the tube axis. This behavior is discussed in detail in Ref. [3].

The fact that preferential emission of modes at the inside edge is proven raises the question of directionality. To prove directional emission we performed measurements mounting the sample on wedges with angles of $\pm 45^\circ$, $\pm 30^\circ$ and 0°. Of course there is a high interest in the emission characteristics around the whole circumference of the microtube. Nevertheless, since the microtube is attached on a substrate and since the tilted sample mounted in a cryostat has still to be accessible with the microscope objective, larger tilt angles were not possible in our setup. All these measurements were accomplished at the same position on the microtube along the z-axis, where the frayed outside edge forms the local kink (see Fig. 2). To ensure comparability, in each measurement the exciting laser spot was positioned between the inside and outside edge, i.e. in the three-layer part of the tube. For each angular position three measurements were performed analyzing light from the inside edge, the position of the laser spot, and the outside edge as described above. All these measurements proved *preferential* emission of resonant modes from the inside edge. For the analysis of the *directionality* of the emission the PL spectra were fitted between 945 and 915 nm by a Gaussian curve for the QW PL signal (leaky modes) and two Lorentz curves for the main mode at 943 nm and the mode at 932 nm. Fig. 3(b) shows the polar plot of the intensity of the main mode emitted at the inside edge and of the leaky signals from both inside and outside edge. To ensure comparability, the intensities are normalized with respect to the intensity of the emission at the laser spot position. The emission of the main mode (dots) shows a strong maximum around 0° [see Fig. 3(a) for the definition of the angles]. In contrast to this, the leaky signal from the inside edge exhibits a more or less continuous increase from -45° to $+45^\circ$. The leaky signal from the outside edge increases from $+45^\circ$ to -45°. Note that the collecting microscope objective has a numerical aperture of 0.5 which means that light is collected in an angle of 30° around the optical axis. Therefore the measured shape of the emission signal is broadened by the aperture. Following conclusion can be made for the emission properties: (i) the optical modes show directed emission from the inside edge around an angle of about 0°. This direction corresponds to an angle of 60° with respect to the tangent at the inside edge in direction to the tube's three-layer part. (ii) The leaky signal both from the inside and from the outside edge seems to be predominantly emitted tangentially in direction to the three-layer part. The polar plot in Fig. 3 (c) shows the intensity ratio of the resonant mode and the leaky signal emitted from the inside edge. This plot demonstrates the different nature of the emission from the inside edge of resonant and leaky modes, respectively.

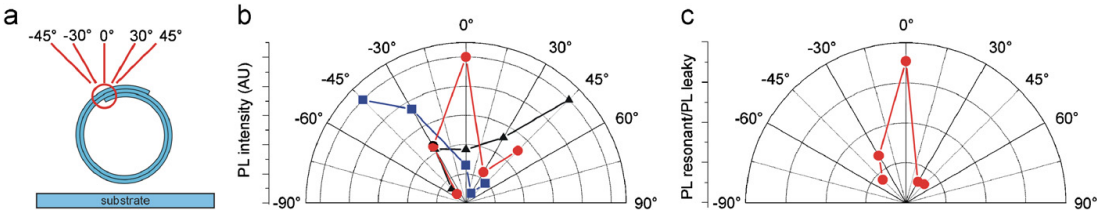

Fig. 3. (a) Sketch of 90° range of tilted positions. (b) Polar plot of the intensity of the resonant mode from the inside edge (dots) and of leaky modes both from the inside edge (triangles) and outside edge (squares). The data points are connected as a guide for the eyes. The curves are normalized to its maximum. (c) Polar plot of the intensity ratio of the resonant mode and the leaky signal emitted from the inside edge.

In summary, we demonstrated preferential and strongly directional emission of resonant modes at the inside edge of a QW microtube ring resonator. This emission occurs in a direction 60° to the tangent. The emission of leaky modes shows an entirely different behavior. Here, tangential emission in direction to the three-layer part of the microtube seems to be preferred at both the inside and the outside edge. Preferential and even directional emission is a substantial argument that the edges of the microtube can be functionalized for a controlled emission. Such a control might be useful for a large number of applications in the field of optoelectronics, like new directional light sources, which can efficiently couple e.g. into waveguides or other microcavities.

We gratefully acknowledge financial support of the Deutsche Forschungsgemeinschaft via the SFB 508 "Quantum Materials" and the Graduiertenkolleg 1286 "Functional Metal-Semiconductor Hybrid Systems".

References

[1] V.Y. Prinz, V.A. Seleznev, A.K. Gutakovsky, A.V. Chehovskiy, V.V. Preobrazhenskii, M.A. Putyato, T.A. Gavrilova, Physica E 6 (2000) 828.
[2] T. Kipp, H. Welsch, Ch. Strelow, C. Heyn, D. Heitmann, Phys. Rev. Lett. 96 (2006) 077403.
[3] Ch. Strelow, C.M. Schultz, H. Rehberg, H. Welsch, Ch. Heyn, D. Heitmann, T. Kipp, Phys. Rev. B 76 (2007) 045303.

4.3 Controlled Axial Light Confinement in Microtube Bottle Resonators

Publication 3 arose out of a close collaboration with the diploma students Christoph M. Schultz and Hagen Rehberg during the time of their diploma thesis. Principally, this publication is strongly motivated by Publication 1. But here, we prepared single well-defined kinks (in the following called lobes) in contrast to Publication 1 where the kinks appeared unintentionally. The microtubes were fabricated of wafer A and wafer B both containing quantum dots as internal emitters.

The findings in this work were the breakthrough for microtube resonators: The lobes modify the photoluminescence spectra of microtube resonators strongly. For frayed edges, as shown in Publication 1, sequences of single azimuthal modes at the positions of the unintentional kinks are observed. For homogeneous unstructured microtubes, as demonstrated in the first work on microtube resonators [Kip06], on the high energy side of each azimuthal mode additional modes with very small mode spacings appear and tend to an inhomogeneous broadening. Contrarily, in this work on microtubes with lobes in the rolling edge we observe groups of sharp and well-ordered modes for every azimuthal mode number. The modes within the groups are localized at the position of the lobe. With increasing energy the axial field distributions exhibit an increasing number of antinodes in axial direction. A controlled three-dimensional confinement is achieved. By this mechanism the mode volume is decreased drastically. As a consequence very recently lasing was observed by us (Publication 6 in this doctoral thesis) and also by another group [Li09] that used this mechanism. But this mechanism exceeds the possibility of controlled axial light confinement: The axial modes can even be tailored by the shape of the lobe which is shown experimentally and theoretically. This can be explained by a very intuitive and accurate model by a quasi-Schrödinger equation in which the circular geometry is introduced as a quasi-potential for each azimuthal mode. The quasi-potential can be calculated from the geometry of the lobe with a modified waveguide model, presented similarly in Publication 1. We observe a nearly perfect agreement between theory and measurements. The accuracy of the model, which is proven by many more experiments in this doctoral thesis, paired with the intuitive character of its solutions, makes the model to an inevitable tool to understand optical modes in microtube resonators.

The sample fabrication as well as the experiments were done by Christoph M. Schultz, Hagen Rehberg and me. The theory and the confinement mechanism was elaborated by me. The publication was written by Tobias Kipp and me.

Publication 3

Optical Microcavities Formed by Semiconductor Microtubes Using a Bottlelike Geometry

Ch. Strelow, H. Rehberg, C. M. Schultz, H. Welsch, Ch. Heyn, D. Heitmann, and T. Kipp

Physical Review Letters **101**, 127403 (2008)

PRL **101,** 127403 (2008) PHYSICAL REVIEW LETTERS week ending 19 SEPTEMBER 2008

Optical Microcavities Formed by Semiconductor Microtubes Using a Bottlelike Geometry

Ch. Strelow, H. Rehberg, C. M. Schultz, H. Welsch, Ch. Heyn, D. Heitmann, and T. Kipp*

Institut für Angewandte Physik und Zentrum für Mikrostrukturforschung, Universität Hamburg, Jungiusstraße 11, 20355 Hamburg, Germany

(Received 12 June 2008; published 19 September 2008)

We report on the realization of optical microtube resonators with a bottlelike geometry. The measured eigenenergies and the measured axial field distributions of the modes can be described by a straight and intuitive model using an adiabatic separation of the circulating and the axial propagation. The dispersion of the axial mode energies follows a photonic quasi-Schrödinger equation including a quasipotential which can be determined for the actual geometry of the microtube in a precise and simple way. We show that tailoring the geometry of the microtube bottle resonators enables the realization of a wide variety of mode distributions and dispersion relations.

DOI: 10.1103/PhysRevLett.101.127403 PACS numbers: 78.66.Fd, 42.55.Sa, 42.82.Fv, 78.20.Bh

Semiconductor microcavities can be used in the fields of photonics, opto-electronics and integrated optics, for example, as passive add-drop filters, as components for novel or superior light sources like low-threshold or thresholdless lasers and single-photon sources. They offer the fascinating possibility of cavity quantum electrodynamics experiments in solid-state systems [1,2]. For all these applications, a detailed understanding and the possibility of an exact tailoring of the optical modes in microcavities is desirable. In this work we report on the realization of microtube resonators with a bottlelike geometry. In spatially and spectrally resolved micro-photoluminescence (PL) measurements we demonstrate that the axial field distributions and eigenenergies of the modes can be precisely tailored by controlling the particular shape of the bottlelike geometry. The mode energies and field distributions can be described by an intuitive theoretical model using an adiabatic separation of the circulating and the axial mode propagation. For axial modes, this ansatz leads to a differential equation, similar to a Schrödinger equation, including a quasipotential which can be tailored experimentally by the detailed form and the dimensions of the bottlelike microtube. This quasi-Schrödinger equation can be solved numerically or, in the case of a parabolic potential, even analytically. We also performed finite-difference time-domain (FDTD) simulations of our bottle resonators, which confirm both our experimental results and the results of the adiabatic separation.

In a pioneering work Prinz *et al.* demonstrated the self-rolling mechanism of strained semiconductor bilayers lifted-off from the substrate [3]. Since then, a wealth of experiments has been performed, with the aim to utilize this mechanism, as recently reviewed in Ref. [4]. It was shown that a microtube fabricated by exploiting the self-rolling mechanism can act as an optical ring resonator [5–8]. Nevertheless, a controlled confinement of light in all three dimensions—particularly in the direction along the microtube axis—has not been reported yet. We reached this controlled confinement by a novel resonator design. Figure 1(a) sketches a microtube resonator with its typical multiwalled geometry and the two rolling edges. Because of the smooth layer interfaces and the high contrast in refractive index of semiconductor and air the light is guided efficiently in the tube wall undergoing multiple total internal reflections [as visualized in Fig. 1(a) by red arrows for the circular propagation]. The most important feature of our new microtube resonators is the structured rolling edge. Exemplarily, in Fig. 1(a) a parabolic lobe is sketched. This lobe turns the structure into a bottle resonator, as will be worked out in the following. Figure 1(b) shows a scanning-electron microscope (SEM) image of a microtube bridge which resulted from rolling-up an *U*-shaped strained mesa. The preparation process and the InAlGaAs-based layer system are similar as described in

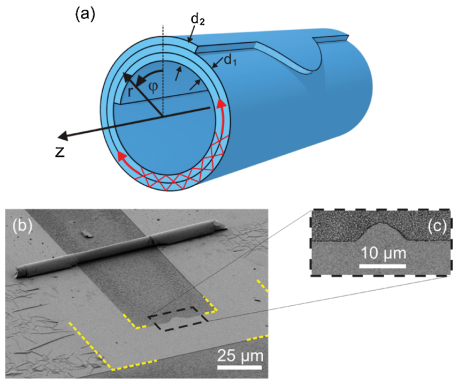

FIG. 1 (color). (a) Sketch of a microtube bottle resonator exhibiting a parabolic lobe on its outside rolling edge. Red arrows illustrate the circular light propagation by multiple total internal reflections. (b) SEM image of a microtube bottle resonator. Yellow lines clarify the edges of the *U*-shaped mesa. (c) Magnified top view on the region marked in (b).

PRL 101, 127403 (2008) PHYSICAL REVIEW LETTERS week ending 19 SEPTEMBER 2008

Refs. [5,6]. In the center part of the tube which is raised from the substrate, the outside edge forms a parabolic lobe which represents a locally increased winding number. The geometrical parameters like radius ($R = 2.6\ \mu$m), winding number ($N = 2.3$), wall thickness ($d_1 = 100$ nm, $d_2 = 150$ nm), the specific shape of the lobe [see Fig. 1(c)], and the distance of the center part of the tube to the substrate are precisely defined by the underlying semiconductor layers, as well as by the optical lithography and the wet etching techniques before rolling-up the U-shaped mesa.

The optical modes are probed by the PL light emitted from InAs quantum dots which are embedded in the tube walls. The sample is mounted in a low-temperature confocal micro-PL setup which images the microtube on the entrance slit of a grating spectrometer. Light from each position along the entrance slit is then dispersed onto a charge-coupled device detector while the spatial information along the slit is conserved. Thus, by aligning the microtube parallel to the entrance slit, we can investigate the near field spectrum with spatial resolution along the tube axis.

Figure 2(a) shows a spatially integrated spectrum from the central part of the microtube depicted in Fig. 1(b). The broad virtually continuous signal of the quantum dot ensemble is dominated by the optical eigenmodes of the microresonator: One observes about six groups of at least seven sharp spectral eigenmodes in each group. The groups resemble each other in their spectrally resolved structure. Within one group the peaks are almost equidistant in energy. Figure 2(b) shows the spatially resolved measurement of the microtube. In this depiction it becomes obvious that the groups are overlapping in their energies and each group consists of up to 11 peaks. Most interestingly, modes within a group are localized in special regions along the tube axis: there are nodes and antinodes in the axial intensity distribution and their numbers increase with increasing energy. This spatial mode distribution demonstrates that the modes are confined at the lobe position and form a system of higher axial harmonics. In principal, the observed sequence of the modes can be explained as follows: The thin wall of the microtube acts as a waveguide for the PL light. The ring structure of this waveguide leads to constructive interference of guided light if the phase of the electromagnetic field matches after one round trip. Thus, in a simple picture, an integer number m of wavelengths has to fit into the circumference. Neighboring groups of modes in Figs. 2(a) and 2(b) differ from each other by their azimuthal mode number m with $\Delta m = \pm 1$. The modes within each group arise from the axial confinement of light which is induced by the lobe. Thus one can regard the three-dimensionally confined modes as superpositions of ringlike modes in the circumference of the tube and back and forth reflected modes along the tube axis. In previous theoretical work on prolate-shaped dielectric resonators, similar modes have been named "bottle modes" in analogy to magnetic bottles in which charged particles can be trapped [9,10]. We adopt this term for our microtube resonators, even though the term "empty-bottle resonator" would be more precise, since we are dealing with hollow microtubes with thin walls.

The measured axial field distributions in Fig. 2(b) remind one of the probability density of a quantum mechanical particle in a parabolic potential. In the following we want to elucidate that the actual profile of the lobe can be translated into a photonic quasipotential which goes into a photonic quasi-Schrödinger equation. The solution of this equation then yields the experimentally observed axial field distributions.

As a first approximation, we assume that we are dealing with electric fields linearly polarized parallel to the tube axis (TE polarization). Indeed, this is what is observed experimentally [5–7] and in FDTD simulations [11].

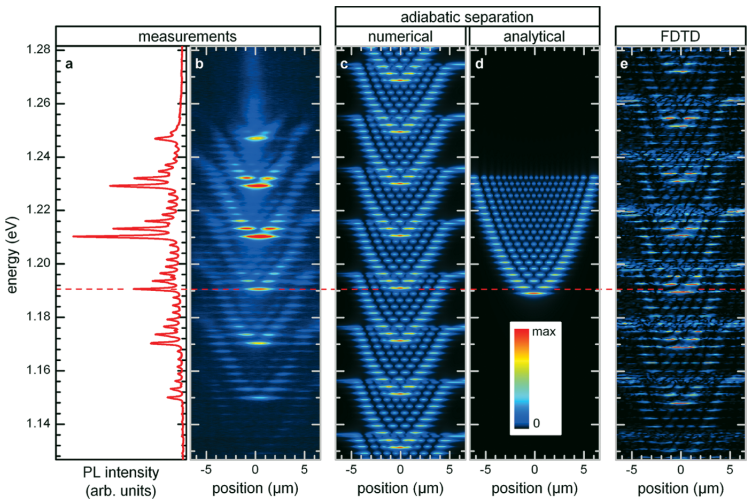

FIG. 2 (color). (a) Spatially integrated and (b) spatially resolved PL spectra of the microtube bottle resonator with a parabolic lobe. (c)–(d) Axial field distributions calculated within the adiabatic approximation. (c) Numerical solution for a finite potential obtained from SEM images of the microtube. (d) Analytical solution for an infinite parabolic potential for one group of axial modes. (e) FDTD simulation of the axial field distribution. Intensities in (b)–(e) are encoded in a color scale as depicted in the inset of (d). Horizontal axes in (b)–(e) give the relative position with respect to the extremum of the lobe. The dashed horizontal line at about 1.19 eV serves as a guide for the eye.

PRL **101,** 127403 (2008) PHYSICAL REVIEW LETTERS week ending 19 SEPTEMBER 2008

Maxwell's equations then result in the scalar wave equation for the z component $E_z(r, \varphi, z)$ of the electric field $-\frac{1}{n^2(r,\varphi,z)}\nabla^2 E_z(r, \varphi, z) = k^2 E_z(r, \varphi, z)$, with the absolute value of the wave vector in vacuum k, and the refractive index of the medium n. The cylindrical coordinates (r, φ, z) are defined in Fig. 1(a). We now apply the adiabatic approximation by writing the electric field as a product of two functions $E_z(r, \varphi, z) = \Phi(r, \varphi, z)\Psi(z)$, where $\Phi(r, \varphi, z)$ is the solution of the circulating propagation for a fixed parameter z and $\Psi(z)$ the solution of the axial propagation. With this ansatz we directly follow the procedure of the adiabatic (or Born-Oppenheimer) approximation given in quantum mechanics textbooks, e.g., in [12], except that we are dealing with a wave equation for electromagnetic fields instead of a Schrödinger equation for quantum mechanical particles. In our ansatz, for each position z along the tube axis, $\Phi(r, \varphi, z)$ has to satisfy the two-dimensional wave equation

$$-\frac{1}{n^2(r, \varphi, z)}\nabla^2_{r,\varphi}\Phi(r, \varphi, z) = k^2_{\mathrm{circ}}(z)\Phi(r, \varphi, z), \qquad (1)$$

where k_{circ} is the absolute value of the wave-vector component of the circular propagation in the r-φ plane. The solutions of Eq. (1) characterize the electromagnetic field in the r-φ plane for fixed values of the coordinate z. Then the axial propagation is described by

$$-\frac{1}{n^2}\frac{\partial^2}{\partial z^2}\Psi(z) + k^2_{\mathrm{circ}}(z)\Psi(z) = k^2\Psi(z). \qquad (2)$$

Since this equation is formally similar to the equation for particle waves, we call it photonic quasi-Schrödinger equation. In contrast to the original Schrödinger equation, in Eq. (2) the eigenenergies k occur squared. The quantity $k_{\mathrm{circ}}(z)$, which also occurs squared in Eq. (2) and which is defined by the solutions of Eq. (1), acts as a quasipotential $V_{\mathrm{eff}}(z)$ for the axial propagation.

In order to solve Eq. (1), we found a good approximation by regarding the thin microtube wall as two coupled planar waveguides with different thicknesses d_1 and d_2, [see Fig. 1(a)] and lengths L_1 and L_2, with $L_1 + L_2 = 2\pi R$. The ring-shaped cross section is taken into account by assuming periodic boundary conditions which ensures phase matching of the light after one round trip [6]. Within this approximation we find the very important result that k_{circ} depends linearly on the quantity $p = L_1/(L_1 + L_2)$ with a deviation from linearity of only 0.1%. By measuring the exact geometry of the lobe in SEM images, we are able to determine p and to calculate the quasipotential $V_{\mathrm{eff}}(z) = k_{\mathrm{circ}}(z)$. We then solve Eq. (2) by a spatial discretization followed by the diagonalization of the resulting algebraic equations. With this procedure arbitrarily shaped quasipotentials can be modeled. Furthermore also the dispersion of the refractive index of the material can be taken into account.

The numerically calculated mode energies and axial field distributions $[|\Psi(z)|^2]$ for the microtube shown in Fig. 1 are depicted in Fig. 2(c). The energy width is assumed to lead to quality factors of $Q = E/\Delta E = 2000$. For the calculations, we took into account the exact geometry of the tube measured from SEM images, including slight asymmetries in the lobe. We observe a very nice agreement with the experimental data in Fig. 2(b) for both, the spatial intensity distribution and the mode energies. The calculations yield groups of eigenmodes each belonging to a discrete solution of Eq. (1) with the eigenvalue $k^{(m)}_{\mathrm{circ}}(z)$, where m gives the azimuthal mode number. Within a group, the almost equidistant eigenmodes are discrete solutions of Eq. (2), for which a new axial mode number $h = 0, 1, 2, \ldots$ can be introduced. Interestingly, also the depth of the quasipotential in which bound solutions exist is reproduced very well. There is a small deviation in the absolute energy between the measured and calculated spectrum which results from slight uncertainties in the radius of the microtube and in the dispersion of the refractive index of the material.

One can estimate the validity of the adiabatic approximation following quantum mechanics textbooks like Ref. [12]. One finds that this adiabatic separation is a good approximation when the sufficient condition $\Delta k_z^2 \ll |(k^{(m)}_{\mathrm{circ}})^2 - (k^{(m+1)}_{\mathrm{circ}})^2|$ is satisfied, with $k_z = \sqrt{k^2 - k^2_{\mathrm{circ}}}$ and $\Delta k_z^2 = |(k_z^{(h)})^2 - (k_z^{(h+1)})^2|$. From experimental data we estimate $\Delta k_z^2/|(k^{(m)}_{\mathrm{circ}})^2 - (k^{(m+1)}_{\mathrm{circ}})^2| \approx 10^{-4}$ which justifies our assumption.

For comparison, we also performed three-dimensional FDTD simulations which take into account the details of the real structure including not only the rolling edges but also the curvature which we neglected in our model so far. Figure 2(e) shows the resulting spatially and spectrally resolved field intensities inside the microtube wall along the tube axis. These calculations agree very well with both the experiment and the above model and demonstrate that our approximations are warrantable. Note that the computing time for the FDTD calculations is more than two magnitudes larger than for the model using the adiabatic separation.

As elaborated above, a parabolic lobe of a microtube leads to a parabolic quasipotential which appears squared in the quasi-Schrödinger equation. Such a potential can generally be expressed as $V_{\mathrm{eff}}(z) = k_{\mathrm{circ}}(z) = az^2 + b$, with the curvature of the lobe a and the wave-vector offset $b = k^{(m)}_{\mathrm{circ}}(0)$ of the mth azimuthal mode. One can show that the fourth order term in $V^2_{\mathrm{eff}}(z)$ can be neglected for small z and typical values of a and b; thus, the squared potential is in good approximation parabolic in z. Then, Eq. (2) can be solved analytically. The eigenenergies read $k = (b^2 + (h + \frac{1}{2})\sqrt{8ab}/n)^{1/2}$ and a Taylor series yields in first approximation $k \approx b + (h + \frac{1}{2})\sqrt{2a/b}/n$. This consideration demonstrates that a squared parabolic potential leads to approximately equidistant axial modes for microtubes with parabolic lobes. Figure 2(d) depicts the first 20 analyti-

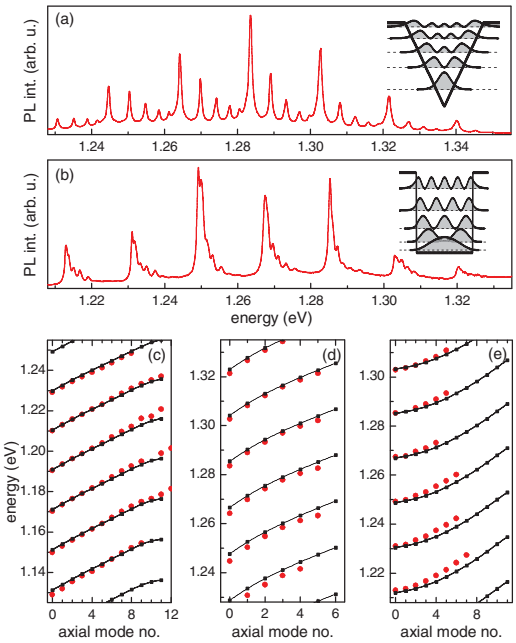

FIG. 3 (color). (a),(b) PL spectra of microtube bottle resonators with a (a) triangular and (b) rectangular lobe. The insets sketch the level spacings in a (a) triangular and (b) rectangular potential. (c)–(e) Axial mode dispersions for a (c) parabolic, (d) triangular, and (e) rectangular lobe. Measured (calculated) values are depicted as red circles (black squares). Connecting lines serve as guides for the eye.

cally obtained solutions of an infinite parabolic quasipotential. It is seen that at least the low-lying axial modes correspond to our measurements and to the numerically obtained solutions for the finite potential induced by the lobe.

The beauty of our microtube bottle resonators and their description within the adiabatic separation is that different field patterns and mode dispersions for a desired application can be precisely tailored. Exemplarily we prepared microtubes with triangular and rectangular lobes. Their PL spectra are presented in Figs. 3(a) and 3(b). Again, one observes groups of axial modes, but, unlike to the parabolic lobe, the axial mode spacings decrease with higher energies for the triangular lobe and increase for the rectangular one. This behavior is even more explicit in Figs. 3(c)–3(e) which depict the measured axial mode dispersions (red circles) for parabolic, triangular and rectangular lobes, respectively. The modes spacings are in direct accordance to the electronic counterparts of differently shaped potentials as sketched in the insets of Figs. 3(a) and 3(b). We also calculated the axial mode dispersions using the adiabatic separation described above, taking into account the exact geometry of the tubes from SEM images. Results are depicted as black squares in Figs. 3(c)–3(e). One can see the overall agreement of experiment and theory. These three types of lobes stand exemplarily for a manifoldness of lobes and mode dispersions: It is possible to tailor the mode dispersion of the axial modes accurately just by a predefined modulation of the rolling edge. One might, e.g., couple two or more lobes in order to fabricate photonic molecules or crystals [13,14].

Regarding possible applications [15,16], microtube bottle resonators are suitable for various opto-electronic devices. In particular, they can act as two port devices like optical filters: using the evanescent fields in the classical axial turning points one can couple light in and out by two waveguides [9,10]. The possibility of tailoring equidistant modes in microtube bottle resonators makes them to good candidates for applications in wavelength division multiplexing schemes or frequency comb generators in future [9,15,16].

In conclusion we have demonstrated experimentally and theoretically that the axial modes in microtubes can be controlled precisely by the preparation of specially shaped lobes in their rolling edge. These lobes turn the microtubes into bottle resonators. The mode energies and axial field distributions can be calculated by an adiabatic separation of the circulating and axial propagation. Both experimental and theoretical results are in good agreement with FDTD simulations that take into account the exact tube geometry.

We thank U. Merkt for stimulating discussions, K. Dietrich for help preparing the figures, and A. Stemmann for her contribution to the MBE growth. We acknowledge financial support by the Deutsche Forschungsgemeinschaft via SFB 508 and Graduiertenkolleg 1286.

*tkipp@physnet.uni-hamburg.de

[1] K. J. Vahala, Nature (London) **424**, 839 (2003).
[2] G. Khitrova *et al.*, Nature Phys. **2**, 81 (2006).
[3] V. Y. Prinz *et al.*, Physica (Amsterdam) **E6**, 828 (2000).
[4] A. Cho, Science **313**, 164 (2006).
[5] T. Kipp *et al.*, Phys. Rev. Lett. **96**, 077403 (2006).
[6] Ch. Strelow *et al.*, Phys. Rev. B **76**, 045303 (2007).
[7] R. Songmuang *et al.*, Appl. Phys. Lett. **90**, 091905 (2007).
[8] S. Mendach *et al.*, Phys. Rev. B **78**, 035317 (2008).
[9] M. Sumetsky, Opt. Lett. **29**, 8 (2004).
[10] Y. Louyer, D. Meschede, and A. Rauschenbeutel, Phys. Rev. A **72**, 031801(R) (2005).
[11] M. Hosoda and T. Shigaki, Appl. Phys. Lett. **90**, 181107 (2007).
[12] A. S. Davydov, *Quantum Mechanics* (Pergamon Press, Oxford, 1995).
[13] M. Bayer *et al.*, Phys. Rev. Lett. **81**, 2582 (1998).
[14] M. Bayer *et al.*, Phys. Rev. Lett. **83**, 5374 (1999).
[15] A. Matsko and V. Ilchenko, IEEE J. Sel. Top. Quantum Electron. **12**, 3 (2006).
[16] V. Ilchenko and A. Matsko, IEEE J. Sel. Top. Quantum Electron. **12**, 15 (2006).

4.3.1 Axial light confinement and mode splitting by broken rotational symmetry

Manuscript 4, which will be submitted to Physical Review B, summarizes the most important findings on three-dimensional light confinement in microtube bottle resonators, starting from their development in the framework of Publication 3 and ending with experiments performed at the end of my doctoral thesis. The aim of this work is to give a detailed derivation of our theoretical model for three-dimensionally confined modes in microtube resonators presented in Publication 3 as well as a complete description of our data analysis that was both not possible due to space limitation in Publication 3. In addition we show experiments on further microtubes with lobes as axial light confinement and present a novel type of axial confinement mechanism. The microtubes containing quantum dots were fabricated of wafer A and wafer B and the microtubes containing quantum wells of wafer E.

The axial light confinement is very important for microtubes since, on the one hand, for fundamental studies of the resonator modes single modes must be studied and, on the other hand, reduced mode volumes and a low number of modes in a spectral range are desired for the observation of quantum electrodynamical effects as well as for efficient laser applications. By microtubes with different lobes we prove experimentally the impact on the number and the energy spacing of the axial modes. We demonstrate that by a very small lobe only one axial mode for each azimuthal mode can be confined. To further improve our microresonators we also searched for further possibilities to confine light in axial direction. We developed a new axial light confinement mechanism that might lead to a stronger light confinement and perhaps to higher quality factors. Motivated by our model we prepared microtubes with etched rings in the microtube wall between which light is confined like in a ridge waveguide. For this axial light confinement we observe for the first time a well pronounced splitting due to the broken rotational symmetry. By analyzing the splitting in FDTD simulations we find that not only the amount of the splitting but also the quality factors oscillate systematically in dependence on the winding number. The findings demonstrate that the fundamental property of the mode splitting can be used to improve the quality factors. Furthermore they explain the absence in microtubes with lobes.

The fabrication of microtubes with lobes was done by Christoph M. Schultz, Hagen Rehberg and me as well as the experiments. The microtubes with etched rings were fabricated by Michael Sauer. For these microtubes the experiments were performed by Michael Sauer and me. The calculations and FDTD simulations were done by me. The manuscript was written by me.

Manuscript 4

Light Confinement and Mode Splitting in Rolled-Up Semiconductor Microtube Bottle Resonators

Ch. Strelow, C. M. Schultz, H. Rehberg, M. Sauer,
H. Welsch, A. Stemmann, Ch. Heyn,
D. Heitmann, and T. Kipp

to be submitted to Physical Review B (2010)

Light Confinement and Mode Splitting in Rolled-Up Semiconductor Microtube Bottle Resonators

Ch. Strelow,* C. M. Schultz, H. Rehberg, M. Sauer, H. Welsch,
A. Stemmann, Ch. Heyn, D. Heitmann, and T. Kipp
Institut für Angewandte Physik und Zentrum für Mikrostrukturforschung,
Universität Hamburg, Jungiusstraße 11, 20355 Hamburg, Germany

(Dated: November 24, 2009)

Abstract

We report on the controlled light confinement in microtube bottle resonators formed by rolled-up strained semiconductor bilayers. We experimentally and theoretically discuss two important properties of these novel kind of microcavities: the axial light confinement and the mode splitting by broken rotational symmetry. We give a detailed theoretical description of the three-dimensionally confined eigenmodes in microtube bottle resonators. By adiabatically separating circular and axial mode propagation we obtain a quasi-Schrödinger equation for the axial propagation whose solutions describe the energies and axial field distributions of all eigenmodes of the microtube in an intuitive and accurate way. The circular properties of the eigenmodes that depend on the specific geometry along the tube axis are introduced as quasi-potential determined by a simple waveguide model. We experimentally investigated two different axial confinement mechanisms: The first mechanism bases on lobes in the rolling edge. In measurements on differently shaped lobes and in comparison to results from our model we show by that the mode energies and axial field distributions can be tailored by the shape of the lobe. We observe a very good quantitative agreement between experiment and theory. The second mechanism is based on two rings etched into the microtube wall. For the axially confined modes in these microtubes we observe only a qualitative agreement between measurement and theory. The modes confined between the rings exhibit a well pronounced splitting by broken rotational symmetry in contrast to the modes in microtubes with lobes. The splitting is discussed in the framework of two-dimensional finite-difference time-domain simulations and the waveguide model. We find an oscillating behavior of the splitting on the winding number for the mode energies, as well as for the quality factors. We demonstrate by comparing the two different axial confinement mechanisms that the axial confinement and the splitting are connected to each other.

I. INTRODUCTION

Since the demonstration of fabricating three-dimensional nano and micro objects by the self-rolling mechanism[1,2]of strained bilayers and later the realization of optical ring resonators by rolled-up microtubes[3] a couple of experiments have been performed to use these structures as optical components. By integrating internal emitters in the microtube walls the emission of optical modes was reported ranging from the near infra red to the visible regime. In (Al)InGaAs/(Al)GaAs-based microtubes emission in the near-infrared regime at cryogenic temperatures was demonstrated by either integrating In(Ga)As quantum dots[3–7] or quantum wells of InGaAs[8] or GaAs[9] inside the tube wall. For microtubes with InGaAs quantum dots also room temperature emission was shown[10]. In Si(O)/SiO_x-based microtubes room-temperature emission in the visible spectral range was reported[11–14]. Here, the internal emitters are Si-Clusters formed in the SiO_x layers during annealing. The self-rolling mechanism has the intrinsic advantage to fabricate three-dimensional structures by well-established two-dimensional lithography on epitaxially grown samples: While the radius and the wall thickness of rolled-up microtubes are adjusted by the thicknesses and compositions of the bilayers during the growth, the winding number can be set by the lithography. It was shown that the mode energies can be precisely tuned by the winding number[8,13]. The fabricated structures have unique properties, like very thin layers with epitaxial smooth surfaces. Due to their strong evanescent fields microtube resonators can be used as refractive index sensors for fluids filled into the microtube[12] and they are highly tunable after fabrication by atomic layer deposition[14]. The thin walls allow us also to easily apply mechanical stress on the microtube and to reversibly tune the emission of single quantum dots into and out of resonance with the microtube modes[4]. In microtubes the emitters are intrinsically positioned close to the antinode of the electric field. Thus, as shown very recently, microtube resonators can also act as microlasers[9,15]. On the one hand due to the epitaxially smooth surfaces these structures have low surface scattering rates. On the other hand the broken rotational symmetry, which arises from the rolling edges, can act conveniently as a strongly directive output coupler[16,17].

For all these experiments a full control of the optical eigenmodes of the microtube is desirable and even necessary, if one wants to observe single and sharp as well as spatially and energetically well-localized modes. In microtubes two features are important in this

context: (i) The axial light confinement and (ii) the mode-splitting due to broken rotational symmetry. In this work we will discuss both features.

Concerning (i) the axial confinement: In general, in cylindrical micro cavities the axial light confinement plays the major role on inhomogeneous broadening of the modes. The strong light confinement in azimuthal and radial direction leads to the formation of ring modes with large energy spacings. They mainly propagate around the circumference of the microtube[3,18,19]. Therefore small inhomogeneities along the microtube axis are sufficient to spatially pin the modes around these inhomogeneities and thus lead to a weak axial confinement. We observed this already in our first experiments on nominally axially unstructured microtubes[3]: On the high energy side of every mode additional modes with very small energy spacings appeared whose energy spacings corresponded to the axial confinement lengths measured in spatially resolved photoluminescence measurements. However, the inhomogeneities and the confinement mechanism were unknown. Typically, for long axial confinement lengths and, thus, small axial mode energy spacings the features on the high energy side tend to smear out and lead to an inhomogeneous and asymmetrical broadening of the modes[3,10–14,18]. The situation changes when the inhomogeneities become more pronounced: In Ref. 8 we showed that kinks in the rolling edge accidentally occurred during the fabrication process lead to a spatially pinning of single modes at the kinks and to considerably large energy shifting along the microtube axis. By a detailed analysis of the special geometry of the inhomogeneities (the kinks) and calculations we found that the apparently chaotic behavior of the modes can be understood in a systematic way. In the present work we report on controlled light confinement in microtube resonators in all three dimensions as demonstrated recently in our previous work[5]. There we showed that special structurings along the microtube axis leads to a predefined formation of the optical eigenmodes, especially along the axis of the microtube. Here, we present the axial confinement demonstrated in Ref. 5 in a more detailed way. In addition we present further measurements and a second axial confinement mechanism.

Concerning (ii) the mode splitting by broken rotational symmetry: Up to now this intrinsical feature of modes in rolled-up microtubes has been shown in two-dimensional finite-difference time-domain (FDTD) simulations[16] but only one group reported on the experimental observation[6,10]. Obviously, in the structures considered up to now this splitting rarely happens or is quite small. In this work we present that a special axial structuring

allows us to observe a clear and well pronounced splitting. We discuss the splitting in the framework of two-dimensional FDTD simulations and with a waveguide model. Further on we will report on the impact of the three-dimensional confinement on the splitting.

This report will be structured as follows: We will start with the description of our sample structures as well as of our experiment in the first section. We will briefly explain a typical spectrum of three-dimensionally confined modes in microtube bottle resonators according findings in our previous work[5]. In the second section we will elaborate the theoretical description of three-dimensionally confined modes in microtubes, presented in Ref. 5, but here in much more detail. The third section deals with experimental results on the axial confinement and we discuss them in the framework of our theoretical description. First, we give a much deeper and more extensive analysis on our data on light confinement by lobes in the rolling edge in Ref. 5, which was not possible for space limitation there. Then, we show further experimental data using the same confinement mechanism. Finally, we introduce a different axial confinement mechanism, that allows us the observation of the pronounced splitting by broken rotational symmetry. The splitting will be discussed separately in the last section.

II. EXPERIMENT AND SAMPLE STRUCTURE

Our strained layer systems used for the fabrication by the self-rolling mechanism are grown by molecular beam epitaxy (MBE). For the microtubes investigated in this work we used two different layer systems with either InGaAs quantum dots or with InGaAs quantum wells as internal emitters. All layer systems were grown on top of a GaAs substrate and a 40 nm AlAs sacrificial layer. The bilayers for the samples containing dots consist of either 20 nm $In_{0.2}Ga_{0.8}As$ (sample A) or 20 nm $In_{0.2}Al_{0.24}Ga_{0.56}As$ (sample B), followed by 30 nm GaAs with one layer InGaAs quantum dots in its center part. The strained layer system of the quantum well sample (sample C) consists of 14 nm $In_{0.16}Al_{0.20}Ga_{0.64}As$, a 4 nm $In_{0.21}Ga_{79}As$ quantum well and 41 nm $Al_{0.24}Ga_{0.76}As$. In the further processing we prepared U-shaped mesas by optical lithography and wet-etching techniques that form self-supporting microtube bridges after rolling-up. Details of the fabrication process are given in Refs. 3 and 8. Figure 1(a) depicts a scanning electron micrograph of a microtube and its U-shaped mesa. Due to additional windings formed by the left and right part of the mesa and a

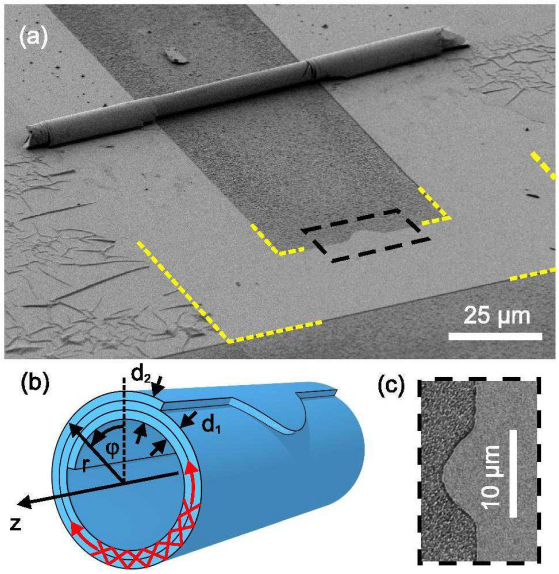

FIG. 1: (a) Scanning electron micrograph of a microtube and its U-shaped mesa, marked by dashed yellow lines. (b) Unscaled sketch of the free-standing part of the microtube. (c) Enlarged view of the parabolic lobe in the dashed black square in (a).

depression between them the center part of the microtube is free-standing. This part that forms the actual resonator is sketched in Fig. 1(b). Due to the large refractive index contrast of air and semiconductor multiple internal reflections give rise to wave guiding inside the microtube wall. After a round trip constructive interference leads to the formation of ring-like eigenmodes that are classified by their azimuthal mode number m that is half the number of antinodes around the circumference. As reported in Ref. 5 we prepared a U-shaped mesa with a well-defined lobe, as shown enlarged in Fig. 1(c). This results in a region of locally increased winding numbers after rolling-up [see Fig. 1(b)] and the special geometry leads to a well-controlled confinement of the eigenmodes along the axis of the microtube.

Our experiments are performed by micro photoluminescence (PL) spectroscopy at low temperatures (T=7K). For excitation a Ti:Sa laser at 800 nm is focussed by a microscope objective (50×, NA=0.5) onto the sample that is mounted in an optical continuous flow cryostat. Electron-hole pairs are generated inside the semiconductor wall forming the microtube and quickly relax into quantum dots or quantum wells that are embedded into the microtube wall as internal light source. The emitted PL light is collected by the same microscope

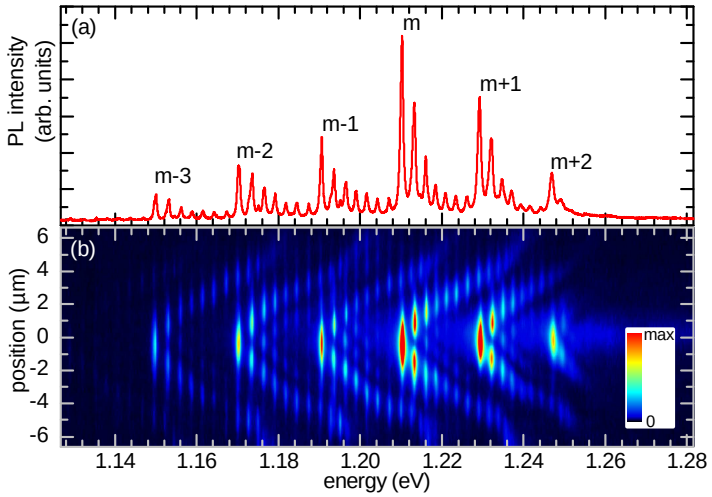

FIG. 2: (a) Spatially integrated PL spectrum of the microtube in Fig. 1(a). (b) Spatially and energetically resolved PL image of (a).

objective, dispersed by a 1 m spectrometer with 1200 lines/mm grating and detected by a cooled charge coupled device (CCD) detector. We mounted the microtube in the cryostat in that way that the tube axis is imaged on the focal plane containing the entrance slit of the spectrometer with the tube axis parallel to the slit. Thus, by the grating the CCD camera image is resolved energetically in horizontal direction whereas in vertical direction the spatial resolution along the microtube axis is kept. Figure 2 (a) depicts the spatially integrated PL spectrum of the microtube in Fig. 1 excited at the position of the lobe. Instead of the broad spectrum of the quantum dot ensemble we observe the regular sequences of sharp optical modes that are typical for microtubes with controlled axial confinement[5]. The modes are arranged in groups. All modes in one group are classified by the same azimuthal mode number m, i.e. the number of wavelengths that fit into the circumference of the microtube. Within the groups the modes differ in their axial confinement. In the spatially resolved measurements in Fig. 2(b) one clearly observes a localization of the modes around the center position of the lobe. With increasing energy the modes in each group exhibit an increasing number of axial antinodes. In this view one observes even more modes within each group whose energies exceed the energy of next higher azimuthal modes. The study of these higher axial modes is the main focus of this work. We will consider the impact of the axial microtube geometry on them in experiments and by calculations. The axial field distributions

resemble the probability density of particle waves in a one-dimensional potential. Indeed, in our previous work we found that the eigenenergies and axial field distributions in every group can be described, in strong analogy to particlewaves, by a quasi-Schrödinger equation with a quasi-potential.[5]. In the next section we demonstrate that by adiabatically separating circular and axial mode propagation the circular propagation induces a quasi-potential for the axial propagation which can be directly determined from the microtube geometry. We will observe a very good agreement between our measurements and the solutions of the quasi-Schrödinger equation for the eigenergies as well as for the axial intensity distributions.

III. THEORETICAL DESCRIPTION

A. Adiabatic Approximation

For the theoretical description of the eigenmodes in microtube bottle resonators we start with the wave equation for the electric fields $\vec{E}(r,\varphi,z)$. Regarding the symmetry of a microtube we use cylindrical coordinates as defined in Fig. 1(b). The wave equation then reads $-\frac{1}{n^2(r,\varphi,z)}\nabla^2\vec{E}(r,\varphi,z) = k^2\vec{E}(r,\varphi,z)$, where k is the wave vector in vacuum and n the refractive index of the microtube material. We assume that the eigenmodes are purely TE-polarized defined as that the electric field vector is polarized along the microtube axis. Actually, this is found in many experiments on axially unstructured microtubes[3,8,11]. Exemplarily on a microtube with a parabolic lobe, we measured that the polarization is only slightly elliptic. Up to now there is only one report on the observation of TM-polarized modes[14]. The observed resonances in Ref. 14 were very weak and had low quality factors and it is not unambiguously clear if not an elliptic polarization of higher axial modes was measured. Since the electric field is not continuous at the interface between microtube and air, TM-polarized modes are very surface-sensitive and especially the rolling edges lead to enhanced scattering losses[16]. For these reasons and for simplicity in this work we regard only TE-polarized eigenmodes. In this case we can solve the Helmholtz equation for the z component $E_z(r,\varphi,z)$ of the electric field:

$$-\frac{1}{n^2(r,\varphi,z)}\nabla^2 E_z(r,\varphi,z) = k^2 E_z(r,\varphi,z). \tag{1}$$

Due to the strong confinement in radial direction and the circular nature of the eigenmodes[3] the main dynamics take part in the $r-\varphi$ plain. Thus we can make an adiabatic (or

Born-Oppenheimer) approximation and separate the circular and the axial propagation. The electric field can be written as a product of two functions $E_z(r,\varphi,z) = \Phi(r,\varphi,z)\Psi(z)$, where $\Phi(r,\varphi,z)$ is the solution for the circular field distribution and $\Psi(z)$ for the axial field distribution. Applying the adiabatic approximation, equation (1) separates into one equation for the circular propagation in the $r-\varphi$ plane and one for the axial propagation. The fields in the $r-\varphi$ plane $\Phi(r,\varphi,z)$ have to satisfy the two-dimensional wave equation for each position z along the axis of the tube:

$$-\frac{1}{n^2(r,\varphi,z)}\nabla^2_{r,\varphi}\Phi(r,\varphi,z) = k^2_{\mathrm{circ}}(z)\Phi(r,\varphi,z). \tag{2}$$

Here, $k_{\mathrm{circ}}(z)$ is the absolute value of the wave vector in the $r-\varphi$ plane at a fixed position z along the tube axis. The function $k_{\mathrm{circ}}(z)$ couples the dynamics of the circular and the axial propagation and goes into the equation for the axial propagation as follows:

$$-\frac{1}{n^2}\frac{\partial^2}{\partial z^2}\Psi(z) + k^2_{\mathrm{circ}}(z)\Psi(z) = k^2\Psi(z). \tag{3}$$

This equation formally looks like a Schrödinger equation for a particle wave in a one-dimensional potential. Thus, we call this equation photonic quasi-Schrödinger equation. By the quantity $k_{\mathrm{circ}}(z)$ the dynamics in the $r-\varphi$ plane induce a quasi-potential $V_{\mathrm{eff}}(z)$ for the axial propagation. In contrast to the original Schrödinger equation the quasi-potential $V_{\mathrm{eff}}(z) = k_{\mathrm{circ}}(z)$ and the eigenenergies k occur squared in equation (3). However, we will show later that the solutions of the quasi-Schrödinger equation correspond to the solutions of the original Schrödinger equation for a particle in a one-dimensional potential. This means that for example a parabolic quasi-potential inserted into the quasi-Schrödinger equation leads to an equidistant mode spacing. But first we have to consider the two-dimensional problem in the $r-\varphi$ plane and solve equation (2) for the circular propagation. We will show by comparing the exact solutions of Maxwell's equations for an ideal ring to solutions of a waveguide guide model that the curvature of the microtubes can be neglected. This allows us to perform all calculations within an expanded waveguide model that can even take into account the rolled-up geometry of real microtubes.

B. Exact solution of Maxwell's equation for a dielectric ring

If one neglects the rolling edges of rolled-up microtubes, the $r-\varphi$ plane can be described as a dielectric ring with rotational symmetry, as sketched in Fig. 3(a). The refractive index

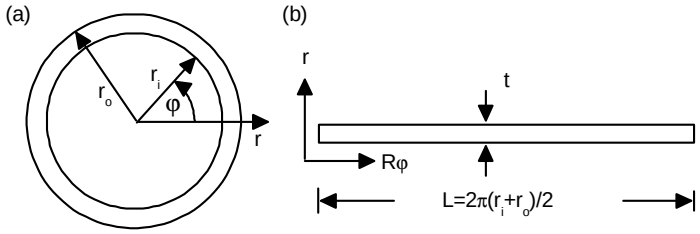

FIG. 3: (a) Cylindrical coordinates for a dielectric ring. (b) Dielectric ring described as a planar waveguide in cartesian coordinates.

jumps at the inner radius r_i from 1 inside the tube to n inside the tube wall and at the outer radius r_o again to 1 outside the tube. The solutions of equation (2) in each one of these three regions are superpositions of the functions $J_m(nk_\mathrm{circ}r)e^{im\varphi}$ and $N_m(nk_\mathrm{circ}r)e^{im\varphi}$ where $J_m(nk_\mathrm{circ}r)$ is the Bessel function and $N_m(nk_\mathrm{circ}r)$ the von Neumann function. Further on it is useful to define the functions $H^1_m(nk_\mathrm{circ}r) = J_m(nk_\mathrm{circ}r) + iN_m(nk_\mathrm{circ}r)$ and $H^2_m(nk_\mathrm{circ}r) = J_m(nkr) - iN_m(nkr)$ that present radially outgoing and radially incoming waves, respectively. Due to the absence of charges inside the microtube the solutions there have to be Bessel functions since the von Neumann function diverges in the origin. Furthermore we assume that the eigenfuctions outside the tube are only outgoing waves. Thus, the field distributions of the eingenmodes in a dielectric ring read:

$$\begin{aligned} A_m\, J_m(k_\mathrm{circ}r) &\qquad \text{inside}(r < r_i) \\ B_m\, H^1_m(nk_\mathrm{circ}r) + C_m\, H^2_m(nk_\mathrm{circ}r) &\qquad \text{wall}(r_i < r < r_o) \\ D_m\, H^1_m(k_\mathrm{circ}r) &\qquad \text{outside}(r_o < r). \end{aligned}$$

The coefficients A_m, B_m, C_m and D_m have to be chosen in a way that certain boundary condition are fulfilled: For TE-polarized light, as defined in this work, the electric field and its derivative have to be continuous, reflecting that the tangential component of the electric and the normal component of the magnetic field at the boundaries are continuous. One obtains a system of equations which only have a non-trivial solution if the system determinant vanishes, i. e.

$$\begin{vmatrix} J_m(k_{\mathrm{circ}}r_i) & -H_m^1(nk_{\mathrm{circ}}r_i) & -H_m^2(nk_{\mathrm{circ}}r_i) & 0 \\ \frac{\partial}{\partial r}J_m(k_{\mathrm{circ}}r_i) & -\frac{\partial}{\partial r}H_m^1(nk_{\mathrm{circ}}r_i) & -\frac{\partial}{\partial r}H_m^2(nk_{\mathrm{circ}}r_i) & 0 \\ 0 & H_m^1(nk_{\mathrm{circ}}r_o) & H_m^2(nk_{\mathrm{circ}}r_o) & -H_m^1(k_{\mathrm{circ}}r_o) \\ 0 & \frac{\partial}{\partial r}H_m^1(nk_{\mathrm{circ}}r_o) & \frac{\partial}{\partial r}H_m^2(nk_{\mathrm{circ}}r_o) & -\frac{\partial}{\partial r}H_m^1(k_{\mathrm{circ}}r_o) \end{vmatrix} = 0. \qquad (4)$$

The solutions of equation (4) are complex k vectors. The real parts describe the energy of the eigenmode and the imaginary parts the losses. Due to the curvature of the ring light can tunnel out of the ring.

But for typical ring geometries investigated in this work these losses lead to quality factors between 10^{11} for small radii and 10^{19} for larger radii. Compared to the experimental quality factors of up to about 3500 these losses can be neglected with respect to other losses. The field distributions are ring modes with $2m$ antinodes around the circumference of the ring. Due to the very thin wall thickness of typical microtubes we observe only modes with one antinode in radial direction. The field is localized inside the wall and decays nearly exponentially inside and outside the tube. Later, we will show solutions of equation (4) in different dielectric rings. But first we want to introduce the second way to calculate the eigenmodes in microtubes by describing it as a rolled-up waveguide. In that case naturally the curvature of the ring is not taken into account.

C. Dielectric rings described as a rolled-up waveguide

If one regards a slab waveguide of the length $L = 2\pi(r_\mathrm{i}+r_\mathrm{o})/2$ and put both ends together, it becomes obvious that a microtube can also be described by a waveguide, as shown in Fig. 3(b). In waveguides the eigenmodes propagate in direction of the waveguide with wavefronts of constant phase velocity. Consequently, the propagation along the waveguide can be treated by a plane wave $e^{i\omega\tau - i\beta\varphi}$. It is convenient to describe this propagation by an effective refractive index n_{eff} and the absolute value of the wave vector k_{circ} in the $r-\varphi$ plane. The propagation can then be described by $\beta = n_{\mathrm{eff}}(k_{\mathrm{circ}}, t)k_{\mathrm{circ}}$. The effective refractive index naturally fulfills the boundary conditions for the electric field at the interface between waveguide and air and depends on the energy and the thickness t of the waveguide. The phases of the eigenmodes of a microtube have to match after a roundtrip. Consequently, an integer number m of wavelengths, here defined as wavelength $\lambda_{\mathrm{circ}} = 2\pi/k_{\mathrm{circ}}$ in the $r-\varphi$

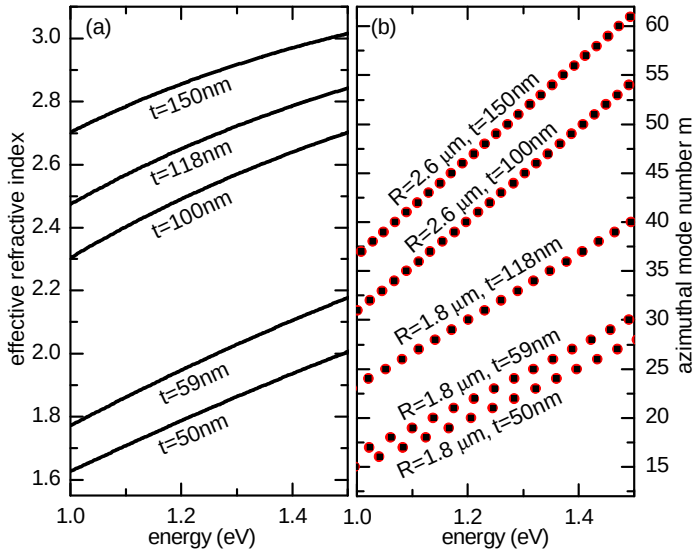

FIG. 4: (a) Dispersion of the effective refractive index for TE-polarized modes for typical wall thicknesses t of our microtube samples. (b) Mode energies for typical inner radii R and wall thicknesses t calculated in waveguide approximation (black squares) and exact as dielectric ring (red circles).

plane, has to fit into the optical ray path along the circumference:

$$2\pi \frac{r_\mathrm{i} + r_\mathrm{o}}{2} n_\mathrm{eff}(\lambda_\mathrm{circ}, t) = m\, \lambda_\mathrm{circ}. \tag{5}$$

The effective refractive index can be calculated by solving Maxwell's equation for a waveguide as known from textbooks like Ref.20 and substituting the propagation constant β by the refractive index and the wavevector k_circ in the $r - \varphi$ plane. For TE-polarized modes one can determine $n_\mathrm{eff}(\omega_\mathrm{circ}, t)$ as numerical solutions of

$$\sqrt{n_\mathrm{eff}^2 - 1} = \sqrt{n^2 - n_\mathrm{eff}^2}\, \tan\left(\frac{t\omega_\mathrm{circ}}{2c}\sqrt{n^2 - n_\mathrm{eff}^2}\right). \tag{6}$$

Due to the numerical determination of n_eff of course a dispersion of n can be taken into account. Note that equation (6) describes only radially symmetric solutions with respect to the waveguide center. In this work we consider only symmetric modes with one antinode in radial direction since these are the modes we observe in our experiments. In Fig. 4(a) we show energy dependencies of the effective refractive index for TE-polarized modes in the typical energy range of our experiments and different typical wall thicknesses. For simplicity

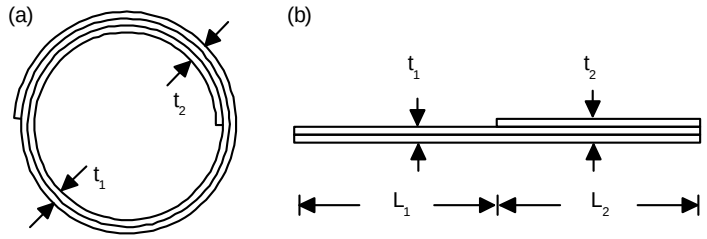

FIG. 5: (a) Unscaled sketch of a microtube in its real rolled-up geometry. (b) Description of a microtube as two coupled waveguide with different thicknesses.

we assumed in Fig. 4 no dispersion but a constant refractive index of n=3.5 for the material and typical waveguide thicknesses of our fabricated samples. Using this dispersions and equation (5) we calculated the mode energies in the waveguide approximation. The results are shown in Fig. 4(b) as black squares. In addition we numerically calculated the exact mode energies for a dielectric ring using the same geometries and equation (4). The results are shown as red circles in Fig. 4(b). We observe a nearly perfect agreement between the two models. Obviously, the curvature can be neglected for the geometries and energies used in this work. For very small wall thicknesses compared to the wavelength the waveguide model breaks down due to long ranging evanescent fields into the surrounding of the microtube and inside the tube. Here, the fields of opposite parts of the ring influence each other. For large thicknesses the model also breaks down. Here, the geometry resembles more and more a microdisk and due to missing reflections at the inner wall the field distribution becomes asymmetric.

Due to this strong validity of the waveguide approach we performed in the following all calculations by solving the much more simple combination of equation (6) and (5). Within this approach the rolled-up geometry including the inner and outer edge of microtubes can be taken into account as will be shown in the following. Figure 5(a) sketches the cross section of a real microtube in rolled-up geometry. Usually microtubes exhibit winding numbers between integer values. In these cases it consists of two waveguides of different thicknesses t_1 and t_2 and lengths L_1 and L_2, respectively. In each of the two waveguides the light propagation along the waveguide can be described by the effective refractive index $n_{\text{eff}}(\lambda_{\text{circ}}, t_1)$ and $n_{\text{eff}}(\lambda_{\text{circ}}, t_2)$, respectively. Following the procedure for microtubes described by a single waveguide we introduce again periodic boundary conditions to require phase matching of

the eigenmodes after a roundtrip. Analogously, an integer number of wavelengths has to fit into the optical ray path length, here, formed by two waveguides:

$$n_{\text{eff}}(\lambda_{\text{circ}}, t_1)L_2 + n_{\text{eff}}(\lambda_{\text{circ}}, t_2)L_2 = m\,\lambda_{\text{circ}}. \tag{7}$$

This equation can be solved analytically if one approximates the effective refractive indices in the regions with the different thicknesses t_1 and t_2 by a quadratic fit $n_{\text{eff}}(\lambda_{\text{circ}}, t_1) = a_1\lambda_{\text{circ}}^2 + b_1\lambda_{\text{circ}} + c_1$ and $n_{\text{eff}}(\lambda_{\text{circ}}, t_2) = a_2\lambda_{\text{circ}}^2 + b_2\lambda_{\text{circ}} + c_2$, respectively. Regarding the energy dependency of n_{eff} in Fig. 4(a) it becomes obvious that a quadratic fit reproduces the energy dependency of n_{eff} very accurately. For small energy ranges even a linear fit is sufficient. Applying the quadratic fit the solutions of equation (7) read:

$$\lambda_{\text{circ}}^m = -\tfrac{u}{2} \pm \sqrt{\tfrac{u^2}{4} - v} \tag{8}$$
$$\text{with } u = \tfrac{L_1 b_1 + L_2 b_2 - m}{L_1 c_1 + L_2 c_2},\ v = \tfrac{L_1 a_1 + L_2 a_2}{L_1 c_1 + L_2 c_2}\ .$$

Equation (7) is the most important equation for the description of microtube modes. It allows us to precisely take into account all important geometrical features of a microtube: radius, wall thicknesses and winding number. Due to the adiabatic approach also the geometry in axial direction is taken into account by this equation: Their solutions for a varying geometry at every position z along the tube axis reflect the quasi-potential $V_{\text{eff}}(z)$ that fully determines the axial dynamics of the eigenmodes. In this context it is important to study how a varying microtube geometry, e.g., along the rolling axis, changes the energy of the propagation in the $r-\varphi$ plane. Figure 6 shows solutions of equation (7) for a changing winding number between 2 and 3. We assumed waveguide thicknesses of t_1=100 nm and t_2=150 nm, a constant refractive index of n =3.5 and an inner radius of r_i=2.6 µm. We observe a nearly perfect linear dependence on the winding number, as exemplarily proven for three modes by a linear approximation between winding number 2 and 3 (red lines). The largest deviations from linearity are only 0.16 % for m=37 and 0.05 % for m=53. This linearity is also observed for a linear dispersion of the refractive index n of the material often assumed in our experiments. The observed linearity is important for the description of three-dimensionally confined modes by lobes in the rolling edge as demonstrated in our previous work[5] and will be shown in detail in this work. Those lobes, as depicted in Fig. 1, are regions where the winding number varies in z direction. According to our calculations in Fig. 6 the shape of the quasi-potential $V_{\text{eff}}(z)$ directly reproduces the lobe shape, which is the axial energy dependence $k_{\text{circ}}(z)$ of the propagation in the $r-\varphi$ plane.

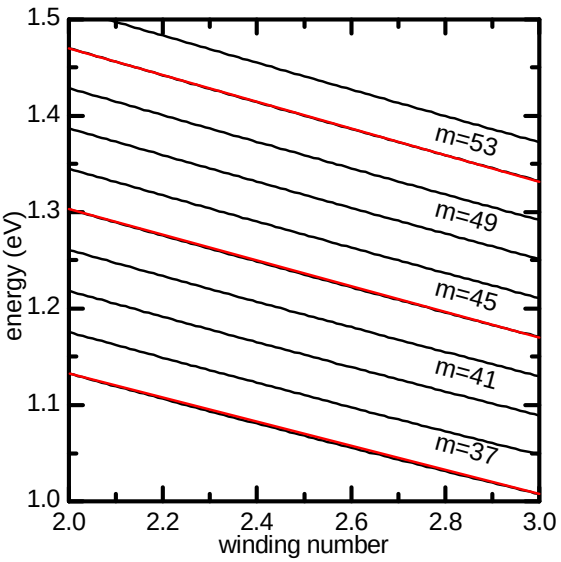

FIG. 6: Mode energy versus winding number. For clarity only modes with odd azimuthal mode number are shown. Exemplarily, the red lines represent a linear approximation between winding number 2 and 3 for three modes.

By solving the quasi-Schrödinger equation (3) for differently shaped quasi-potentials we will show later that the modes in axial direction indeed act like particle waves in a one-dimensional potential and can be calculated accurately within this approach.

D. Solutions of the quasi-Schrödinger equation

The solutions of equation (7) in waveguide approximation directly generate the quasi-potential $V_{\text{eff}}(z) = k^m_{\text{circ}}(z)$ for every azimuthal mode m. In principal, all variations of the tube geometry along the axis are taken into account in the quasi potential. Thus the complete three-dimensionally confined eigenmodes for every azimuthal mode m should be found as solutions of the quasi-Schrödinger equation (3). First we will show how one can get analytical solutions for parabolic lobes. Later we will describe how we can solve equation (3) for arbitrarily shaped quasi-potentials.

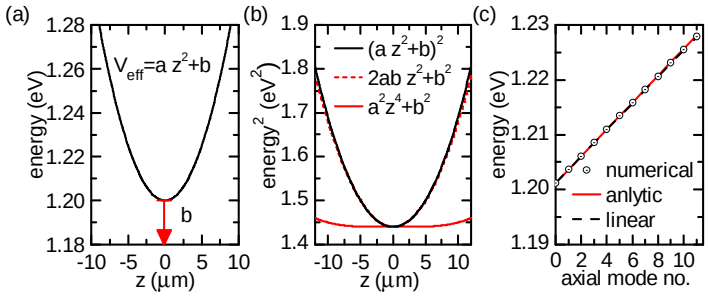

FIG. 7: (a) Parametrization of a parabolic quasi-potential. (b) Squared parabolic quasi-potential as is (black line), neglecting the fourth order term (red line) and only fourth order term and offset (red dots). (c) Mode energies calculated by numerical calculation (open circles), analytical calculation (red line) and linear approximation of the analytic solution (black dashed lines). The lines serve as a guide to the eye.

1. Analytical solution for a parabolic lobe

A parabolic lobe is defined as a rolling edge of a microtube that changes the winding number of the tube quadratically in a finite region along the tube axis. Due to the linear energy dependence of k_{circ} on the winding number the quasi-potential can be parameterized as

$$V^*_{\mathrm{eff}}(z) = \frac{\hbar c}{e} k_{\mathrm{circ}}(z) = az^2 + b, \tag{9}$$

where the offset b is the energy of the propagation in the $r-\varphi$ plane for z=0 and a is the curvature of the quasi-potential. To directly derive the solutions in eV all wave vectors are multiplied by the reduced Planck constant $\hbar$ and the velocity of light in vaccuum c and devided by the elementary charge e. The quasi-potential is sketched in Fig. 7(a). Since $k_{\mathrm{circ}}(z)$ occurs squared in equation (3) the quasi-potential appears as $V^{*2}_{\mathrm{eff}}(z) = a^2z^4 + 2abz^2 + c^2$. Hence, the problem can not be solved analytically as a harmonic oscillator. However, we can show that the fourth order terms can be neglected with high accuracy. Figure 7(b) depicts the squared quasi-potential as black lines in comparison to the quantity neglecting the fourth order term (dashed red line) as well as only the fourth order term and the offset (solid red line). We used a=1.2 eV and b=$10^{-3}eV/\mu m^2$ which are typical values of the curvature and the energy offset for our microtubes with a parabolic lobe. We find that neglecting the fourth order term does not change $V^{*2}_{\mathrm{eff}}(z)$ with an accuracy of better

than 99.9 % for $|z| < 12\mu$m which is larger than the typical size of parabolic lobes in axial direction. Consequently, we can write equation (3) for typical parabolic quasi-potentials as

$$-\frac{\hbar^2 c^2}{e^2 n^2}\frac{\partial^2}{\partial z^2}\Psi(z) + (ab\,z^2 + b^2)\Psi(z) = E^2\Psi(z), \tag{10}$$

which is the differential equation of the quantum mechanical harmonic oscillator. The eigenenergies read $E = (b^2 + (h+\frac{1}{2})\sqrt{8ab}\frac{\hbar c}{ne})^{\frac{1}{2}}$ and the eigenfunctions $\Psi_h(z) = \sqrt{\frac{1}{2^h h!}}\,(\frac{ne}{\hbar c}\frac{\sqrt{ab}}{\pi})^{\frac{1}{4}}\,e^{-\frac{en}{\hbar c}\frac{\sqrt{ab}}{2}z^2}\,H_h\left(\sqrt{\frac{en}{\hbar c}\sqrt{ab}}\,z\right)$, where $H_h(z)$ are the Hermite polynomials and $h = 0, 1, 2, \ldots$ the axial mode numbers. For typical values of a and b we find that the mode spacing is nearly equidistant, more accurately E^2 is equidistant: Since the right-hand side of the equation for the eigenenergies is small compared to b^2, a Taylor series yields in first approximation $E \approx b + \left(h+\frac{1}{2}\right)\sqrt{2a/b}\frac{\hbar c}{en}$ with an accuracy of about 99.9 % for the first 20 modes. Figure 7(c) shows mode energies for the parabolic quasi-potential in Fig. 7(a) calculated by equation (10) compared to the linear approximation by the Taylor series and to results from numerical calculations including the fourth order term. We observe a very good overall agreement. Parabolic lobes induce a parabolic quasi-potential for the mode propagation along the z axis and, indeed, the eigenenergies of the axially confined modes exhibit an equidistant mode spacing. This important result was not unambiguously expectable, since the quasi-potential and the eigenenergies occur squared in equation (3). Later we will show by further calculations and experiments that appropriate statements can be expanded on arbitrarily shaped lobes and quasi-potentials: The shape of lobes in the rolling edge of microtubes induces a quasi-potential of the same shape and the higher axial eigenmodes act like particle waves in a one-dimensional potential of corresponding shape.

2. Numerical solutions for arbitrarily shaped quasi-potentials

In general, microtubes can not be described by a parabolic quasi-potential. Even the finiteness of the quasi-potential can naturally not be described by a purely parabolic quasi-potential. Additionally, slight geometrical inhomogeneities in fabricated structures lead to a deviation from a planed parabolic shape. On the other hand the manifoldness of possible quasi-potential shapes including also slight deviation from the parabolic potential bear interesting new features. These cases should all be described or in the best case even be predicted by our theory. To take into account all cases of quasi-potentials we developed a

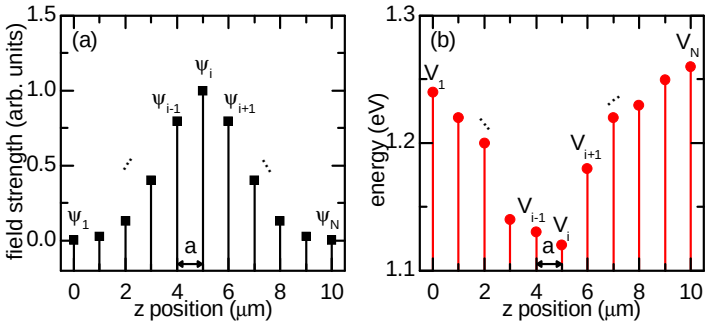

FIG. 8: Parametrization for a discrete description of the electric field (a) and the quasi potential (b).

method that can solve the quasi-Schrödinger equation on a discrete spatial grid for arbitrarily shaped quasi-potentials. Figure 8 sketches how the axial electric field distribution $\Psi(z)$ and the quasi-potential V_{eff} are described. The z space is projected on a grid of N grid points with the distance a. In each grid point i one value of the electric field Ψ_i and one value of the quasi-potential V_i is defined. Thus any field distribution is described by the vector $\vec{\Psi}$ formed by the N values Ψ_i at the grid points. In this description the operator of the quasi-potential $\hat{V}_{\text{eff}}$ is defined as $V_{ij}^{\text{eff}} = V_i^{\text{eff}}\,\delta_{ij}$. $\hat{V}_{\text{eff}}^2$ is a $N \times N$ diagonal matrix containing the squared values $(V_i^{\text{eff}})^2$ of the quasi-potential in the main diagonal. The derivative $\frac{\partial}{\partial z}$ has to be replaced by a differential quotient $\frac{\Delta\Psi_i}{a} := (\Psi_i - \Psi_{i-1})/a$. Analogously, for the second derivative follows:

$$\Delta^2\Psi_i/a^2 := \frac{\Psi_{i+1} - 2\Psi_i + \Psi_{i-1}}{a^2}. \tag{11}$$

In matrix notation the operator of the second derivative $\hat{D}$ reads $D_{ij} = -2\delta_{ij} + \delta_{ij+1} + \delta_{ij-1}$. $\hat{D}$ is an $N \times N$ matrix with 1 in the main diagonal, -2 in the secondary diagonal and 0 elsewhere. To calculate the eigenenergies and eigenfunctions in this description one has to solve

$$-\frac{1}{n^2a^2}\,\hat{D}\,\vec{\Psi} + \hat{V}_{\text{eff}}^2\,\vec{\Psi} \;=\; k^2\,\vec{\Psi}, \tag{12}$$

which means diagonalyzing the matrix $-\frac{\hat{D}}{n^2a^2} + \hat{V}_{\text{eff}}^2$. The extracted eigenvalues are the squared mode energies and the extracted eigenvectors are the axial field distributions. Exemplarily, in Fig. 9 a quasi-potential and some intensity distributions are shown. The quasi-potential is determined from a real structure by measuring the exact geometry in scanning electron micrographs and solving equation (7) with the measured properties along

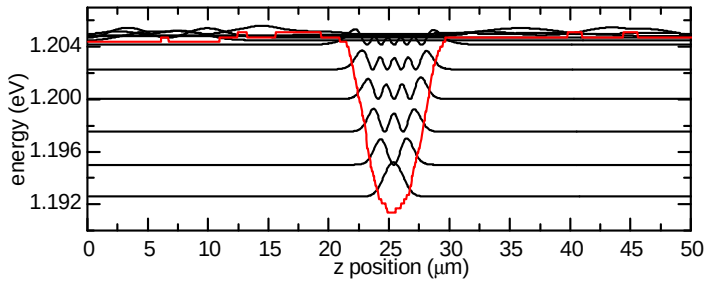

FIG. 9: Quasi-potential determined from a real structure and the 12 calculated solutions with the lowest energies. N=1000 grid point with a spacing of 50 nm were used. The field distributions are squared and shifted by its corresponding eigenenergy.

the axis. The simulation length was chosen to be 50 μm which is much wider than the quasi-potential to avoid artifacts from the artificial boundaries. We observe 7 bound eigenstates. Due to the fact, that all eigenfunctions of equation (12) vanish at the boundaries, solutions that are not bound in the quasi-potential quantize on the artificial length of the simulation area. Those solutions are no real bound eigenstates. However, they reflect light with high k_z vectors that is not bound in the quasi-potential and propagates along the microtube axis. In the experiments one often observes resonances that are similar to those solutions.

IV. DISCUSSION OF EXPERIMENTS AND CALCULATIONS ON THE AXIAL LIGHT CONFINEMENT

A. Axial light confinement by lobes in the rolling edge

In this section we describe in detail our experimental results on light confinement by lobes in the rolling edge. We also present calculations done with the methods presented in the theoretical description and compare them to the measurements. We give a detailed description how the actual geometry of the microtube is taken into account in our calculations. In the first part we concentrate on three microtubes with differently shaped lobes in the rolling edge. Figure 10 depicts the parameters of the microtubes as they are defined on the mesa before rolling-up. From these parameters the microtube geometry can be determined. After measuring the radius the spiral shape of the microtube can be calculated and the lengths L_1 and L_2 as defined in Fig. 5, can be extracted.

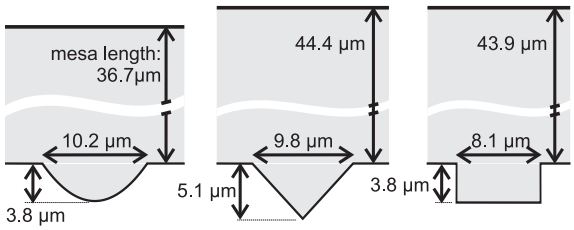

FIG. 10: Parameters defined on the mesa for three microtubes with a parabolic, a triangular and a rectangular lobe in the rolling edge.

Figure 11 shows the measurements on the microtube with the parabolic lobe as depicted in Fig. 1. Here, in addition to Fig. 2, the measurements are compared to results from different calculations and FDTD simulations. The axes are rotated to scale the energy in horizontal direction and the space in vertical direction as typical for potentials. In this view the analogy of Fig. 11 (b) to the probability density of particle waves in a one-dimensional potential becomes evident. By comparing the measurements to the results from calculations in Fig. 11 (c) and (d) this becomes even more clear, since the solutions are, mathematically, indeed one-dimensionally confined waves in a one-dimensional quasi-potential. For the calculations we followed the procedure in our theoretical description and separated the circular propagation in the $r-\varphi$ plane from the axial propagation. The circular problem was solved by the waveguide model for each axial position along the tube axis as follows: In scanning electron micrographs we measured the exact shape of the mesa including slight asymmetric deviations from the planned structure as well as the radius. This asymmetry can clearly be observed in Fig. 1(c) and is included in the following numerical calculations. From this geometrical data we calculated the lengths L_1 and L_2 for each position z along the axis of the tube, as defined in Fig. 5(b). From the sample parameters (sample A, as described above) and the length of the mesa we determined the wall thicknesses to be t_1=100 nm and t_2=150 nm which means that the tube has a winding number between 2 and 3. For the dispersion of the refractive index n of the semiconductor material we assumed $n(E) = 3.46 + (E[eV] - 1.1)/2$ following our previous work[3]. With these values we numerically solved equation (6) to determine the dispersions of the effective refractive indices $n_{\text{eff}}(\lambda_{\text{circ}}, t_1)$ and $n_{\text{eff}}(\lambda_{\text{circ}}, t_2)$ and fitted the data quadratically. Finally, we calculated the solutions of the circular equation for a finite number of points along the microtube axis as solutions of equation (8). This results in a discrete

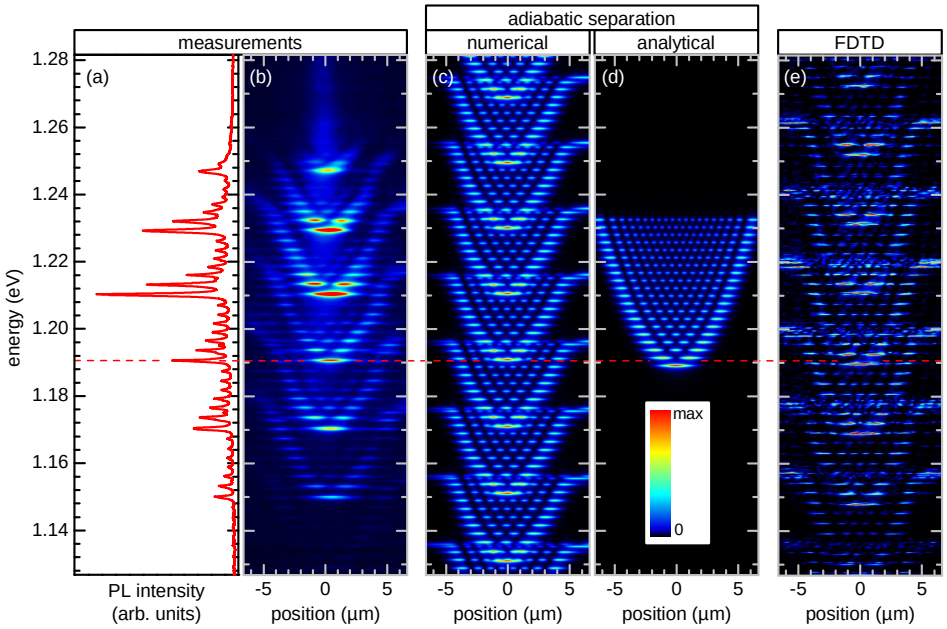

FIG. 11: (a) Spatially integrated PL spectrum of a microtube with a parabolic lobe in the rolling edge. (b) Spatially resolved measurement of (a). (c-d) Calculated mode energies and intensity distributions using the method of adiabatic separation. (c) Numerical solutions. (d) The 20 first analytical solutions for an infinite parabolic quasi-potential for one azimuthal mode number. (e) Intensity distributions and mode energies calculated by FDTD simulations. All intensities are encoded in false colors.

description of the quasi-potential for the axial propagation for each azimuthal mode number m. An example of such a quasi-potential is given in Fig. 9 as a red curve. In the next step we calculated the eigenenergies and field distributions of the bound states in the quasi-potential following the procedure of numerically solving the quasi-Schrödinger equation. The dispersion of the refractive index is taken into account by iteratively solving equation (12): We determine the refractive index for a start value E_0 of the energy in the desired energy range and calculate the mode energy E_1. With this value we again calculated the refractive index. This procedure is repeated until the mode energy converges. The results are shown in Fig. 11(c). The modes are energy-resolved in vertical direction and spatially resolved along the tube axis in horizontal direction. The energies as eigenvalues of equation (12) are artificially broadened in Fig. 11 assuming a quality factor Q, defined as $Q = E/\Delta E$ of

2000. The intensities in form of the squared values of the eigenfunctions of equation (12) are encoded in false colors. We observe a very good agreement to the measurement. The energy of the fundamental mode in each quasi-potential as well as the energy of the highest bound mode are reproduced. This directly reflects the validity of the waveguide approximation by which the quasi potential was calculated. Also the number of bound modes in every potential and the axial field distributions agree with the measurements. This demonstrates on the one hand not only the validity of the adiabatic separation but, on the other hand, that also our procedure to integrate the exact geometry is very accurate. In a closer look one observes a slight asymmetry of the measured intensity distributions that can also be found in the numerically calculated results which arise from the actual asymmetric shape of the experimental mesa (see above). Our picture to regard the modes to be axially confined in a quasi-potential that is induced by the circular propagation seems to be right.

As demonstrated in the theoretical description in the case of a parabolic lobe one can also calculate analytical solutions as solutions of equation (10). Here, we neglected the slight geometrical asymmetry. To find the parameters a and b we calculated the quasi-potential as described above and made a quadratic fit. Due to the linear dependence of the circular mode energy on the winding number (see Fig. 6) the parameters can also be calculated directly from the geometrical shape of the lobe. Figure 11 (d) shows the first 20 mode energies and field distributions exemplarily for one azimuthal mode number as solutions from the harmonic oscillator according equation (10). The picture was generated in the same way as the numerical solutions. We also observe a good agreement to the measurements as well as to the numeric calculations. Deviations result only from neglecting the slight asymmetry the lobe geometry from the parabolic case. The analytic description has the important advantage that the calculation can be reversed in a simple way: One can choose an energy offset and a mode spacing and calculate the parameters a and b. Due to the linear dependence on the winding number the quasi-potential can then be translated back into the winding number of the structure and can serve as an input parameter to fabricate tailored microtubes.

A third method to calculate the modes in dielectric cavities there are FDTD simulations. Those simulations numerically solve the time evolution of the electromagnetic fields on a discrete spatial and temporal grid. Those simulations allow us in principal to calculated arbitrarily complex geometries, if the grid is chosen fine enough. Thus all geometrical features can be taken into account. The disadvantage is that much computation power is

required. For the FDTD calculations we used the commercial software "Lumerical FDTD Solutions". The simulation was set up as depicted in Fig. 12. The geometry of the tube was generated by putting together half tubes each with different constant radii. The lobe was composed by 300 arc elements whose lengths were defined by a parabola equation obtained from a fit to the real structure neglecting the slight asymmetry. The refractive index of the semiconductor was set to n=3.5 without dispersion. The microtube structure was centered in a simulation area of 7µm×7µm×15µm resolved by 300 mesh points in each direction. In order to avoid unnecessary reflections of light at the boundaries the simulation area was terminated by perfectly matching layers. The time step was set to 0.0517 fs and the duration of the simulation was set to 30000 fs. For excitation we chose a plane wave starting at the inside rolling edge (brown box in Fig. 12) and propagating azimuthally in direction of the lobe (green arrow in Fig. 12). It was chosen asymmetric in z direction to excite both symmetric and asymmetric axial modes. The source emitted a Gaussian pulse having a center frequency of 294 THz and a spectral width of 26 THz. The polarization of the electric field was set in z direction [yellow arrow in Fig.12(b)]. To determine the eigenfrequencies and their axial field distributions of the resonator we recorded the time evolution of the axial component of the electric field along a line situated near the inside rolling edge [dark blue line and cross in Fig. 12(b) and (d), respectively]. The time dependent signals in each grid point along the line were Fourier-transformed. The simulations were performed calculating parallel with 4 cores of an 8 core Intel Xeon E5440 Processor with 2.83 GHz. The total duration of the calculations was about 145 hours. The results are shown in Fig. 11 (e).

However, if we want to compare the results in Fig. 11 (e) to our measurements or to our calculations, we have to be careful. For two-dimensional FDTD simulations on a perfect ring of 100 nm wall thickness and the same diameter we found that the energy of the simulated modes deviates about 6.5 meV from the analytic solution evaluated from equation (4). Thus the results from the three-dimensional simulations can be compared to our other data only in a qualitative way. To simulate our microtube with a sufficiently fine grid and in adequate time was not possible for us up to now due to our limited computation power. This shows the mentioned disadvantage of three-dimensional FDTD simulations to be very time-consuming. In this context it is worthwhile to search for other methods as done in this work. Nevertheless, by qualitative comparison the simulations underline the validity of our statements since the measurement in Fig. 11(b) and our calculations in Fig. 11(c) are

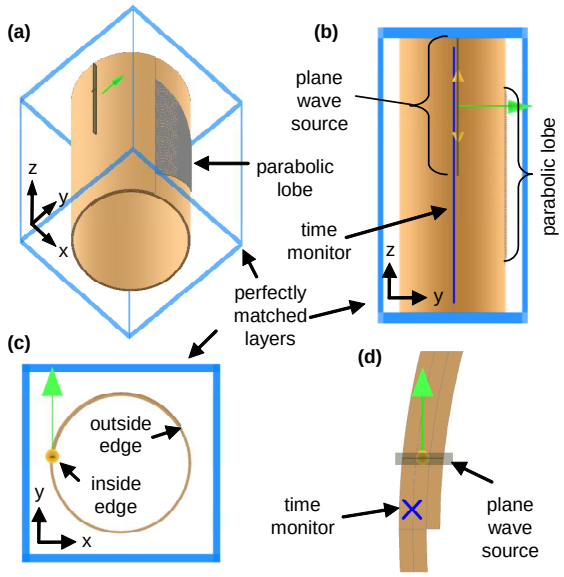

FIG. 12: Three-dimensional view (a), top view (b) and side view (c) of the microtube geometry as implemented in the simulation. (d) Enlarged view of the azimuthal and radial position of the time monitor and the source near the inside edge of the microtube.

generally reproduced. For example, we can conclude that the emitted intensity pattern in the measurements really reflects the intensity distributions inside the tube which would not be possible without the FDTD simulation.

Our theoretical description shows that parabolic lobes and thus parabolic quasi-potential actually lead to an equidistant mode spacing of the axially confined modes with the same azimuthal mode number m. Here, we want to prove that in our experiment. But we also want to show that the statement can be expanded to lobes and thus quasi-potentials with different shapes. This is discussed exemplarily by experiments and calculations on microtubes with lobe shapes as defined in Fig. 10. In Fig. 13 (a) and (b) we present the spatially integrated spectra of the microtubes with a triangular and a rectangular lobe, respectively. The microtubes were fabricated using sample B. The first important finding is that also in these structures the typical mode spectrum of three-dimensionally confined modes is observed. Regarding the mode spacings in the groups of the same m we find that indeed the mode spacings behave as known from particle waves in one-dimensional potentials [see the insets in Fig. 13 (a) and (b)]: For a triangular lobe and thus a triangular quasi-potential we observe a decreasing mode spacing and for the rectangular lobe an increasing mode spac-

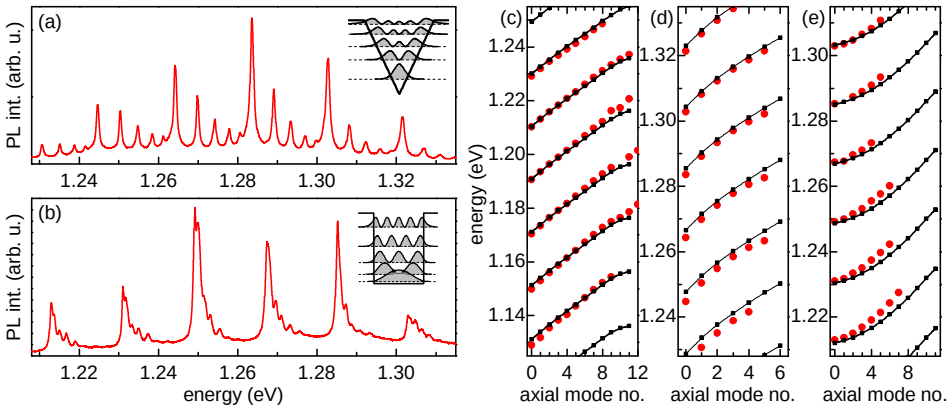

FIG. 13: (a) Spatially integrated spectrum of a microtube with a triangular lobe, (b) with a rectangular lobe. The insets sketch the respective quasi-potentials and bound field distributions. (c-e) Measured (red dots) and calculated (black squares) mode energies for a parabolic (c), a triangular (d), and a rectangular lobe (e). The lines serve as guide to the eye.

ing with higher energy. We also performed numerical calculations for the microtube with the triangular and the rectangular lobe. We proceeded in the same way as described for the parabolic lobe and determined the quasi-potential from the actual geometry followed by numerically solving equation (12). The calculated and measured mode energies versus their axial mode number h are shown in Figs. 13(c), (d) and (e) for the parabolic, the triangular and the rectangular lobe, respectively. In this view it becomes obvious that by differently shaped lobes a corresponding quasi-potential is induced and the confined modes behave as expected: Parabolic lobes lead to an equidistant, triangular lobes to a decreasing and rectangular lobes to an increasing mode spacing with higher energy. In comparison to our calculation we again find a good qualitative agreement. This is a very important finding because it proves on the one hand the general validity of our model. On the other hand one can predict the behavior of the modes and can plan the sample structure. We also believe that the three special shapes of lobes stand exemplarily for the manifoldness of lobe shapes and mode dispersions. Consequently, it is possible to tailor the mode dispersion of the modes with the same azimuthal mode number just by the shape of the lobe. This could be very useful to balance a change of the mode spacing due to the dispersion of the refractive index of the material. For example in applications for the telecommunication or information procession equidistant frequency channels are desired. For very small microtubes the tailoring

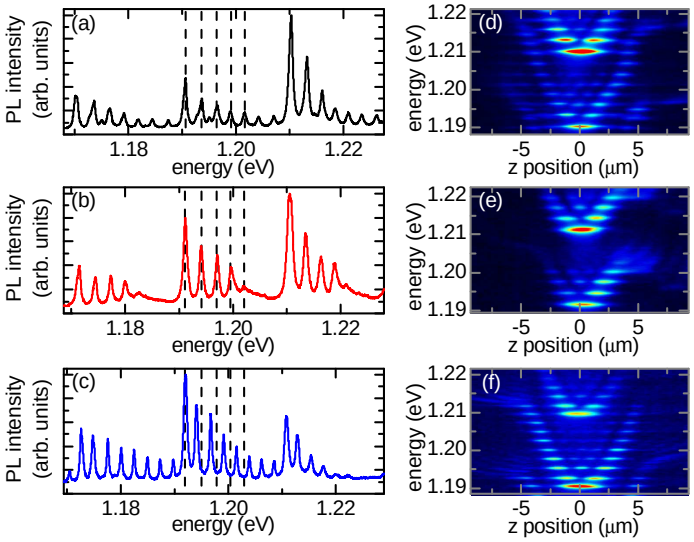

FIG. 14: (a)-(c) Details of spectrally integrated PL spectra of microtubes with differently shaped parabolic lobes on an expanded energy scale. The spectrum in (a) that is part of the spectrum in Fig. 11(a) is compared to a microtube with the same lobe curvature but different height (b) and a microtube with a lobe with different curvature (c). The dashed lines are guides to the eye. (d)-(f) show the corresponding spatially resolved PL measurements to (a)-(b), respectively. The intensity is encoded in false colors.

of the axial confinement becomes even more prominent: Microtubes with small radii exhibit a very large azimuthal mode spacing that only the axial modes of one m are observed in a finite energy range. In this case actually all observed modes can be tailored.

In the following we want to give further examples of microtubes with different lobes. We focus on microtubes with parabolic lobes, as parameterized in Fig. 10 and study experimentally, how the different parameters change the mode spectrum. In Fig. 14 on an expanded energy scale spatially integrated, as well as spatially resolved spectra of two further microtubes are compared to the spectra shown in Fig. 11(a) and (b). Figures 14 (a) and (d) show again details of the measurements depicted in Fig. 11. In Figs. 14 (b) and (e) the spectra are compared to measurements of a microtube with the same lobe curvature but a smaller lobe height of 1.9 μm. All other microtube parameters like radius and winding number are the same in both experiments. Nevertheless, also nominally identical microtubes show slightly different spectra due to slight inaccuracies in the fabrication resulting

mostly in a constant shift of all modes. Thus to compare only the influences of the axial confinement by the lobe the spectra are shifted by a constant energy to horizontally align the mode energy of the fundamental modes. In the spatially integrated spectra we observe nearly the same energies of the higher axial modes in both measurements as expected for lobes, and consequently also quasi-potentials, of the same curvature. In addition, we find fewer axially confined modes due to a more shallow quasi-potential, as we expect from our model. In the spatially resolved measurements this is becomes even clearer. We also find that the axial intensity distributions spread very similarly in axial direction. In Figs. 14 (c) and (f) we show measurements of a microtube with a lobe curvature that is about 30% smaller. The height of 3.7 µm is roughly the same as for the measurements in Figs. 14 (a) and (d). Here, we observe that the energies of the higher axial modes are smaller than in the compared experiments. This also accords to our model. The axial intensity distributions are dimensioned wider in axial direction compared to the other measurements. Note that one must not compare the field distributions of modes with the same axial mode number, but modes with the same energy, since in parabolic potentials the confinement length changes with energy. These three microtubes demonstrate that the experimental spectra of microtubes with lobes in the rolling edge can be understood in a very intuitive way in terms of our model. The spectra can actually be tuned in a very sensitive way by the shape of the lobe.

As a last example for a microtube with a lobe as axial confinement mechanism we study a microtube with a very small lobe. On the one hand this proves a possible limit for lobe geometry, one the other hand it is often a goal to reduce the number of modes that are confined in a cavity. This is useful for example for single-mode and low-threshold lasing or for experiments on quantum electrodynamics with single quantum dots. Figures 15(a) and (b) depict spatially integrated and spatially resolved PL measurements on a microtube with a very small lobe, respectively. The lobe has dimensions of approximately 700 nm height and about 1 micron width. It is shown in the inset of Fig. 15 (a). Indeed, in Fig. 15 (a) one principally observes only the fundamental mode in the very shallow quasi-potential induced by the lobe. Instead of the higher axial modes on the high energy side one observes only the onset of a weak broad band. This becomes even more clear in the spatially resolved measurement in Fig. 15 (b). Here, the resonances on the high energy side appear smeared out in energy and space. Those resonances are typical for all microtubes with lobes and

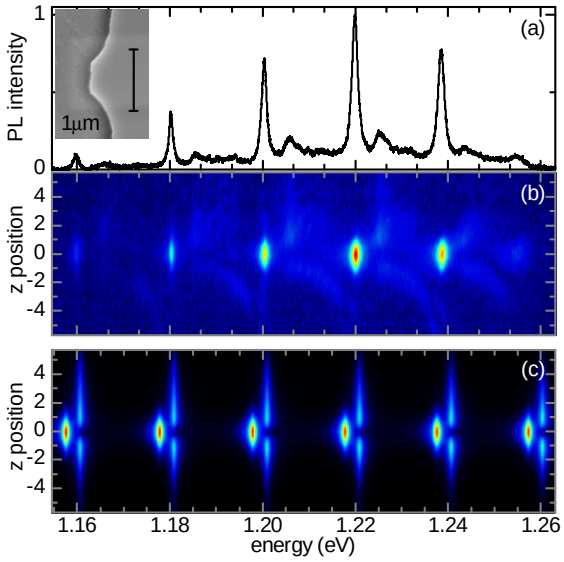

FIG. 15: (a) Spatially integrated PL spectrum of a microtube with a very small lobe, as shown in the inset. (b) Corresponding spatially resolved PL measurement. The intensity is encoded in false colors. (c) Results from numerical calculations taking into account the exact lobe geometry.

can be found, more or less pronounced, in all our spatially resolved measurements. They appear at the energy edge of the quasi-potential. With increasing energy the higher axial modes smoothly change from bound modes in the quasi-potential to modes with too high k_z vectors to be bound which thus are only scattered by the quasi-potential. This means that we indeed realized a microtube that only confines one mode per azimuthal mode number.

Now, we want to check our model for this small lobe geometry. Figure 15 (c) shows the results of calculations, following again the procedure of measuring the exact geometry, calculating a quasi-potential by the waveguide model and numerically solving the quasi-Schrödinger equation. Also for this very small geometry we find a good agreement. The field distributions of the fundamental modes are reproduced nicely and the calculated energies are only a little bit too small. In general, one can not expect that the absolute energies are reproduced by the model so accurately, since they depend sensitively on the measured geometries like radius and winding number. Moreover the spacing of the azimuthal mode numbers has to be compared, which nevertheless gives a nice agreement. This confirms only our two-dimensional description by the waveguide model. We can not check if the deviations might also derive from our three-dimensional treatment. Up to now we always compared

the energy spacings between the higher axial modes, but here only one mode is found in the experiments. In the calculations two bound states are found. But the field distribution of the second mode already spreads very widely in axial direction, indicating that its energy is close to the edge of the quasi-potential. We believe that here our model is limited. In general our approach treats the system as closed. By the adiabatic separation the light is confined by the strong boundary condition of the quasi-potential and the solutions are time independent: A mode is either bound in the quasi-potential or not bound. But in reality the system is open and the modes can leave the system reflected in the finite Q factors. Modes that have energies close to the edge of the quasi-potential are only temporarily influenced by the lobe and thus not described correctly. The smooth change from bound to unbound in the experiments as described above is not described correctly by our model. If we associate the second bound state with the resonances on the high energy side, we find that the energy spacing to the fundamental mode is much higher in the experiment. This demonstrates that our model can not describe modes that have energies very close to the quasi-potential edge. Nevertheless, the number of confined modes can be estimated quite well and makes our method a nice tool to plan the microtube design concerning the three-dimensional confined modes by lobes in the rolling-edge.

We shortly summarize the findings on axial light confinement by lobes in the rolling edge: Obviously, this mechanism allows to control the axial eigenmodes in a very precise way and over a wide range of geometries. In addition, this mechanism can be described by an intuitive model that reproduces the experimental findings. For the highest axial modes the model exhibits inaccuracies which become important for very small lobes. Nevertheless, a good qualitative agreement is also achieved for very small lobes.

B. Axial light confinement by etched rings

The theory to describe the axial light confinement by the Schrödinger equation allows in general all kinds of modulations of the microtube geometry to axially confine the light when it causes an attractive quasi-potential along the axis. This can, for example, be done by a radius modulation which was shown very recently for a dielectric prolate shaped cavity formed by a tapered glass fiber.[21] But this is very difficult to realize in microtube resonators since the radius is driven by the strain built up during the growth process. Here, we present

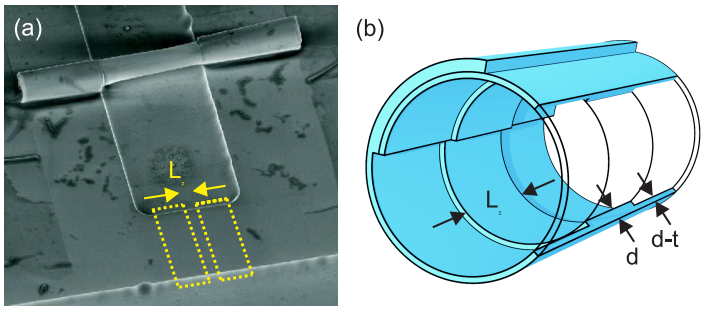

FIG. 16: (a) Scanning electron image of a microtube with its U-shaped mesa. The regions before rolling up that form etched rings in the microtube after rolling are marked by dashed yellow line. (b) Sketch of the center part of the rolled-up microtube.

a different axial confinement mechanism based ona modulation of the wall thickness. Besides the axially confined modes this allows us also a clear observation of the splitting by broken rotational that has not been observed in such clarity up to now. In this section we discuss the axial confinement by comparing experiments and calculations. In the next section we analyze the splitting. The axial confinement is achieved by an axial microtube design similar to ridge waveguides, but here in a rolled-up form. Fig. 16 (a) shows a scanning-electron micrograph of such a microtube. In principal we prepare those microtubes, as shown in Refs. 3,8, without a lobe in the rolling edge. But before rolling-up we etch two stripes of a distance L_z and a depth of about t=4 nm into the U-shaped mesa, as depicted by yellow dashed lines in Fig. 16(a). After rolling up the free-standing part of the sample looks as sketched in Fig. 16(b). A ring of larger wall thickness d is formed, situated between rings with thinner wall thicknesses of $d - t$. This leads to a jump of the effective refractive index n_{eff} from large between the etched rings to smaller within the etched rings and, consequently, to a higher energy of one azimuthal mode m within the etched rings as compared to between the rings. In terms of our model a rectangular quasi-potential is induced. Figures 17 (a),(b) and (e),(f) show PL measurements on two microtubes with L_z=4.3 µm and L_z=3.3 µm distance of the etched rings, respectively. The microtubes have diameters of, respectively, 3.5 µm and 3.6 µm and approximately 1.3 windings. The wall thickness of the single layer part is 59 nm (sample C).

As internal light source the PL of a 4 nm InGaAs quantum well is used (see the sample structure of sample C). Thickness fluctuations in the quantum well lead to the localization

of excitons and thus to a considerable broad PL emission widely ranging to lower energies as shown in our previous work for a very similar sample.[8] The emission is strongly modified by the emission of the microtube modes. To assign the modes correctly one has to consider the spatially resolved measurements in Fig. 17 (b) and (f). Here, it becomes obvious that we observe only modes of one azimuthal mode number that differ in their axial confinement. But, in contrast to the measurements on microtubes with lobes, all modes are split into two resonances. It is unambiguously clear that we observe a pronounced mode splitting by broken rotational symmetry since all modes with the same axial number of antinodes appear twice, as clearly observed in Fig. 17 (b-d). This splitting will be analyzed in the next section. In the following we want to focus on the higher axial modes. As expected for a rectangular quasi-potential the mode spacing increases with higher energy. But actually it turned out that these structures can be described by our model only in a qualitative way. To demonstrate this we anyhow calculated the axial modes analogously to microtubes with lobes. To determine a quasi-potential for these structures we calculated the energy of the azimuthal mode in the desired energy range within the etched rings and between them. We determined the effective refractive indices for the two waveguide parts d_1 and d_2 between the rings and d_1-t and d_2-2t within the etched rings by equation (6) and calculated the mode energy by equation (7). The energy jumps like in a finite rectangular potential. For this quasi-potential we followed the procedure of numerically solving equation (12). The results are shown in Fig. 17(c) and (g). Since the dispersion of the refractive index n of the material is not known for this structure (we assumed n=3.5), the absolute values of the calculated modes strongly deviated from the measurements. To compare the axial modes to the experiments we energetically aligned the calculated axial fundamental modes to the mean value of the split fundamental modes in the experiment. Naturally, the splitting is not found in the calculations. The spacings between the axial modes deviate strongly from the mode spacing between the mean values of the split modes. In the experiment the axial mode spacings are much larger than in the calculations. However, the axial intensity distributions are reproduced very well by the calculations. To check if some additional unknown confinement mechanisms are involved we performed further calculations. The strongest axial mechanism that confines a wave on a length L_z leads to vanishing field amplitudes at the boundaries and thus to an axial wave vectors $k_z = h\,\pi/L_z$, where h is the number of axial antinodes. The field functions between the rings then read $\sin(h\,\pi/L_z\,z)$ and the total wave vector is calculated by $k = \sqrt{k_{\mathrm{circ}}^2 + k_z^2}$.

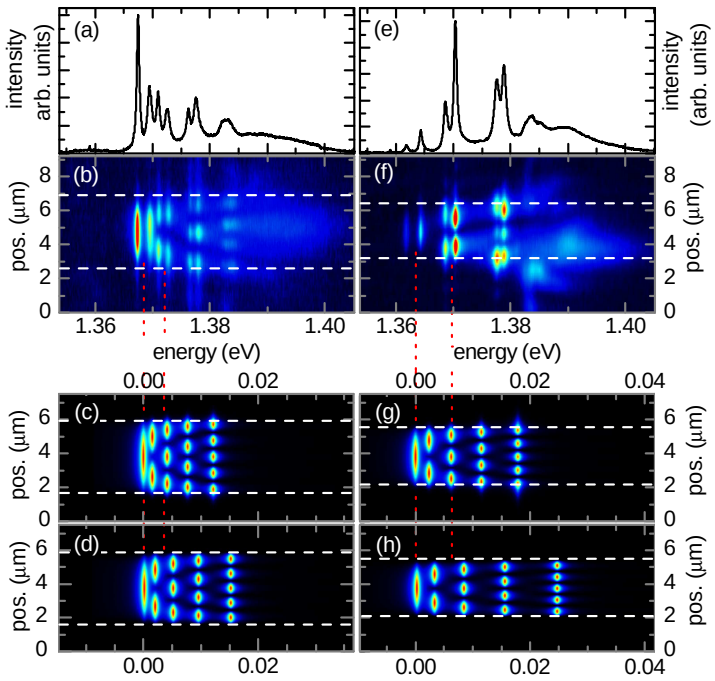

FIG. 17: (a),(e) Spatially integrated PL spectra of microtubes with different axial confinement lengths. (b),(f) Spatially resolved measurements corresponding to (a) and (e). The intensity is encoded in false colors. (c),(g) Strongly deviating results of calculations with a finite rectangular quasi-potential as well as (d),(h) of an infinite rectangular quasi-potential (see text). Dashed white lines mark the region between the etched rings. Vertical red dashed lines serve as guide to the eye.

The intensity distributions and mode energies calculated by this approach are shown in Fig. 17(d) and (h). Also by this strongest possible confinement mechanism the experimental mode energies can not be explained. Obviously, this mechanism is much more complicated as the modes can be described quantitatively by our approach. First hints on the origin of this different behavior we obtained by polarization dependent measurements. Actually, we found that these modes are not purely linearly polarized with the electrical field vector along the tube axis, as found in many previous works[8,11,14]. By analyzing the emitted intensity behind a rotated $\lambda/2$ plate and a linear polarizer we measured a minimum extinction of the modes of still 10%. Thus the modes are polarized slightly elliptically in contrast to our assumption of TE-polarized light in our waveguide approach. In addition by the etched rings the microtube has more interfaces also in axial direction [see Fig. 16(b)]. Under these

considerations the electrodynamics of the modes become very complicated, since many more boundary conditions have to be satisfied. We can not give a solution for this problem but we can motivate how the larger axial splitting could be explained. In a simple picture the k vector, the magnetic and the electric field vector are situated perpendicular to each other. For no k_z contribution the electric field vector can direct only in axial direction not depending on the contributions of k_r and k_φ to the total wave vector. For increasing k_z the electric field vector directs more and more out of the microtube surface. This leads to a stronger confinement in radial direction and increases the mode energy. In the case of the lobes we in principal also have high k_z contributions. But here we have nearly no interfaces in axial direction and at the classical turning points, where most of the mode intensity is situated, the k_z vector is zero. Indeed, we measured for these structures also a slight elliptical polarization but the measured extinction, as defined above, was only about 4%. Our explanation is supported when we consider the measurements and the calculations on the microtube with a rectangular lobe in Fig. 13 (e). Here, the experimental values are also slightly larger than in the calculations since for rectangular lobes the axial interfaces are larger than for other lobe shapes and the abrupt change of the quasi-potential leads to high k_z vectors also at the boundaries.

V. MODE SPLITTING BY BROKEN ROTATIONAL SYMMETRY

Due to the inner and outer rolling edge rolled-up microtubes exhibit a broken rotational symmetry. In general one expects a splitting of each mode due to the coupling of clockwise and counterclockwise propagating modes with azimuthal mode number m and $-m$, respectively. Applying two-dimensional FDTD calculations one finds various amounts of splittings of a few meV, as reported in Ref. 16. However, the splittings observed in the experiments were not very pronounced[6,7,10]. A prerequisite for the observation is, on the one hand, a well-defined axial confinement to consider single modes and, on the other hand, spatially resolved measurements to distinguish between the splitting and higher axial modes. Here, we discuss the splitting for the modes axially confined due to the etched rings by analyzing it on the hand of two-dimensional FDTD simulations and in comparison to the waveguide model. Finally, we investigate the impact of the three-dimensional confinement on the splitting, by measurements on microtubes with lobes.

The three-dimensional confinement has a high impact on the microtube modes. Nevertheless, for the axial light confinement by etched rings, in first order, at all axial positions between the rings the cross section is the same. Thus all axial modes with the same azimuthal mode number m should be influenced in the same way by the rolling edges. This is actually what we observed in our experiments in Fig. 17 and will also be motivated below. Consequently, two-dimensional FDTD solutions should approximately describe the dynamics in the cross section of the microtube and can be performed with sufficiently fine spatial grids. We assumed a microtube with a radius of 1.8 µm and a single-wall thickness of 59 nm. The winding number was varied in 20 steps between 1.5 and 1.56. Similar to the simulations shown in Fig. 12, we positioned time monitors at different positions in the ring that record the time evolution of the electric fields. As a source we chose a plane wave positioned diagonal within the thicker part of the ring and emitting along the circumference. In this way all modes can be excited in contrast to a dipole source where the dipole might accidentally be positioned in a node of a mode. The time evolution of the electric field in axial direction recorded by the time monitors was Fourier-transformed. Figure 18(a) depicts the summed intensity from all time monitors depending on the energy and the winding number. The modes are found as dark features implying high intensity. Besides a decrease of the energy with increasing winding number, we observe an oscillating behavior of the mode splitting. Obviously, the splitting depends on the winding number in a systematic way. To elucidate this we also performed calculations with our waveguide model. The results are shown as red lines and black dashed lines in Fig. 18(a). The red lines are the solutions of equation (7), for which an integer number of wavelengths has to fit into the optical ray path that is formed by the two waveguides with their two effective refractive indices $n_{\text{eff}}(\lambda, t_1)$ and $n_{\text{eff}}(\lambda, t_2)$ and lengths L_1 and L_2. The dashed black lines are calculated by assuming each waveguide as a single resonator. For these resonators we assumed that an integer number of half wavelengths has to fit into the optical ray path length, here formed by the length of the single waveguides and their single effective refractive indices. Naturally, the resonance energy of the thicker waveguide decreases with increasing winding number and increases for the thinner waveguide since one part becomes longer and one shorter. To compare these results to the results from the FDTD simulations we shifted the energy scale of the lines by a constant value to higher energy. The small deviations are caused by the approximation of our model and by a small error due to the finite convergence criterium of the FDTD

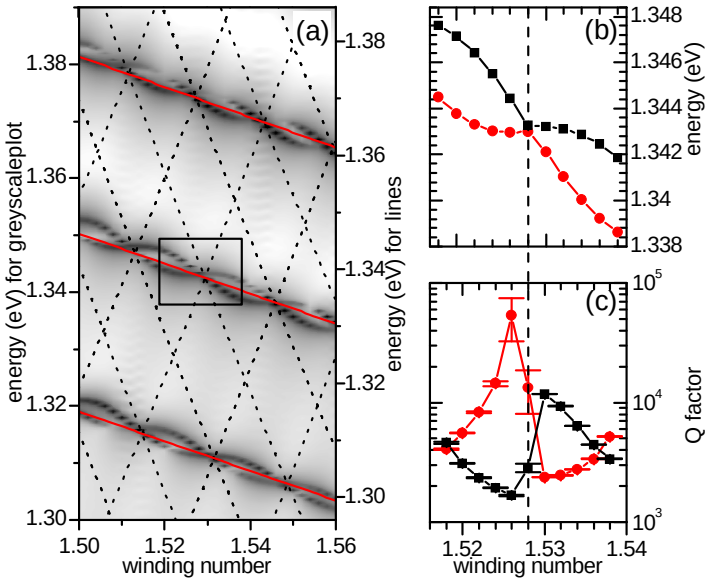

FIG. 18: (a) Greyscale plot: Intensity versus energy and winding number in the cross section of a microtube obtained by FDTD simulations. The intensity is scaled logarithmically, dark means high intensity. The red lines are results from calculations by a waveguide model. The dashed lines show the resonance energies of the single waveguide parts. (b),(c) Lorentz fits in the region marked by the square in (a). (b) Energy and (c) width (FWHM).

simulation. Interestingly, the points of zero or very small splittings in the FDTD simulation coincide with the points in which the mode is resonant in both single waveguide parts. In Ref. 16 it is reported on the hand of a special mode in a single geometry that one of the split modes has a node at the inside rolling edge and the other mode a node at the outside rolling edge. The different energies arise from the different lengths of the mode trajectories around the opposite rolling edges. Here, we studied the problem more generally, since we investigate a couple of geometries and thus all potential arrangements of nodes and antinodes, with respect to the rolling edges. To find zero or very small splittings in the doubly resonant points extracted from our waveguide approach is in absolute agreement with this previous work. In these special points both modes can principally arrange both nodes at the rolling edges. But the split modes have to be orthogonal and consequently the field distributions repel each other. To study the modes around such doubly resonant points more detailed we fitted the spectra marked by the square in Fig. 18(a) by two Lorentzians. The resulting energies E

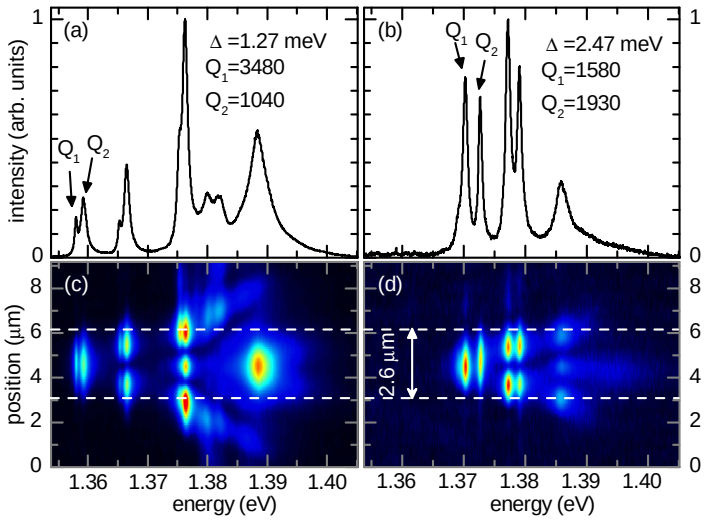

FIG. 19: (a),(b) Spatially integrated PL spectra of two microtubes and (c),(d) the corresponding spatially resolved PL measurements. The dashed white lines mark the region between the etched rings. The intensity is encoded in false colors.

and quality factors Q, defined as $Q = E/\Delta E$ (ΔE = FWHM), are shown in Fig. 18(b) and (c), respectively. We observe the interesting behavior that the quality factors of the modes behave contrarily to the mode energies. When the energy splitting is large the splitting of the quality factors is small and, even more interestingly, at the doubly resonant point where the energy splitting is minimized the quality factors are split strongly. Especially, very close to the doubly resonant point we find one broad mode with strong losses and a very sharp mode with low losses. In a theoretical work the formation of long-lived modes near avoided resonance crossings was reported as a typical feature of open mesoscopic systems[22]. The coupling of the modes is described as so called external coupling, where the losses can be redistributed by interference of the modes in the far field. Such a behavior was also observed for two coupled photonic crystal cavities[23].

In Fig. 19 we show PL measurements on two microtubes with approximately the same axial confinement lengths L_z but different radii and winding numbers. In both spectra we observe about the same energy spacing of the axial modes, but a different splitting due to the broken rotational symmetry. In Fig. 19 (a),(c) the splitting is only 50 % of the splitting observed in Fig. 19 (b),(d). For the axial fundamental modes we determined the quality factors of the split mode. Indeed, we observe for the smaller energy splitting a larger

splitting of the quality factors which directly follows the behavior in Fig. 18. In addition we find that the higher axial modes of the same azimuthal mode number m exhibit nearly the same splitting. We attribute the deviations to a varied geometries of the cross section within the etched rings. Microtube modes with very small splittings are considerably seldom, since the winding number has to fit the resonance conditions very accurately. We observed much more often microtubes with intermediate splittings and the quality factors usually ranged between 2000 and 1500. This agrees with the FDTD simulations and underlines that the modes in Fig. 19(a),(c) are modes that redistribute their losses by the external coupling mechanism[22]. A predefined coupling of the split modes is very useful to achieve higher quality factors and could make single mode lasing possible. By this mechanism the laser threshold could be lowered since the high quality mode would start lasing first. A predefined design of microtubes exhibiting modes with small splittings is very difficult since the winding number has to fit very accurately. Much more promising is to tune the modes after fabrication. Very recently it was shown that post fabrication tuning by atomic layer deposition can precisely tune the modes[14]. By additional layers the resonance energy of the thinner waveguide part would be tuned stronger than the thicker one and for a distinct thickness the doubly resonant points can be reached.

The question arises why a well pronounced splitting of the modes, as found in the two-dimensional FDTD simulations, is only observed in microtubes with this axial confinement mechanism. We believe this is caused by the fact that only in these microtubes the winding number along the axis is constant. For parabolic or triangular lobes the axial mode distribution averages over different winding numbers and thus the different splittings cancel out. For rectangular lobes we should in principal also find pronounced splittings. But in our samples the edges of the rectangular lobes tend to round during the fabrication which leads also to the described averaging effect. We in general observed that the splittings tend to average out if the microtube exhibits inhomogeneities like changes of the radius or the winding number along the axis. However, observations of splittings were also reported for structured rolling edges[6,7,10]. Indeed, we can also find splittings in some of our measurements on the parabolic lobes, e.g. in Fig. 14 (c) and (f), if one evaluates the spatially resolved measurements more accurately. This is demonstrated in Fig. 20 (a). We determined two different spatially integrated spectra from the spatially resolved measurement: First we integrated only signals from the classical turning points from positions of the upper part of the tube (marked by the

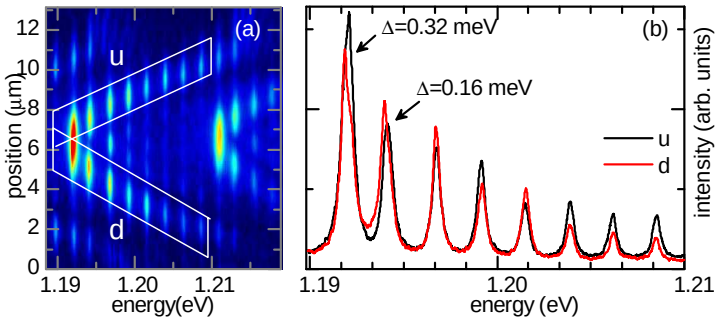

FIG. 20: (a),(b) Spatially integrated PL spectra of two microtubes and (c),(d) the corresponding spatially resolved PL measurements. The dashed white lines mark the region between the etched rings. The intensity is encoded in false colors.

white lines and labeled with u) and afterwards only signals from positions of the lower part of the tube (marked with d). The two spectra are compared in Fig. 20 (b). We observe that the first and the second axial mode are split and that their contributions on the emission from the upper and the lower microtube part are different. For the other axial modes we can not decide whether they are split or the splitting can not be resolved. By carefully regarding SEM images of the lobe we found that it is slightly asymmetric at its center part. We believe that, as described above, a varying winding number over the axial field distribution of the modes, e.g. by lobes, averages out the splittings, but that asymmetries can also enlarge the splitting. The repelling of the field distributions of the degenerated azimuthal modes due to orthogonality is transferred to the axial direction by the asymmetries. It might be that for perfectly symmetric lobes with changing winding number for all azimuthal modes external coupling and redistribution of the losses is a fundamental property. But to check this more theoretical work on the three-dimensional properties of the modes or experiments on improved perfectly symmetric as well as systematically asymmetric structures have to be done.

VI. CONLUSION

We presented controlled three-dimensional light confinement in rolled-up microtube bottle resonators. We showed that the axial confinement plays an important role for the observation of well defined optical modes in these structures. We demonstrated that the axial light confinement can be achieved by lobes in the rolling edge or rings etched in the microtube before rolling-up. Both mechanisms allow us to precisely tune the modes by the axial structuring. In the case of microtubes with lobes in the rolling edge the energies of modes with the same azimuthal mode number m can even be tailored by the shape of the lobe. For microtubes with etched rings we observe a well-pronounced splitting by broken rotational symmetry in contrast to microtubes with lobes. For different microtubes we observed not only different energy splittings but also splittings of the quality factors, i.e., a redistribution of the losses. Our experimental findings concerning the axial light confinement are in good agreement with a model based on the adiabatic separation of circular and axial light propagation. The circular propagtion can be described excellently by a waveguide model. By comparing the exact solutions of Maxwell's equations to the waveguide model for ideal rings we found that the curvature of the microtube can be neglected. The waveguide model can include the exact geometry of the microtube along the axis in the calculations. The calculated energies of the circular propagation along the microtube axis act like a quasi-potential for the axial propagation. All eigenmodes are solutions of the axial equation which is similar to the Schrödinger equation for particle waves in a one-dimensional potential. This analogy leads to intuitive solutions. For microtubes with lobes we find a good quantitative agreement and for microtubes with etched rings only a qualitative agreement between calculations and measurements. The splitting is discussed by two-dimensional FDTD simulations. We find a systematic behavior on the winding number that can also be understood in our waveguide model. By comparing the two different confinement mechanisms we find that the splitting and the axial confinement are directly related to each other.

We thank Jan Wiersig for fruitful discussions concerning the mode splitting. We acknowledge financial support by the Deutsche Forschungsgemeinschaft via SFB 508 and Graduiertenkolleg 1286.

* Electronic address: cstrelow@physnet.uni-hamburg.de

[1] V. Y. Prinz, V. A. Seleznev, A. K. Gutakovsky, A. V. Chehovskiy, V. V. Preobrazhenskii, M. A. Putyato, and T. A. Gavrilova, Physica E **6**, 828 (2000).

[2] O. G. Schmidt and K. Eberl, Nature **410**, 168 (2001).

[3] T. Kipp, H. Welsch, Ch. Strelow, Ch. Heyn, and D. Heitmann, Phys. Rev. Lett. **96**, 77403 (2006).

[4] S. Mendach, S. Kiravittaya, A. Rastelli, M. Benyoucef, R. Songmuang, and O. G. Schmidt, Phys. Rev. B **78**, 035317 (2008).

[5] Ch. Strelow, H. Rehberg, C. M. Schultz, H. Welsch, Ch. Heyn, D. Heitmann, and T. Kipp, Phys. Rev. Lett. **101**, 127403 (2008).

[6] S. Vicknesh, F. Li, and Z. Mi, Appl. Phys. Lett. **94**, 081101 (2009).

[7] F. Li, Z. Mi, and S. Vicknesh, Opt. Lett. **34**, 2915 (2009).

[8] Ch. Strelow, C. M. Schultz, H. Rehberg, H. Welsch, Ch. Heyn, D. Heitmann, and T. Kipp, Phys. Rev. B **76**, 045303 (2007).

[9] Ch. Strelow, M. Sauer, S. Fehringer, T. Korn, C. Schüller, A. Stemmann, Ch. Heyn, D. Heitmann, and T. Kipp, Appl. Phys.Lett., accepted (2009).

[10] F. Li, S. Vicknesh, and Z. Mi, Electron. Lett. **45**, 645 (2009).

[11] R. Songmuang, A. Rastelli, S. Mendach, and O. G. Schmidt, Appl. Phys. Lett. **90**, 091905 (2007).

[12] A. Bernardi, S. Kiravittaya, A. Rastelli, R. Songmuang, D. J. Thurmer, M. Benyoucef, and O. G. Schmidt, Appl. Phys. Lett. **93**, 094106 (2008).

[13] G. S. Huang, S. Kiravittaya, V. A. B. nos Quiñones, F. Ding, M. Benyoucef, A. Rastelli, Y. F. Mei, and O. G. Schmidt, Appl. Phys. Lett. **94**, 141901 (2009).

[14] V. A. B. nos Quiñones, G. Huang, J. D. Plumhof, S. Kiravittaya, A. Rastelli, Y. Mei, and O. G. Schmidt, Opt. Lett. **34**, 2345 (2009).

[15] F. Li and Z. Mi, Opt. Express **17**, 19933 (2009).

[16] M. Hosoda and T. Shigaki, Appl. Phys. Lett. **90**, 181107 (2007).

[17] Ch. Strelow, H. Rehberg, C. Schultz, H. Welsch, Ch. Heyn, D. Heitmann, and T. Kipp, Physica E **40**, 1836 (2008).

[18] S. Balakrishnan, Y. Gun'ko, Y. P. Rakovich, J. F. Donegan, T. S. Perova, and R. A. Moore, Appl. Phys. Lett. **89**, 143113(2006).

[19] J. R. Rodriguez, J. G. C. Veinot, P. Bianucci, and A. Meldrum, Appl. Phys. Lett. **92**, 131119 (2008).

[20] N. S. Kapany and J. J. Burke, *Quantum Electronics* (Academic Press, 1972).

[21] M. Pöllinger, D. O'Shea, F. Warken, and A. Rauschenbeutel, Phys. Rev. Lett. **103**, 053901 (2009).

[22] J. Wiersig, Phys. Rev. Lett. **97**, 253901 (2006).

[23] K. A. Atlasov, K. F. Karlsson, A. Rudra, B. Dwir, and E. Kapon, Opt. Express **16**, 16255 (2008).

4.3.2 Axial light confinement by radius modulations

As reported in Publication 3 and Manuscript 4 the axial light confinement in microtubes can be achieved by lobes in the rolling edge, i.e., a modulation of the winding number along the microtube axis, and by etched rings in the microtube wall, i.e., a modulation of the wall thickness along the microtube axis. We also tried to achieve axial light confinement by a radius modulation along the microtube axis. In terms of our model this radius modulation induces a quasi-potential along the microtube axis with its lowest energy in points with the largest radius. The idea based on two theoretical works that describe prolate-shaped dielectric bottle resonators [Sum04, Lou05]. Those bottle resonators can be fabricated of tapered glass fibers. Very recently, also an experimental realization was reported exhibiting ultrahigh quality factors of $3.6 \cdot 10^8$ [Pöl09]. Our idea was to induce a radius modulation by a squeezing of the microtube with additional windings. Figure 4.1(a) depicts a sketch of such a microtube and its underlying mesa. The U-shaped mesa has two very long rectangular lobes that form the additional windings during the rolling process. Figure 4.1(b) sketches the tube in a cross section of the $r-z$ plane and a parametrization of the radius modulation. The additional windings are forced to roll-up with a slightly larger rolling radius and thus exhibit additional strain energy to squeeze the first windings. Figure 4.2 shows experimental results on two microtubes of the described geometry with different distances between the rings. The microtubes were prepared of wafer A. I first discuss the measurement on the microtube with the widely spaced additional windings. The effects of the additional windings are only visible in the spatially resolved measurement in Fig. 4.2(c). The enclosed false color bar stands for all following false color images in this work. Indeed, we observe that modes are located between the rings. Many higher axial modes overlap spatially and energetically and smear out to a complex pattern. However, we find increased energies for the modes that are localized in larger distances to the center. This is

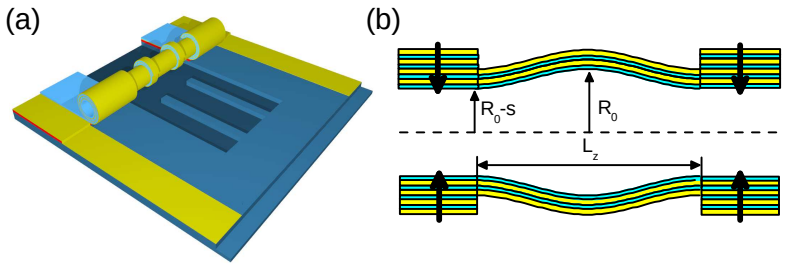

Figure 4.1: (a) Sketch of a microtube with rings formed by additional windings and the underlying mesa. (b) Cross section of the $r-z$ plane the microtube. The thick black arrows symbolize a squeezing of the inner windings which cause a radius modulation.

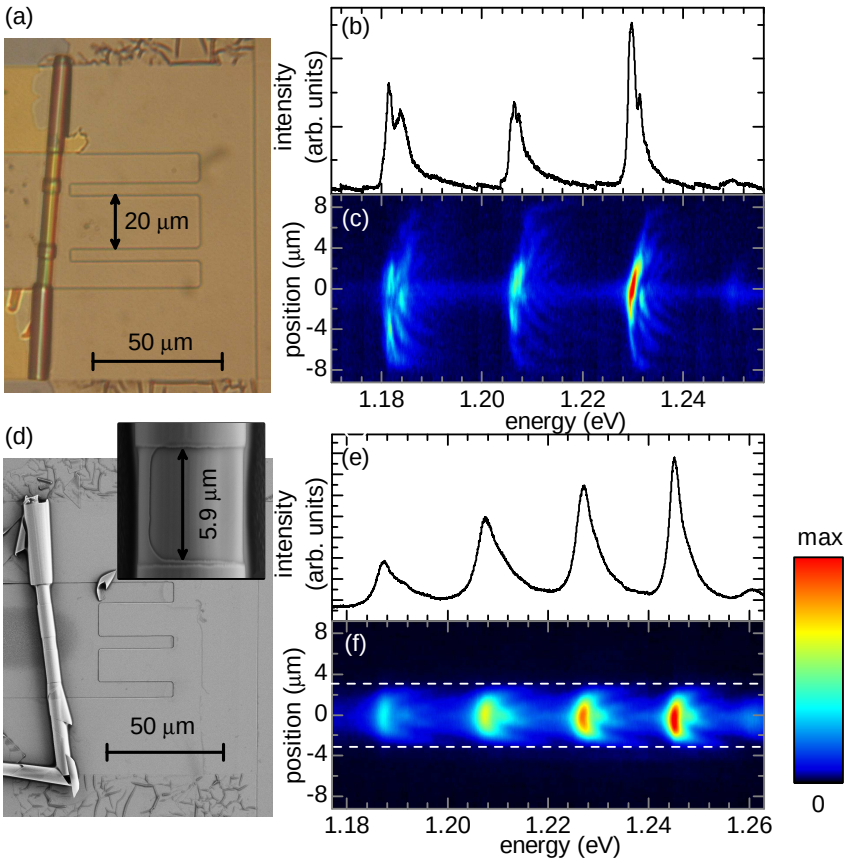

Figure 4.2: (a) Light microscope image of a microtube with rings formed by additional windings with a large distance. (b)-(c) Spatially-resolved (b) and spatially-integrated (c) photoluminescence measurements on the microtube in (a). (d) Scanning-electron micrograph of a microtube with a small distance between the rings. (e)-(f) Spatially-resolved (e) and spatially-integrated (f) photoluminescence measurements on the microtube in (d). Intensities are encoded in false colors.

what we expect since a decreasing radius leads to an increasing energy of the circular propagation and a decreasing energy of the axial propagation. Consequently, the light wave is reflected back to larger radii. However, the axial confinement length is too large to resolve individual higher axial modes, as demonstrated for other axial confinement mechanisms. Figure 4.2(e) and (f) show the measurements on the microtube with a smaller distance between the rings. In general, we observe a similar mode pattern in the spatially resolved measurements to Fig. 4.2(c). On the one hand, here we can identify the numbers of axial antinodes and allocate individual higher axal modes but, on the other hand, the modes are strongly spectrally broad-

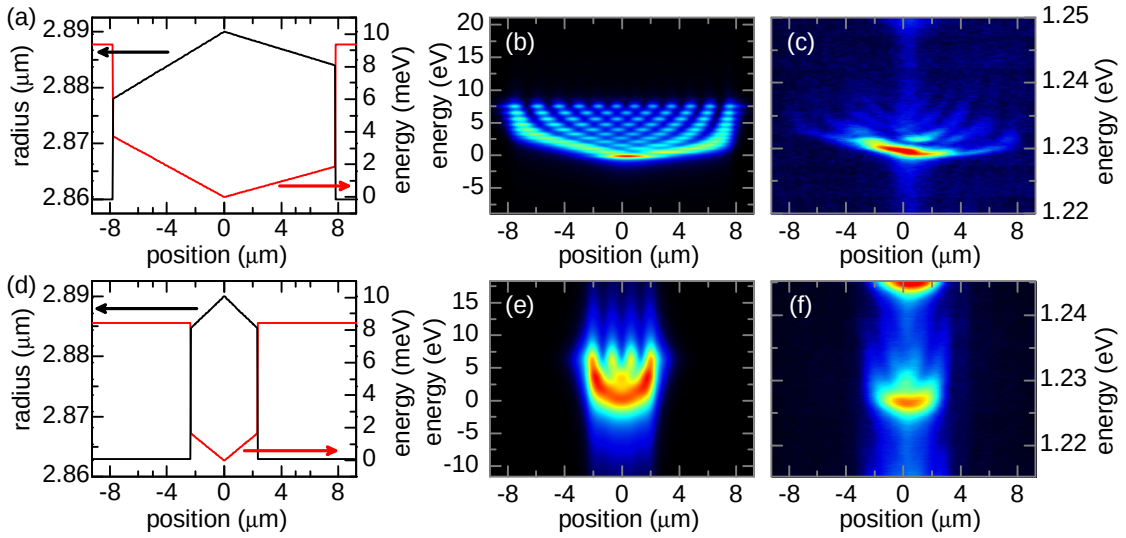

Figure 4.3: (a),(d) Calculated radius modulations and corresponding quasi-potentials obtained by fitting the results from the calculations shown in (b) and (e) to the measurements in (c) and (f), respectively. (b),(e) Calculated energies and axial intensity distributions fitted to the measurements in (c) and (f), respectively. The intensity is encoded in false colors. (a), (b) and (c) describe the sample with a large distance between the addition windings, (d), (e) and (f) the sample with a small distance.

ened. We believe that the effect of the squeezing leads only to a weak axial light confinement described by a shallow quasi-potential. For smaller axial confinement lengths the modes range widely into the barriers of the quasi-potential, as known for particle waves in shallow potentials. Consequently, for smaller axial confinement lengths the axial field distributions reach the additional windings and are affected by scattering losses at the rings. In scanning-electron micrographs we could not resolve any systematic radius modulation, but in the following I will show that very small radius modulations are sufficient to achieve a quasi-potential that confines the modes in axial direction. The problem will be solved in backward direction, which means that we consider the measurements and try to fit the results from the calculations to the measurements by changing the assumed radius modulation. For the calculations we used the procedure of numerically solving a quasi-Schrödinger as described in Manuscript 4. From the used test quasi-potential we calculate the estimated radius modulation. The simplest model is a rectangular quasi-potential with an axial confinement length of the distance between the rings. But this model failed. Moreover, we directly determined the quasi-potential from the spatially-resolved PL measurements. In principle, the line defined by the intensity maxima at the lowest energy of each axial position depicts the quasi-potential. Figure 4.3

shows the results from the fitting procedure compared to the measurement and the recalculated radius modulation. We observe that a nearly perfect agreement can be achieved between the fitted calculations and the measurements. For Fig. 4.3(b) and (d) we assumed quality factors of 1500 and 400, respectively. The depth of the quasi-potential is roughly estimated as the distance between the mode with the lowest and the highest energy in the measurements. The largest radius modulations obtained by this fitting procedure were only 30 nm for the large distance and only 27 nm for the small distance between the additional windings. This is in agreement with the fact that we could not resolve the modulation with our scanning-electron microscope. Resolving a modulation of 30 nm on a three-dimensional microtube of 2.8 µm diameter was not possible, especially, since images of microtubes tend to underly aberrations caused by charging effects by the e-beam. In Fig. 4.3 the calculated radius modulation is shown. Obviously, the squeezing induces a short-ranging change of the radius close to the rings and a weaker long-ranging modulation. In the case of Fig. 4.3(a) the modulation is slightly asymmetric. Shortly summarizing our findings on axial confinement by squeezing by additional windings we found that the mechanism in principle works. However, the effect is very weak. This leads to low quality factors by scattering at the additional windings for small confinement lengths and to the absence of individually resolved modes for long axial confinement lengths. Nevertheless, this mechanism has great potential, since the axial confinement is very smooth and thus should lead to low losses. In further experiments the radius modulation has to be increased. This would lead to a larger energetical mode spacing of the axial modes and a better localization between the rings. It might be realized by depositing rings of additional stressed material on top of the sample. Recently it has been shown that there are a couple of possibilities to engineer strain, e.g., by depositing material with different thermal expansion coefficients at different temperatures [Mei08].

4.3.3 One-dimensional photonic crystals in microtube resonators

The ability to tailor the mode energies and axial field distributions by the shape of lobes in the rolling edge demonstrated in Publication 3 and Manuscript 4 opens a wide field of possible realizations of axial mode dispersions. The generality of the theoretical description by the quasi-Schrödinger equation predicts also coupling effects of eigenmodes confined by lobes that are situated very close to each other. It should be possible to fabricate photonic molecules of even linear photonic crystals by coupling the eigenmodes of two or more lobes situated very close to each other. For laterally coupled micropillars it is reported on the realization of photonic molecules [Bay98] and linear photonic crystals [Bay99]. Very similar to the

electronic counterparts one observes mode splittings in binding and anti-binding states or the formation of energy bands with energy gaps. In this section a first approach to realize one-dimensional photonic crystals by coupled lobes will be discussed. Figure 4.4(a) sketches the geometry of a photonic crystal microtube. The rolling edge is modulated by sinusoidal lobes. If the height and the distance of the lobes is chosen small enough the eigenmodes can couple and form delocalized field distributions. Figure 4.4(b) shows an scanning-electron micrograph of a fabricated microtube with its outside rolling edge on its top. The lobes are 300 nm high and have a period of 2 µm. In the center part the microtube exhibits a defect in the periodicity. Unfortunately, these defects were produced during the e-beam writing of the shadow masks and are transferred to the geometry for all microtubes prepared with this shadow mask. Figure 4.4 depicts measurements on a microtube with nominally the same parameters of the microtube in Fig. 4.4(b). The microtube was prepared of wafer A. By scanning the microtube along the axis we found that only one half of the microtube exhibits considerably sharp modes. As described above these microtubes exhibit a defect in the center part. We determined that 6 lobes contribute to the spectrum in Fig. 4.4(c) and (d). Utilizing a cylindrical lens we excited the microtube with a line shaped focus to excite all lobes simultaneously. The spectrum consist of 4 groups of modes differing in their azimuthal mode number. In the spatially-resolved measurements we observe in each group that fundamental modes are localized in 5 of the 6 lobes [lobe 2 to 6 in Fig. 4.4(d)] indicated by the intensity maxima at the lobe positions. Between these intensity maxima at slightly higher energy we found a mode pattern formed by further modes. These modes arise from the second spatial harmonics of each lobe. Since we observe mode intensity at one energy from more than one lobe position we conclude that these second modes are coupled. For a more detailed study we also performed calculations for the microtube. In Fig. 4.5 the results are shown together with the measurement. For the calculations we used the procedure of numerically solving the quasi-Schrödinger equation for arbitrarily shaped quasi-potentials, as described in Manuscript 4. In each image the 30 modes with the lowest energy were taken into account. Calculated modes with higher energies were neglected. Fig. 4.5(b) depicts results of calculations assuming identical lobes. The quasi-potential is calculated with the parameters listed above. To compare the results to the measurements in Fig. 4.5(a) the energy offset for the fundamental modes is set to zero and aligned approximately to the measured fundamental modes. In the calculations the modes of all lobes couple and form bands. The gap between the fundamental mode band and the second states band is reproduce well by the calculation. In addition the pattern formed by the second states is very similar to the measurements. The strongest deviations are found for the individual fundamental modes. To analyze the measurements further we performed additional calculations. Ensuring that the observed effects are caused by the lobes we also calculated the mode pattern for a zero quasi-potential. Here,

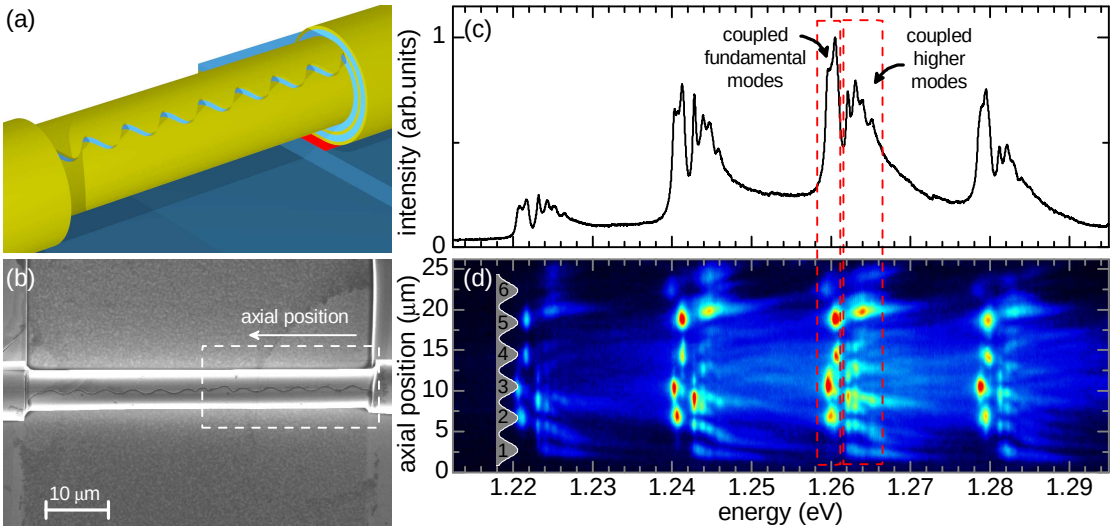

Figure 4.4: (a) Sketch of a photonic crystal microtube with a sinusoidally shaped outside rolling edge. (b) Scanning-electron micrograph of a fabricated microtube with the outside edge on top. (c)-(d) Spatially integrated (c) and spatially resolved (d) photoluminescence measurements on a different microtube, as shown in (b), but with the same geometry. The intensity is encoded in false colors. The measurements were taken in a region marked by the dashed white lines in (b). The lobe positions are sketched in (d).

the modes are confined in the artificial potential formed by the simulation area, as described in Manuscript 4. We observe a completely different mode pattern and no gap. Obviously, the measured pattern is caused by the lobes. Figure 4.5(d) shows a superposition of mode patterns that were calculated for each individual lobe in absence of the other lobes. One clearly observes an energy spacing between the band formed by the fundamental modes and by the higher modes. But the mode pattern is different for the higher modes. This clearly demonstrates that the second modes are coupled in the experiment. By a very close view one observes also that the gap is larger in the case of the coupled lobs indicating the delocalization of the modes. In a next step I tried to fit the calculations to the measurements. Therefore, I changed the depth of the quasi-potential for the individual lobes. In scanning-electron micrographs we found that the left lobe (no. 6 in Fig. 4.4) was a little bit wider than the other ones and the right lobe (no. 1 in Fig. 4.4) was very shallow. Since the lobes in this case are very small, the deep mesa etching step was performed very shortly not to destroy the lobe shape in lateral direction. Thus we could not resolve the exact geometry of the lobes from the mesa as input for the calculation. Nevertheless, the calculations shown in Fig. 4.5(e) for the estimated quasi-potential are very similar to the measurements. For slightly different lobes we find that the fundamental

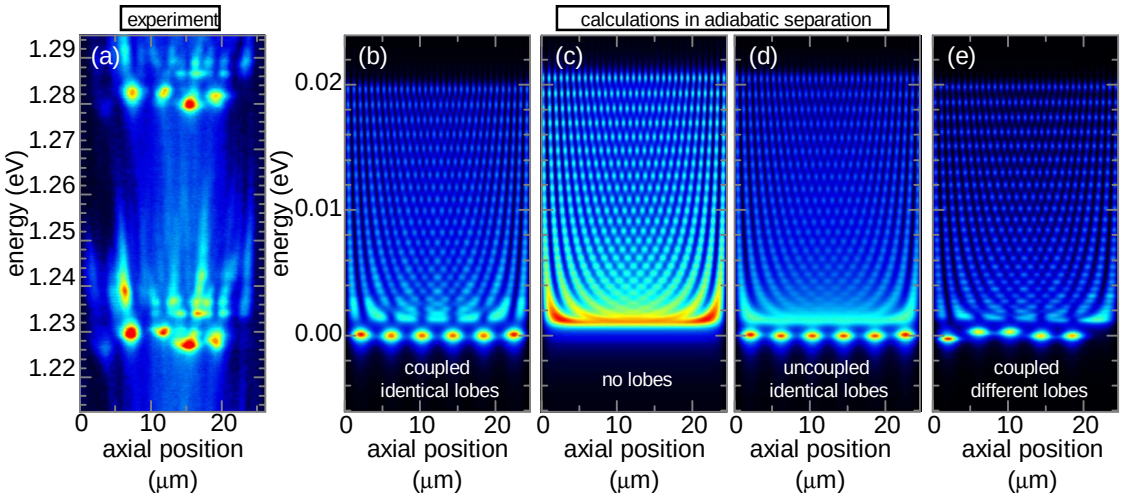

Figure 4.5: (a) Enlarged view of a part of the measurement in Fig. 4.4(d). (b)-(e) Energies and axial field distributions for one azimuthal mode number m calculated by numerically solving the quasi-Schrödinger equation for different quasi-potentials: (b) a sinusoidal potential over 6 periods, (c) the zero potential (artificial confinement in the simulation area), (d) superposition of the results for the individual lobe quasi-potential in absence of the other ones, (e) sinusoidal quasi-potential over 6 periods with different amplitudes in the different periods. The field intensity is encoded in false colors.

modes partly decouple, whereas the higher modes stay coupled. Although the calculation with the different lobes is very similar to the measurement, we cannot state that differently shaped lobes fully explain the deviations of the measurements to the calculations. In our calculations the splitting by the broken rotational symmetry is not taken into account. In Manuscript 4 we observed that this splitting can have a large impact on the energetical position of the modes. In conclusion, we observed that it is indeed possible to fabricate linear photonic crystals by microtubes with lobes in the rolling edge. However, the influence of defects in the periodicity has to be studied more extensively. In general, photonic crystal microtubes could be very interesting to achieve a more smooth axial light confinement by the formation of stop bands. This might increase the quality factors.

4.3.4 Three-dimensional FDTD simulations on microtubes with etched rings

In this section I present additional results on microtubes with etched rings obtained by three-dimensional FDTD simulations with the commercial software "Lumerical

FDTD Solutions". The design of the simulation area is depicted in Fig. 4.6. The geometry of the microtube is chosen similarly to the ones fabricated from wafer E. The microtube has a radius of 1.8 µm and 1.2 windings which is very close to the geometry of the microtube investigated in Fig. 19 (b) in Manuscript 4. The structure is formed by 240 cuboids that are arranged in a spiral to realize the rolled-up structure of the tube. The refractive index was set to n=3.5. As depicted in Fig. 4.6 (b) and (c) by the dashed black lines we defined a ring of 2.65 µm length and 59 nm thickness between two rings of 55 nm thickness. As the source we chose a plane wave source, emitting in the thicker ring but only over the half axial ring length [see Fig. 4.6(c)], to excite both symmetric and antisymmetric modes in axial direction. The wavelength was set to 885 nm with a FWHM of 200 nm. The polarization was set to linear with 45 degree to the z axis, as shown in Fig. 4.6 (a) and (c). The time evolution of the field was recorded in all positions of a line-shaped time monitor. We simulated for 20000 fs in a region of 5 µm×5 µm×5.5 µm resolved by $270 \times 270 \times 270$ grid points, terminated by perfectly-matching layers (PML) that completely absorb incident light. The results are shown in Fig. 4.7. The time evolution of the electric field in each point of the time monitor was Fourier-transformed. The intensities in dependence on the energy and axial position are encoded as false colors in Fig. 4.7(b) and spatially integrated in Fig. 4.7(a). Before discussing the results, I have to point out that the spatial resolution of the grid is not sufficient to make quantitative statements. However, the simulations demonstrate the qualitative behavior of the system. In rough checks of the convergence, I found that the absolute energy still decreases with refined grids, whereas the axial spacings were affected only little.

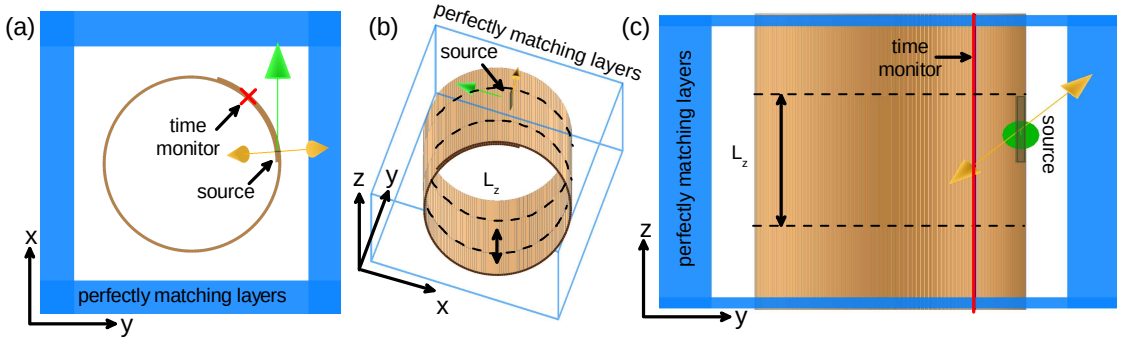

Figure 4.6: Setup for three-dimensional FDTD simulations on a microtube with etched rings in different views. (a) Cross section of the $r - \varphi$ plane of the microtube. (b) Three dimensional view. The interfaces between the thick ring in the center and the thinner rings are marked by dashed black lines. (c) Side view of the microtube to elucidate the axial positions of the source and the time monitor.

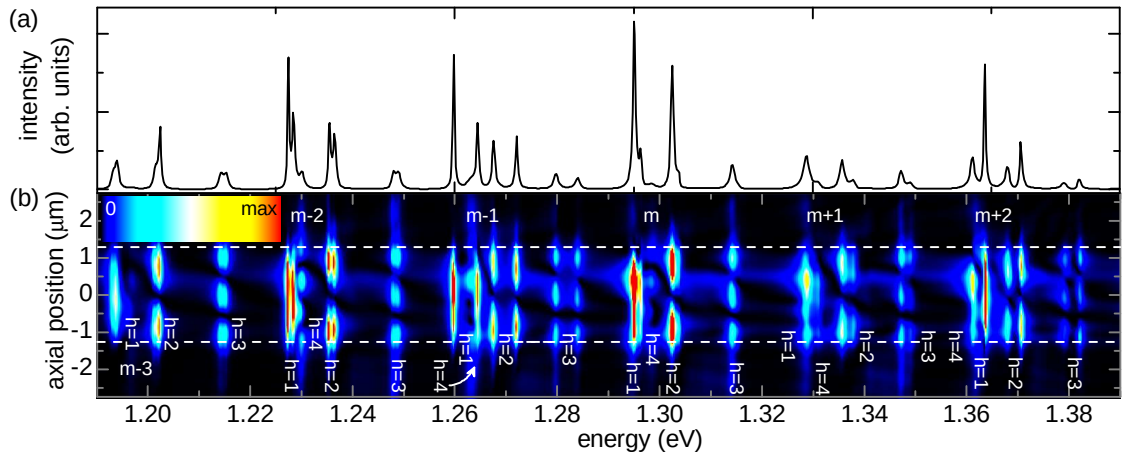

Figure 4.7: Spatially-integrated (a) and spatially-resolved (b) intensities recorded in the line shaped time monitor depicted in Fig. 4.6. The false colors encode the intensity. The modes are labeled with azimuthal mode number m and axial mode numbers h.

In Fig. 4.7 one clearly observes the splitting by broken rotational symmetry, as found in the measurements shown in Manuscript 4. The splitting is different for different azimuthal mode numbers m, but equal for all axial modes h with the same m. This is an important finding since it ensures that the splitting in microtubes with etched rings is only induced by the broken rotational symmetry in the $r - \varphi$ plane and not affected by the axial geometry. However, this statement is only valid for axially symmetric microtubes. Axial asymmetries can influence the splitting, as demonstrated in Manuscript 4. In the simulation we observe also other interesting features. Especially, the higher axial modes tent to have an increased field intensity in the etched rings which is not expected in the framework of our model with the quasi-potentials. I believe that this effect is caused by couplings to modes with smaller m but higher h. For example at 1.33 eV the $m+1, h=1$ and the $m, h=4$ modes have nearly the same energy. Here, it might be that the intensities are not only a superposition of the intensity distributions of the single modes but the modes form hybridized modes. These couplings might not only be possible with modes bound between the etched rings but also with free axial modes and could be an important loss channel. Interestingly, all h=3 modes exhibit well pronounced intensity contributions in the etched rings. This might be because of a coupling with quasi-free modes that are confined in axial direction by the PML. It is known that the PML reflect parts of light waves that do not incident normaly on the PML.

Finally, I want to address the amount of the axial mode splitting. In Manuscript 4 we found that the measured axial mode splittings are much larger than predicted by

the model with the quasi-potentials. At about 1.37 eV we find a splitting between the $h = 1$ and the $h = 2$ modes of about 7.4 meV. In Manuscript 4 we observed in our experiments that the axial mode splitting is larger than in the calculations using the adiabatic separation, even if an infinite quasi-potential is assumed. In the measurements shown in Fig. 19 (b) in Manuscript 4 we measured 6.8 meV. Both values are in considerably good agreement but, more important, they are both larger than the calculated splitting in the adiabatic separation. Actually, the three-dimensional confinement leads to the deviation between our measurements and our model and other unknown effects like, for example, strain can be excluded.

4.4 Optical Modes Excited by Evanescent-Wave-Coupled Nanocrystals

Publication 5 arose out of a close cooperation with the diploma student Kay Dietrich during his diploma thesis. The microtubes were fabricated from wafer C and contained no internal emitters.

The advantage of microtubes resonators is that emitters can be positioned very close to the field maximum of the optical microtube mode during the growth by MBE. Thus emitters centered within the strained bilayer can couple very efficiently to the light field of the microtube modes. But the multi-walled structure formed by the self-rolling mechanism allows us also to position material between the bilayers which is situated automatically very close to the field maximum in the rolled-up structure. The material can simply be brought onto the bilayer before rolling up. This offers the unique possibility to use chemically synthesized nanocrystals as emitters in MBE grown microcavities which is very difficult for other microcavities since the emitters has to be embedded during the growth. But up to now we could not solve the problem that the nanocrystals get destroyed by the HF etch which is necessary in the selective etching process during the self-rolling.

The second idea was to bring the nanoparticles into evanescent coupling with the microtube modes. The thin walls exhibit the unique property of very long reaching evanescent fields inside and outside the microtube. First experiments failed trying to bring a solution of nanocrystals on top of rolled-up microtubes after the HF etching by spin-coating. The solution was either to much concentrated and covered the whole sample by a film or the PL signal of the nanocrystals was to weak in the case of lower concentrations. Finally, we succeeded in filling the solution of nanoparticles inside the hollow core of the microtube using a micropipette and a micro-positioning system. We observed the typical spectrum of microtube bottle resonators with an astonishingly large signal-to-background signal. An important

point for the realization was also the axial light confinement. In this time the axial light confinement by etched rings was developed.

As described in Publication 5 the realization of this experiment touches strongly the field of optofluidics [Mon07] in which microtubes should be ideal candidates in microfluidic networks, e.g. in "lab-on-a-chip" devices. In addition hybrid systems of chemically synthesized nanoparticles and rolled-up microtubes might be a new type of laser device. Due to the long ranging evanescent fields a large fraction of the field intensity lies outside of the microtube wall and thus the embedded nanocrystal solution could deliver a high modal gain. All in all this experiment is an absolute key experiment and new further experiments should be performed.

The sample fabrications, the fluid filling and all experiments were done by Kay Dietrich. Details of the development process described above can be found in his Diploma thesis [Die08]. The development of the axial confinement and the calculations were done by me. The publication was written by me and Tobias Kipp.

Publication 5

Optical Modes Excited by
Evanescent-Wave-Coupled PbS Nanocrystals
in Semiconductor Microtube Bottle Resonators

K. Dietrich, Ch. Strelow, C. Schliehe, Ch. Heyn, A. Stemmann,
S. Schwaiger, S. Mendach, A. Mews, H. Weller,
D. Heitmann, and T. Kipp

Nano Letters **10 (2)**, 627–631 (2009)

NANO LETTERS

pubs.acs.org/NanoLett

Optical Modes Excited by Evanescent-Wave-Coupled PbS Nanocrystals in Semiconductor Microtube Bottle Resonators

Kay Dietrich,[†] Christian Strelow,*[,†] Constanze Schliehe,[‡] Christian Heyn,[†] Andrea Stemmann,[†] Stephan Schwaiger,[†] Stefan Mendach,[†] Alf Mews,[‡] Horst Weller,[‡] Detlef Heitmann,[†] and Tobias Kipp*[,†,‡]

[†]Institut für Angewandte Physik und Zentrum für Mikrostrukturforschung, Universität Hamburg, Jungiusstrasse 11, 20355 Hamburg, Germany, and [‡]Institut für Physikalische Chemie, Universität Hamburg, Grindelallee 117, 20146 Hamburg, Germany

ABSTRACT We report on optical modes in rolled-up microtube resonators that are excited by PbS nanocrystals filled into the microtube core. Long ranging evanescent fields into the very thin walled microtubes cause strong emission of the nanocrystals into the resonator modes and a mode shift after a self-removal of the solvent. We present a method to precisely control the number, the energy and the localization of the modes along the microtube axis.

KEYWORDS Optical microcavities, rolled-up semiconductors, microtube bottle resonators, PbS nanocrystals, evanescent fields

Optical semiconductor microcavities have gained considerable interest in the past due to their unique potential in studying fundamental light-matter interaction and for applications in optoelectronic devices. The research on active microcavities with incorporated nanoemitters focused mainly on structures fabricated from epitaxially grown layer systems including self-assembled quantum dots.[1,2] Despite all advantages of epitaxial growth, like extreme low defect density, high-purity, and atomic layer precision, it also strongly limits the properties of the embedded nanoemitters. Many of these limitations concerning, for example, material, size, shape, density, and emission energy, do not exist for wet-chemically prepared nanoemitters. Thus, the combination of wet-chemically prepared, colloidal nanocrystals (NCs) with epitaxial microcavities is of fundamental interest.[3−5] We show that passive optical semiconductor microtube resonators fabricated from epitaxial layer systems can indeed be efficiently coupled to wet-chemically synthesized NC emitters. These novel hybrid systems open up new perspectives of research since they allow for a much larger variety of combinations of different NC emitters with optical resonators as all-epitaxial systems do. Attractively, this hybrid system is fully compatible to the research field of optofluidics. This field combines (i) microfluidics and (ii) microoptics, for example, in "lab-on-a-chip" devices, in which fluids are either analyzed by optical devices acting as sensors or fluids are used to dynamically change the optical properties of such devices.[6]

The research on micro- and nanotubes fabricated by exploiting the self-rolling mechanism of strained semiconductor layer systems lifted off from a substrate started about one decade ago.[7,8] Since then many different paths to functionalize these three-dimensional structures have been investigated. Relating to (i) microfluidics, the capillary-forces driven filling of such tubes with liquids has been demonstrated by monitoring the fluorescence of dyes[9] or colloidal NCs[10] solved in the liquid. Furthermore, the integration of microtubes into a microfluidic device has been shown.[11] Relating to (ii) microoptics, it has been demonstrated that freestanding microtube bridges with optical emitters embedded inside their walls can act as active optical microcavities.[12] Here, the tubes' walls serve as waveguides for the luminescence light of the internal emitters. The azimuthally guided light interferes after a round trip along the circumference of the tube, which leads to optical modes for constructive interference. Extensive studies of such microtube resonators[12−23] deal with different material systems, based on, for example, InGaAlAs or Si, and different emitters, like, for example, epitaxially grown quantum dots or quantum wells. The ringlike cross-sectional shape of a microtube has the strongest impact on the optical modes since it ensures a two-dimensional light confinement in azimuthal and radial direction. Recently it was shown that a precisely tailorable confinement of light also along the tube axis can be achieved by structuring the rolling edges of a microtube, leading to so-called microtube bottle resonators.[17] Microtube resona-

* To whom correspondence should be addressed. E-mail: (C.S.) cstrelow@physnet.uni-hamburg.de; (T.K.) kipp@chemie.uni-hamburg.de.
Received for review: 11/5/2009
Published on Web: 01/05/2010

DOI: 10.1021/nl9036966 | *Nano Lett.* **2010,** *10,* 627-631

NANO LETTERS

tors exhibit the striking features of a nearly perfect overlap between embedded emitters and the intensity maximum of the optical modes. Furthermore, because of the thinness of the waveguiding tube walls, strong evanescent fields of the optical eigenmodes occur in the vicinity of the thin walls. These evanescent fields are the reason that active microtube resonators can act as sensitive refractometers for liquids inside the microtube core, as has been recently demonstrated.[20]

In this work, we investigate the combination of passive rolled-up microtube resonators with chemically synthesized PbS NCs. The microtube resonators are based on the InGaAlAs material system and exhibit a novel confinement mechanism for light propagating along the tube axis. The NCs dispersed in toluene are brought into the microtube core by fluid filling. Spatially and energy resolved photoluminescence (PL) measurements prove an efficient evanescent-field coupling of the NCs to the optical modes of the microtube resonator. We demonstrate that hybrid systems of microtubes and chemically synthesized nanocrystals can be very useful components in microoptical devices and in optofluidic networks.

Starting point for the fabrication of our microtube resonators is a layered sample grown by molecular beam epitaxy on a GaAs substrate consisting of a 40 nm AlAs sacrificial layer and a strained bilayer of 15 nm $Al_{0.31}In_{0.15}Ga_{0.54}As$ and 25 nm $Al_{0.20}Ga_{0.80}As$. The Al concentration in the strained bilayer was chosen to maximize the bandgaps but still allow for a selective etching of only the sacrificial layer in the later HF etching step. The further processing principally follows the one described in refs 12 and 15, a U-shaped strained mesa is prepared onto the sample that forms freestanding microtube bridges when it is lifted off from the substrate by selectively etching the sacrificial layer. Figure 1a shows a light microscope image of the microtube on which all measurements described in the following have been performed. Here, the U-shaped mesa is outlined by the coarsely dashed line. The freestanding part of the tube has a diameter of 5.48 μm and exhibits 2.31 revolutions. Total internal reflection leads to waveguiding in the tube wall and to the formation of ring modes by constructive interference after a round trip.[12] In contrast to other cylindrical microcavities our microtubes also allow a precise control of the axial light confinement. In earlier experiments we achieved a controlled three-dimensional confinement of light by lithographically defining lobes in the rolling edges of the strained mesa before rolling it up.[17] Here, we report on a different axial confinement mechanism induced by lithographically defining two regions of a thinner bilayer, by etching about $t = 3.7$ nm into the U-mesa before the rolling process. These regions are marked by the yellow dashed squares in Figure 1a. The lengths of the squares are chosen to equal the circumference of the microtube. Figure 1b sketches the geometry of the freestanding part of the microtube when the U-shaped mesa has rolled-up. The definition of the

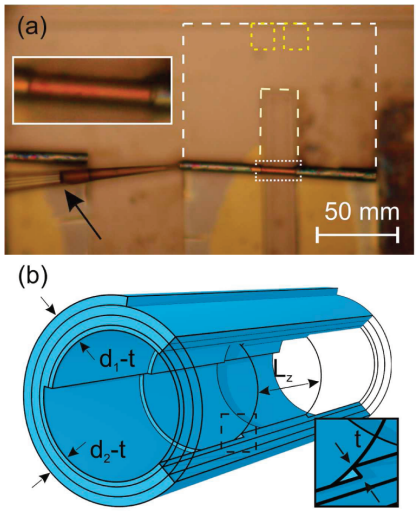

FIGURE 1. (a) Light microscope image of a microtube during the filling process. The filling level in the micropipet (arrow), the etched regions (yellow squares) forming the thinner rings in the rolled-up microtube, and the U-shaped mesa (dashed white lines) are marked. The inset gives an enlarged view of the freestanding part of the microtube marked by the dotted rectangle. (b) Unscaled sketch of the freestanding part of the microtube. One part of the wall is left transparent for better view.

squares results in a slightly thicker ring of the width $L_z = 5.8$ μm in the middle part of the microtube enclosed by thinner rings on both sides. This preparation leads to a very precise localization of the resonator modes between the etched rings as will be discussed in detail below.

As nanoemitters to be injected into the core of the passive microtube, we chose PbS NCs. These NCs were fabricated by the hot injection synthesis as described in ref 24. They were dispersed in a toluene solution. Transmission electron microscope images reveal diameters of the NCs around 3.4 nm. The PL spectrum of a NC ensemble at low temperature $T \sim 7$ K peaks out at 1.3 eV with a full width at half-maximum of about 0.1 eV due to an inhomogeneous size distribution of the emitters. The emission energy of the NCs is below the bandgap of the microtube material, thus, the microtube is transparent for the emitted light.

For the filling of the microtubes, we used a micropipet that is connected to a syringe and that is attached to a micro positioning system. Figure 1a shows the micropipet inserted into the microtube. It is partly filled with a solution of nanocrystals which appears dark (see the black arrow). Depending on the wall thickness of the investigated tube the filling level of the microtube can in most cases be controlled by a weak contrast in the microscope view. We observed that on a time scale of about 1 day after the filling the solution has spilled out of the tube. Shadows in the microscope view indicate that the spilled-out solution has partly wetted the microtube. In this situation, the syringe-coupled micropipet was used to suck in the spilled-out liquid from

DOI: 10.1021/nl9036966 | *Nano Lett.* **2010,** *10,* 627-631

NANO LETTERS

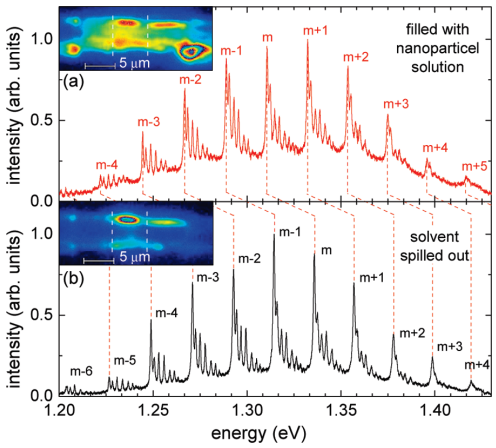

FIGURE 2. (a,b) Spatially integrated micro PL spectra of the microtube in 1 filled with PbS nanocrystal solution (a) and with spilled-out solvent (b). The modes are marked by their azimuthal mode number m. The insets depict PL emission images of the filled and the spilled-out microtube in the region of the inset in Figure 1a.

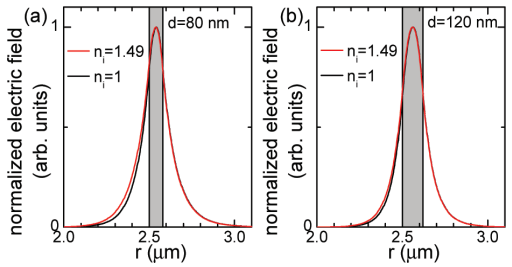

FIGURE 3. Radial field distribution calculated for a ring with the diameter of our tube and a wall thickness of (a) $d_1 = 80$ nm and (b) $d_2 = 120$ nm. The refractive indices of the tube wall (gray shaded region) is assumed to be 3.3. Outside the tube we set $n = 1$. For the red (black) curve a refractive index inside the tube of $n_i = 1.49$ for toluene ($n_i = 1$ for vacuum) is used.

the sample. Interestingly, the spilled-out liquid was now clear in contrast to the inserted solution. This already indicates that a large amount of the dispersed NCs stayed inside the microtube while the solvent spilled out.

We performed micro PL measurements on the microtube shown in Figure 1a (i) in its original state before filling with NCs, (ii) after filling with the nanocrystal solution, but before the leakage of the solvent, and (iii) after the leakage of the solvent. For the measurements, the sample was mounted in a low-temperature ($T = 7$ K) micro-PL setup that images the tube on the entrance slit of a grating spectrometer. Light from each position along the entrance slit is dispersed onto a charge coupled device detector. Thus by aligning the tube image parallel to the entrance slit we can investigate the spectrum with spatial resolution along the tube axis. For the excitation we used a Ti:sapphire laser with a wavelength fixed to 800 nm. The focus was widened by a cylindrical lens to obtain a line focus along the tube axis.

Measurements on the original microtube reveal no signal from the tube itself. This is because the excitation energy is below the bandgap of the microtube material. The spectra drastically change for the filled microtube. Figure 2a shows a spectrum of the microtube filled with the nanocrystal solution spatially integrated over the region of the thicker ring in the center of the tube (cf. Figure 1b). One observes the typical mode sequences of microtube bottle resonators,[17] groups of modes that differ from each other in the azimuthal confinement ($2m$ antinodes in azimuthal direction) and the modes in each group that differ in the axial confinement (h antinodes in axial direction). The axial confinement mechanism of the investigated microtube will be addressed in detail below. The superposition of sharp optical modes on the rather broad emission peak of the NCs clearly demonstrates the coupling of the NCs' PL light to the bottle resonator via its evanescent fields.

By solving Maxwell's equations for dielectric rings (as shown, for example, in refs 25 and 26) the radial field distribution and particularly the evanescent fields can be calculated. Figure 3 shows the radial field distributions calculated for a ring with the diameter of our tube and a wall thickness of (a) $d_1 = 80$ nm and (b) $d_2 = 120$ nm. The refractive index of the tube wall was set to 3.3. For the red curve, we assumed a refractive index of $n_i = 1.49$ for toluene inside the tube. (For comparison, the black curve is calculated for $n_i = 1$). The evanescent fields inside the tube decay nearly exponentially with a decay length of about (a) 86 and (b) 64 nm. The respective field strength on the surface is still (a) 82 and (b) 68 % of the maximum field strength inside the microtube. The large fraction of the field distribution inside the tube is peculiar for rolled-up microtube resonators with their very thin waveguiding walls. It ensures an efficient coupling of the external emitters to the optical modes and opens up, for example, the possibility to reach evanescent-field-coupled lasing of external emitters in microtube resonators. A similar laser scheme has been demonstrated for a dye solution flowing through a polystyrene coated fused-silica capillary with an inner diameter about 30 times larger than our microtubes.[27] Rolled-up microtubes' capability of lasing has been very recently demonstrated, but with embedded quantum wells as internal gain instead of external NCs.[28] Lasing of NCs has been, for example, reached by coupling to whispering-gallery modes of solid microcylinders[29] or microspheres.[30]

Figure 2b shows a measurement corresponding to the one in panel a but after the solvent spilled out of the microtube. Interestingly, also the spilled-out microtube exhibits signals from the nanocrystals, actually proving that a large amount of the dispersed NCs stayed inside the microtube while the solvent spilled out. Compared to the filled microtube, the spectrum of the microtube with the spilled-out solvent shows an energy shift of all modes and an enhancement of the mode-to-background ratio. The shifting

DOI: 10.1021/nl9036966 | Nano Lett. 2010, 10, 627-631

NANO LETTERS

is again an effect induced by the large evanescent fields in the microtube core, since they make the modes very sensitive to the environment inside the tube. By solving again Maxwell's equations for dielectric rings with the diameter of our microtube and with a core refractive index of either 1.49 (toluene) or 1 (vacuum) we find a blue shift of 23.9 and 10.1 meV for a ring thickness of $d_1 = 80$ nm and $d_2 = 120$ nm, respectively, leading to an average blue shift of about 19.8 meV for our microtube geometry. In finite-difference time-domain simulations for the real rolled-up geometry we found a value of about 19.3 meV. These values are in good agreement with the blue shift indicated by the dashed lines in Figure 2 (25.6 meV for a mode energy around 1.3 eV). The very sensitive behavior of microtube modes on the refractive index inside the tube has also been reported in ref 20 and demonstrates that microtube resonators can be used as very sensitive sensors in optofluidic networks.

The enhancement of the mode-to-background ratio for the spilled-out microtube compared to the filled one is because, in the case of the spilled-out solvent, all the NCs inside the tube are located close to the tube wall and can easily couple to the evanescent field of the resonator modes. In contrast, for the filled microtube a considerable amount of NCs is located away from the tube wall without the possibility to couple to the evanescent fields. Their emission thus leads to an increase of the background signal. This behavior also becomes obvious in the emission images of the filled and the spilled-out microtube shown in the insets of Figure 1a,b, respectively. In each image the microtube is nearly horizontally aligned (like in the inset of Figure 1a) and the region of the thicker ring in the center of the tube roughly extends between the two dashed vertical lines (with a distance of $L_z = 5.8\,\mu$m). In both cases, one observes strong emission from regions close to the walls of the microtube, but the filled microtube shows much stronger emission from particles from the center of the tube not coupling to the evanescent fields of the resonant modes.

The procedure of depositing chemically synthesized nanocrystals inside the tube and removing the solvent is a very elegant way to place emitters very close to the wall and allows for a very efficient coupling of light into the resonator without integrating them directly into the resonator material. It provides significant flexibility in the preparation of novel microoptical devices with a large variety of possible emitters. The coupling of emitters in the case of a filled microtube enables one to change the emission of the microtube after fabrication and integration in a device by changing the inserted emitters. Consequently, rolled-up microtube resonators are very flexible components in "lab-on-a-chip" devices.

In the following, we want to focus on the light confinement for the modes along the tube axis and, especially, on the novel confining mechanism. In Figure 4a, we present a part of the spectrum in Figure 2b of the spilled-out microtube together with its related spatially resolved measurements in

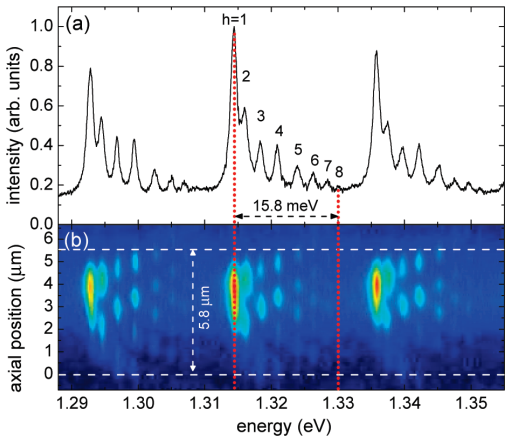

FIGURE 4. (a) Part of the spatially integrated micro PL spectrum in Figure 2b. Exemplary, the modes are labeled with their axial mode number *h*. (b) Spatially resolved PL image of the spectrum in (a). The region between the etched rings is marked by white dashed lines.

Figure 4b. One observes that all modes are localized in a special region along the tube axis. This region, that is marked by dashed white lines, can be identified as the region between the etched rings. The axial intensity distributions of the modes in every group exhibit an increasing number h of antinodes with increasing energy. In ref 17, we showed for microtube bottle resonators with specially structured rolling edges that the modes arise from a superposition of circulating light propagation around the circumference and back- and forth- reflected light along the tube axis. The axial modes can be interpreted as standing waves in a quasi-potential along the tube axis. This quasi-potential is induced by the circulating part of the light propagation and can be determined by the microtube geometry. In the case of this work the quasi-potential can be determined as follows: The energy of the circular part of the light propagation of an eigenmode jumps from the region between the etched rings labeled with L_z in Figure 1b to the region with edged rings. These jumps leads to a rectangular quasi-potential for the axial propagation. We can calculate the amount of the energy jumps using our model introduced in ref 15. The cross section of the tube can be described as two connected wave guides of different thicknesses d_1 and d_2 between the etched rings and d_1-t and d_2-t within the etched rings, respectively. To account for the ringlike structure, azimuthal eigenmodes have to fulfill periodic boundary conditions at the ends of the connected waveguides. We calculate an energy difference of 16.2 meV for the microtube in this work. From Figure 4, we can estimate the experimentally observed depth of the actual quasi-potential. The energy difference between the $h = 1$ mode, which is the ground state in the quasi-potential, and the $h = 8$ mode, which is the highest axial mode in the quasi-potential, is about 15.8 meV. This is in very good agreement with the theoretical value, espe-

DOI: 10.1021/nl9036966 | *Nano Lett.* **2010,** *10,* 627-631

NANO LETTERS

cially if one keeps in mind that the depth of a potential is always larger than the energy separation between the lowest ($h = 1$) and the highest ($h = 8$) bound state. The novel axial confinement mechanism presented here allows a precise localization of the resonator modes in regions along the microtube axis that are predefined by the etched rings. The shape of the quasi-potential, that is, the depth and the width L_z, can be adjusted in a simple way by the etching depth and the separation of the etched rings, respectively. This enables one to tailor the number and the energies of the confined axial modes. We think that, generally, the formation of three dimensionally confined modes is an intrinsic feature of tubular microcavities; since the modes mainly propagate in azimuthal direction around the tube axis, very small inhomogeneities, like changes of the radius, wall thickness, refractive index, and so forth, that are present in all fabricated structures lead to total refection also in axial direction. This results in an arbitrary pinning of modes at axial inhomogeneities and, for weak axial confinements, to an inhomogeneous broadening of the high-energy side of optical modes, as observed in many experiments.[12,14,20−22,31] Thus, for applications of tubular microcavities in, for example, novel light sources and/or integrated optofluidic networks, the axial light confinement is very important in order to control axial mode localization and to achieve well-defined, sharp modes. As shown above, axial light confinement in rolled-up microtube resonators can be controlled in a simple and precise way.

In conclusion, we demonstrate efficient evanescent-field coupling of NC emitters to optical modes of passive rolled-up microtube bottle resonators. The NCs are brought into the microtube core by fluid filling. These hybrid systems offer a considerable flexibility in the combination of semiconductor microcavities fabricated from epitaxially grown samples with wet-chemically synthesized NCs of different optical properties induced by different material, size, and shape. Microtube bottle resonators are excellent components for the integration into optofluidic networks. The fabrication process allows to prepare fluid channels with very thin walls that can simultaneously act as optical microcavities with long ranging evanescent fields. Therefore, on the one hand they can be excited efficiently by chemically synthesized nanoparticles that are filled into the microtube after fabrication. On the other hand, they can act as sensitive sensors for fluids in the microtube. The precise control of the axial light confinement allows one a localization of tailored modes in small and predefined regions, which is an important feature for components in optofluidic networks.

Acknowledgment. We acknowledge financial support by the Deutsche Forschungsgemeinschaft via SFB 508, Graduiertenkolleg 1286, and grant no. KI 1257/1-1.

REFERENCES AND NOTES

(1) Vahala, K. J. *Nature* **2003**, *424*, 839.
(2) Khitrova, G.; Gibbs, H. M.; Kiraz, M.; Koch, S. W.; Scherer, A. *Nat. Phys.* **2006**, *2*, 81.
(3) Woggon, U. *J. Appl. Phys.* **2007**, *101*, 081727.
(4) Vignolini, S.; Riboli, F.; Intonti, F.; Belotti, M.; Gurioli, M.; Chen, Y.; Colocci, M.; Andreani, L. C.; Wiersma, D. S. *Phys. Rev. E* **2008**, *78*, 045603.
(5) Barth, M.; Stingl, J.; Kouba, J.; Nüsse, N.; Löchel, B.; Benson, O. *Phys. Status Solidi B* **2009**, *246*, 298.
(6) Monat, C.; Domachuk, P.; Eggleton, B. J. *Nat. Photonics* **2007**, *1*, 106–114.
(7) Prinz, V. Y.; Seleznev, V. A.; Gutakovsky, A. K.; Chehovskiy, A. V.; Preobrazhenskii, V. V.; Putyato, M. A.; Gavrilova, T. A. *Phys. E* **2000**, *6*, 828.
(8) Schmidt, O. G.; Eberl, K. *Nature* **2001**, *410*, 168.
(9) Deneke, C.; Schmidt, O. G. *Appl. Phys. Lett.* **2004**, *85*, 2914.
(10) Giordano, C.; Todaro, M. T.; Salhi, A.; Martiradonna, L.; Viola, I.; Passabí, A.; Carbone, L.; Gigli, G.; Passaseo, A.; Vittorio, M. D. *Microelectron. Eng.* **2007**, *84*, 1408–1411.
(11) Thurmer, D. J.; Deneke, C.; Mei, Y.; Schmidt, O. G. *Appl. Phys. Lett.* **2006**, *89*, 223507.
(12) Kipp, T.; Welsch, H.; Strelow, C.; Heyn, C.; Heitmann, D. *Phys. Rev. Lett.* **2006**, *96*, 77403.
(13) Mendach, S.; Songmuang, R.; Kiravittaya, S.; Rastelli, A.; Benyoucef, M.; Schmidt, O. G. *Appl. Phys. Lett.* **2006**, *88*, 111120.
(14) Songmuang, R.; Rastelli, A.; Mendach, S.; Schmidt, O. G. *Appl. Phys. Lett.* **2007**, *90*, 091905.
(15) Strelow, C.; Schultz, C. M.; Rehberg, H.; Welsch, H.; Heyn, C.; Heitmann, D.; Kipp, T. *Phys. Rev. B* **2007**, *76*, 045303.
(16) Kipp, T.; Strelow, C.; Welsch, H.; Heyn, C.; Heitmann, D. *AIP Conf. Proc.* **2007**, *893*, 1127–1128.
(17) Strelow, C.; Rehberg, H.; Schultz, C. M.; Welsch, H.; Heyn, C.; Heitmann, D.; Kipp, T. *Phys. Rev. Lett.* **2008**, *101*, 127403.
(18) Strelow, C.; Rehberg, H.; Schultz, C.; Welsch, H.; Heyn, C.; Heitmann, D.; Kipp, T. *Phys. E* **2008**, *40*, 1836–1839.
(19) Mendach, S.; Kiravittaya, S.; Rastelli, A.; Benyoucef, M.; Songmuang, R.; Schmidt, O. G. *Phys. Rev. B* **2008**, *78*, 035317.
(20) Bernardi, A.; Kiravittaya, S.; Rastelli, A.; Songmuang, R.; Thurmer, D. J.; Benyoucef, M.; Schmidt, O. G. *Appl. Phys. Lett.* **2008**, *93*, 094106.
(21) Huang, G. S.; Kiravittaya, S.; Bolaños Quiñones, V. A.; Ding, F.; Benyoucef, M.; Rastelli, A.; Mei, Y. F.; Schmidt, O. G. *Appl. Phys. Lett.* **2009**, *94*, 141901.
(22) Bolaños Quiñones, V. A.; Huang, G.; Plumhof, J. D.; Kiravittaya, S.; Rastelli, A.; Mei, Y.; Schmidt, O. G. *Opt. Lett.* **2009**, *34*, 2345–2347.
(23) Vicknesh, S.; Li, F.; Mi, Z. *Appl. Phys. Lett.* **2009**, *94*, 081101.
(24) Nagel, M.; Hickley, S. G.; Froemsdorf, A.; Kornowski, A.; Weller, H. *Z. Phys. Chem.* **2007**, *221*, 427–437.
(25) Hentschel, M. Ph.D. Thesis, Technische Universität Dresden, 2001.
(26) Rodriguez, J. R.; Veinot, J. G. C.; Bianucci, P.; Meldrum, A. *Appl. Phys. Lett.* **2008**, *92*, 131119.
(27) Moon, H.-J.; Park, G.-W.; Lee, S.-B.; An, K.; Lee, J.-H. *Appl. Phys. Lett.* **2004**, *84*, 4547–4549.
(28) Strelow, C.; Sauer, M.; Fehringer, S.; Korn, T.; Schüller, C.; Stemmann, A.; Heyn, C.; Heitmann, D.; Kipp, T. *Appl. Phys. Lett.* **2009**, *95*, 221115.
(29) Kazes, M.; Lewis, D.; Ebenstein, Y.; Mokari, T.; Banin, U. *Adv. Mater.* **2002**, *14*, 317.
(30) Snee, P.; Chan, Y.; Nocera, D.; Bawendi, M. *Adv. Mater.* **2005**, *17*, 1131.
(31) Rakovich, Y.; Balakrishnan, S.; Donegan, J.; Perovaa, T.; Moore, R.; Gun'ko, Y. *Adv. Funct. Mater.* **2007**, *17*, 1106–1114.

DOI: 10.1021/nl9036966 | *Nano Lett.* **2010,** *10,* 627-631

4.5 Lasing in Microtube Bottle Resonators

Publication 6 arose out a of close collaboration with the diploma student Michael Sauer as well as Dr. Tobias Korn in the group of Prof. Dr. Christian Schüller from the University of Regensburg where we performed the time-resolved measurements. The investigated microtube was fabricated from wafer F.

Since the development of microtube ring resonators they suppose to be good candidates for low-threshold lasing since they bear a nearly perfect overlap between the embedded gain material and the microtube mode. Despite, only recently we succeeded in the observation of lasing in active microtube resonators. The main problem in the experiments under continuous wave (cw) excitation in Hamburg were highly evaluated temperatures since the microtubes offer only a slow heat transfer through their thin walls. We observed that for higher excitation powers the PL emission saturated and even decreased. In addition the spectral emission as well as the modes shifted to the red. This all indicates strongly elevated temperatures in the microtube wall. We tried quantum dots and quantum wells as gain material and, especially the latter, should be able to deliver enough gain to overcome the threshold. However, we observed no threshold behavior of the emitted photoluminescence. We believe that before the threshold is reached the evaluated temperatures destroy the gain.

In the experiments in Regensburg the microtubes were excited with a pulsed laser. Since temperature develops on a longer time scale compared to the PL emission the lasing has finished before the temperature develops in the system. Between two exciting laser pulses the system has time to cool down again. But even in the pulsed measurements we observed heating effects for the highest excitation powers. Obviously, the time between two excitation pulses is not long enough to let the system cool down in the high power regime. The observed threshold powers are quite high since charge carriers were excited only inside the quantum well and not inside the barriers.

Interestingly, also another group succeed in the observation of lasing in microtube resonators [Li09]. Astonishingly, they observed lasing on nearly identical microtubes containing quantum dots as we used in previous experiments and even at room temperature under cw excitation. In addition the observed threshold power was much lower than in our experiments in Regensburg. Naturally two question arise: (i) Why are our threshold powers so high compared Ref. [Li09], and (ii) why did we not observe lasing at low temperatures in our samples containing quantum dots. In principal the questions are related to each other. The answer to the first question (i) is simple. The quality factors in Ref. [Li09] are with 3500 much higher than 1000 in our experiments. In addition they estimated a Purcell Factor of 12 for their system which leads to an enhanced coupling of the spontaneous emission into

the laser mode. In our case no enhancement is expected. The answer to the second question (ii) is related to the energy shift of the quantum dots from low temperature to room temperature. Typically, this shift is in the order of 100 nm. In Ref. [Li09] the emission from the $s - s$ transition of the quantum dots is situated at 1240 nm at room temperature and in Hamburg at 1080 nm at low temperature. Our quality factors of the quantum dot microtubes range around 2000. Since the Purcell factor is proportional to the quality factor and to $1/\lambda^3$ one finds a two times larger Purcell factor for the values in Ref. [Li09]. Consequently, the higher quality factor and the higher Purcell factor might be the difference between our system and and the system in Ref. [Li09]. Perhaps, we could also observe lasing in our samples at room temperature, but up to now we do not have a detector that is sensitive in the desired spectral range. It might also be possible, that our quality factors would be larger for the modes observed at room temperature, since modes with larger wavelengths are not affected as much by the rolling edges as modes with shorter wavelengths. Interestingly, all our experiments showed the slight trend that modes at longer wavelengths have larger quality factors.

Consequently, both systems can hardly be compared since they differ in nearly all properties. The higher threshold power is obviously an offering to study the fast operation under nearly resonant excitation of microtubes containing quantum wells and at much shorter wavelengths, as shown in Publication 6.

The sample fabrication was done by Michael Sauer and me. The experiments were performed by Dr. Tobias Korn, Michael Sauer and me. The data analysis and the calculations were done by me. The publication was written by me.

Publication 6

Time-Resolved Studies of a
Rolled-Up Semiconductor Microtube Laser

Ch. Strelow, M. Sauer, S. Fehringer, T. Korn, C. Schüller,
A. Stemmann, Ch. Heyn, D. Heitmann, and T. Kipp

Applied Physics Letters, **95**, 221115 (2009)

APPLIED PHYSICS LETTERS **95**, 221115 (2009)

Time-resolved studies of a rolled-up semiconductor microtube laser

Ch. Strelow,[1,a)] M. Sauer,[1] S. Fehringer,[2] T. Korn,[2] C. Schüller,[2] A. Stemmann,[1] Ch. Heyn,[1] D. Heitmann,[1] and T. Kipp[1,b)]
[1]*Institut für Angewandte Physik und Zentrum für Mikrostrukturforschung, Universität Hamburg, Jungiusstraße 11, 20355 Hamburg, Germany*
[2]*Institut für Experimentelle und Angewandte Physik, Universität Regensburg, D-93040 Regensburg, Germany*

(Received 17 September 2009; accepted 11 November 2009; published online 4 December 2009)

We report on lasing in rolled-up microtube resonators. Time-resolved studies on these semiconductor lasers containing GaAs quantum wells as optical gain material reveal particularly fast turn-on times and short pulse emissions above the threshold. We observe a strong redshift of the laser mode during the pulse emission which is compared to the time evolution of the charge-carrier density calculated by rate equations. © *2009 American Institute of Physics*.
[doi:10.1063/1.3271176]

The most studied semiconductor microcavity lasers are micropillars,[1,2] microdisks,[3,4] and photonic crystals.[5,6] Their small size combined with high quality factors exhibits the possibility of low threshold lasing and single mode operation. Besides the pursuit of lowering the threshold also fast turn-on times are desirable.[4,5] Presently the fastest turn-on times were achieved by using quantum wells (QWs) as gain material[5] which have the disadvantage of high nonradiative recombination rates in the vicinity of the structured surfaces. To overcome this problem the surface can be passivated.[7,8] Quantum dots offer a much lower surface recombination rate[9] but have the disadvantage of a low carrier capture rate[10] which lengthens the turn-on times. In this work we present lasing in microtubes. These structures have the intrinsical advantage of nearly no unpassivated surfaces. Exploiting the self-rolling mechanism of thin strained semiconductor bilayers[11] we fabricated multiwalled microtubes that act as optical ring resonators.[12] As optical gain medium we chose a GaAs QW. Applying subpicosecond optical pumping we measured the time evolution of the photoluminescence (PL) emission at low temperature.

Our samples were grown by molecular beam epitaxy on GaAs(001) substrates. On top of a 40 nm AlAs sacrificial layer a 42 nm thick layer system is grown consisting of a 16 nm thick pseudomorphically strained barrier layer of $In_{0.16}Al_{0.30}Ga_{0.54}As$, a 4 nm GaAs QW, and a 22 nm $Al_{0.20}Ga_{0.80}As$ barrier. By selectively etching the sacrificial layer a predefined U-shaped mesa rolls up and forms a freestanding microtube bridge. Details of the fabrication are described in Refs. 12 and 13. The tube investigated in this work is shown in Fig. 1(a). It has a diameter of 5.74 μm and 1.1 revolutions. In the freestanding part total internal reflection leads to waveguiding in the tube wall and to the formation of ring modes by constructive interference after a roundtrip.[12] Very recently we showed that a fully three-dimensional control of the eigenmodes can be achieved by the definition of lobes in the rolling edge.[14] In this work we used a different axial confinement mechanism. By etching two $t=4$ nm deep stripes of a distance $L_z=1.43$ μm before rolling up, we fabricated a rolled-up ridge waveguide, as shown schematically in Fig. 1(b). Here, it also becomes obvious that microtubes should have low surface recombination rates due to the nearly complete absence of gain material at the surface.

Our experiments were performed with a tunable Ti:sapphire laser with 600 fs pulse length and 81 MHz repetition rate. The laser was focused by a 40× microscope objective (numerical aperture=0.4) onto the sample mounted in a continuous flow He cryostat at 4 K. The PL light is collected by the same objective, dispersed by a 25 cm spectrometer with 600 lines/mm grating and detected either by a streak camera (Hamamatsu Synchroscan) or a Si charge coupled device camera. The time resolution of the setup is 9 ps, measured from the full width at half maximum (FWHM) of the pump laser. The excitation wavelength was set to 750 nm which excites only the QW and not the barriers, since the band gap of the InAlGaAs layer is increased by compressive strain inside the microtube structure. Figure 2 shows excitation power dependent measurements on our microtube. Emission spectra of the microtube for three different excitation powers (measured as time-averaged power of the pulsed laser) are shown in Fig. 2(b). The QW emits around 797 nm with a FWHM of about 4.5 nm. Its emission is modified by optical modes. We rule out strong-coupling effects since all estimated charge carrier densities exceed the saturation density for strong coupling.[15] The strong mode at 800 nm is an axial fundamental mode[14] with one antinode in axial direction, determined from spatially resolved measurements (not shown). Figure 2(a) depicts the time evolution of the PL emission of the mode for different excitation powers. With

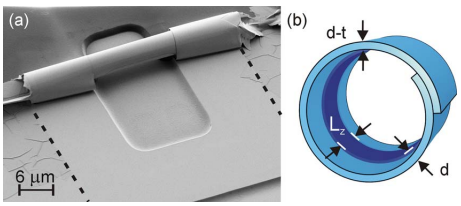

FIG. 1. (Color online) (a) Scanning electron micrograph of a microtube and its U-shaped mesa (dashed lines). (b) Unscaled sketch of the freestanding part of the tube.

a)Electronic mail: cstrelow@physnet.uni-hamburg.de.
b)Present address: Institut für Physikalische Chemie, Universität Hamburg, Grindelallee 117, 20146 Hamburg, Germany.

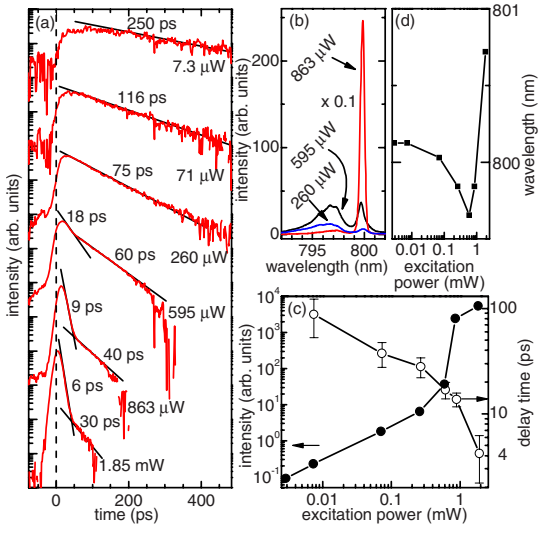

FIG. 2. (Color online) Excitation power dependent measurements of the microtube in Fig. 1. (a) Time evolution of the emitted PL light. (b) PL spectra. (c) Time-integrated PL intensity and delay time between pump pulse and PL emission. (d) Wavelength of the lasing mode in the time-integrated spectra.

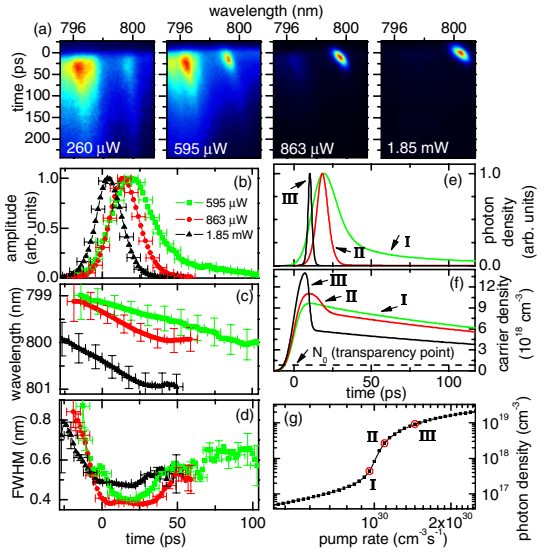

FIG. 3. (Color online) (a) False-color images by the streak camera for different excitation powers. [(b)–(d)] Time evolution of the amplitude, wavelength, and width of the lasing mode obtained by Gaussian fits at all times in (a). [(e)–(g)] Results for the time evolution of the photon density (e) and the charge carrier density (f) for three pump rates marked in the pump rate dependent photon density in (g), calculated by rate equations.

increasing excitation power one clearly observes a shortening of the lifetime from 250 ps down to about 6 ps, determined by fitting the decay in a period longer than the time resolution (at least 20 ps) and calculating the 1/e lifetime. In addition we find a threshold behavior in the light-input/light-ouput (L-L) curve depicted in Fig. 2(c). Above a threshold between 260 and 595 μW the system starts lasing. With increasing excitation power more and more stimulated emission shortens the decay times and a short pulse appears at the onset of the PL emission. For 863 μW a single laser mode dominates the spectrum, as shown in Fig. 2(b). Interestingly, the decay times already shorten well below the threshold. We believe that between 7.3 and 71 μW population inversion is reached and amplified spontaneous emission shortens the decay time. The threshold power is quite high compared to values for microdisk lasers[9,16] and photonic crystal laser.[5,10] This is caused by the large surface to volume ratio of microtubes. In finite-difference time-domain simulations, assuming that only the quantum well absorbs power, we calculated that less than 2% of the laser power are absorbed by the microtube. The threshold power might be much lower if one overcomes the difficulties of optical pumping, e.g., by electrical pumping.

Figure 2(c) depicts the delay between the arrival of the pump pulse, determined by the stray light of the excitation laser, and the maximum of the PL emission. A clear drop of the turn-on times with increasing excitation power is observed. For 863 μW, we measured about 14 ps. By exciting with light linearly polarized perpendicular to the mode polarization[12,13] and measuring successively parallel and perpendicularly to the mode polarization, turn-on times even below the conventional time resolution can be determined. For 1.85 mW we find 4 ± 1.5 ps. Our turn-on times are quite fast in comparison to values in Refs. 5 and 9, despite the absence of a fastened spontaneous decay rate by the Purcell effect. We attribute this to the nearly-resonant carrier excitation directly in the QW and the fast carrier relaxation in the QW. In addition we observed no relaxation oscillations in our experiments as often observed in microdisks.[4,9] This is because microtubes have no charge-carrier reservoir such as microdisks. In QW microdisk lasers diffusion from the middle part to the active region is a prerequisite in order to balance gain losses due to the very strong nonradiative surface state recombination.

Figure 2(d) shows the center wavelength of the time integrated lasing mode in dependence on the excitation power. Up to 595 μW we observe a strong blueshift followed by a strong redshift for higher excitation powers. The blueshift is caused by a change of the refractive index with an increasing charge carrier density for increasing excitation powers. Although untypical for pulsed measurements we attribute the redshift to heating which even destroys microtubes when excited with powers of typically 4 mW. Probably the thin microtube walls offer only a slow heat transfer to the substrate. A wavelength shift is also observed during the short PL emission and gives insight into the charge carrier dynamics on short time scales: Fig. 3(a) depicts false-color images taken by the streak camera at different excitation powers. Obviously, the lasing mode around 800 nm shifts to red during the emitted light pulse and the shift becomes larger for higher excitation powers. We fitted the spectral profiles at different times with Gaussians for the highest three excitation powers in Fig. 3(a). The results in form of amplitude, wavelength and width are depicted in Figs. 3(b)–3(d). Interestingly, we also observe a dynamic change of the spectral width besides the redshift. The first photons emitted after excitation are emitted spontaneously and the line width reflects the cavity life time. Indeed, the width of 0.8 nm at the onset of PL emission is the same as measured well below the threshold in the time-integrated spectra. Then, the width decreases by

50% within about 20 ps, stays constant for 30 ps (when the maximum of the PL emission is reached) and again increases at the end of the PL pulse. We attribute this behavior to the dynamic change into the coherent light state, when the system lases, and back into the spontaneous emission regime when the lasing turns off. Line-width narrowing with increasing pump power is reported for other microlasers,[6] but here we observe it on the time scale.

To explain the time evolution of the emitted PL intensity and the wavelength of the lasing mode we numerically solved rate equations for the charge-carrier density N and the photon density S

$$\dot{N} = -\Gamma S G_0 (N - N_0) - \frac{N}{\tau_{sp}} + P(t), \tag{1}$$

$$\dot{S} = \Gamma S G_0 (N - N_0) + \beta \frac{N}{\tau_{sp}} - \frac{S}{\tau_p}. \tag{2}$$

Here, we assumed a constant differential gain of $G_0 = 5 \times 10^{-6}$ cm^3/s and a value of $N_0 = 1.16 \times 10^{18}$ cm^{-3} for N at the transparency point.[4] For the optical confinement factor Γ we calculated 0.0563 and for the spontaneous emission factor β we assumed 0.01. According to the experiment we chose the spontaneous life time to $\tau_{sp} = 250$ ps [see Fig. 2(a) for low excitation power]. We neglected nonradiative decays since for our comparative studies significant nonradiative decay rates do not change the results qualitatively. From the experimentally obtained cavity quality factor $Q = 1000$ we determined a photon lifetime τ_p in the cavity of 0.424 ps. The pump pulse we assumed to be Gaussian, i.e., $P(t) = P_0 e^{-(2t/w\sqrt{\ln 2})^2}$ with a FWHM of $w = 10$ ps. The time-integrated photon density versus the pump rate is shown in Fig. 3(g). A qualitative agreement to the experimental data in Fig. 2(c) is observed. Figures 3(e) and 3(f) depict the time evolution of S (normalized) and N for pump rates roughly corresponding to the excitation powers in the Figs. 3(b)–3(d). The calculated curve of S qualitatively reproduces the experimental data in Fig. 3(b). The time evolution of N can be compared to the time evolution of the wavelength in Fig. 3(c). N changes the refractive index linearly[17] which on the other hand causes a linear shift of the mode wavelength. Consequently, the wavelength shift is a direct measure for N. Slightly above the threshold (pump rate I) N decays mainly spontaneously and thus exponentially. Well above the threshold (pump rates II, III) dominating stimulated emission leads to the observed fast drop of N. This behavior can directly be found in the measurements: At 595 μW (slightly above the threshold) the wavelength shift is slow and at 863 μW (well above the threshold) it changes from fast during the pulse emission to slow at its end. For 1.85 mW the shift does not become faster in contrast to the calculations. We believe that here the assumption of a constant gain breaks down. The mode might have shifted to different gain or the gain itself has changed, e.g., due to saturation or renormalization effects or heating. The absolute values of the wavelength are generally not reproduced by the calculations. For high excitation powers heating leads to an additional redshift of the laser mode.

In summary, we report on the demonstration of lasing in active microtube resonators. We observed fast turn-on times as compared to other microlasers and a characteristic redshift of the laser mode during pulsed emission. This behavior is reproduced by a rate equation model.

We acknowledge financial support by the Deutsche Forschungsgemeinschaft via Grant Nos. SFB 508 and 689 and Graduiertenkolleg 1286 and 638.

[1] M. Schwab, H. Kurtze, T. Auer, T. Berstermann, M. Bayer, J. Wiersig, N. Baer, C. Gies, F. Jahnke, and J. P. Reithmaier, Phys. Rev. B **74**, 045323 (2006).
[2] S. M. Ulrich, C. Gies, S. Ates, J. Wiersig, S. Reitzenstein, C. Hofmann, A. Löffler, A. Forchel, F. Jahnke, and P. Michler, Phys. Rev. Lett. **98**, 043906 (2007).
[3] S. L. McCall, A. F. J. Levi, R. E. Slusher, S. J. Pearton, and R. A. Logan, Appl. Phys. Lett. **60**, 289 (1992).
[4] K. J. Luo, J. Y. Xu, H. Cao, Y. Ma, S. H. Chang, S. T. Ho, and G. S. Solomon, Appl. Phys. Lett. **77**, 2304 (2000).
[5] H. Altug, D. Englund, and J. Vučković, Nat. Phys. **2**, 484 (2006).
[6] S. Strauf, K. Hennessy, M. T. Rakher, Y.-S. Choi, A. Badolato, L. C. Andreani, E. L. Hu, P. M. Petroff, and D. Bouwmeester, Phys. Rev. Lett. **96**, 127404 (2006).
[7] U. Mohideen, W. S. Hobson, S. J. Pearton, F. Ren, and R. E. Slusher, Appl. Phys. Lett. **64**, 1911 (1994).
[8] D. Englund, H. Altug, and J. Vučković, Appl. Phys. Lett. **91**, 071124 (2007).
[9] K. J. Luo, J. Y. Xu, H. Cao, S. H. Chang, S. T. Ho, and G. S. Solomon, Appl. Phys. Lett. **78**, 3397 (2001).
[10] B. Ellis, I. Fushman, D. Englund, B. Zhang, Y. Yamamoto, and J. Vučković, Appl. Phys. Lett. **90**, 151102 (2007).
[11] V. Y. Prinz, V. A. Seleznev, A. K. Gutakovsky, A. V. Chehovskiy, V. V. Preobrazhenskii, M. A. Putyato, and T. A. Gavrilova, Physica E **6**, 828 (2000).
[12] T. Kipp, H. Welsch, Ch. Strelow, Ch. Heyn, and D. Heitmann, Phys. Rev. Lett. **96**, 077403 (2006).
[13] Ch. Strelow, C. M. Schultz, H. Rehberg, H. Welsch, Ch. Heyn, D. Heitmann, and T. Kipp, Phys. Rev. B **76**, 045303 (2007).
[14] Ch. Strelow, H. Rehberg, C. M. Schultz, H. Welsch, Ch. Heyn, D. Heitmann, and T. Kipp, Phys. Rev. Lett. **101**, 127403 (2008).
[15] R. Houdré, J. L. Gibernon, P. Pellandini, R. P. Stanley, U. Oesterle, C. Weisbuch, J. O'Gorman, B. Roycroft, and M. Ilegems, Phys. Rev. B **52**, 7810 (1995).
[16] V. Zwiller, S. Fälth, J. Persson, W. Seifert, L. Samuelson, and G. Björk, J. Appl. Phys. **93**, 2307 (2003).
[17] J. G. Mendoza-Alvarez, F. D. Nunes, and N. B. Patel, J. Appl. Phys. **51**, 4365 (1980).

4.5.1 Lasing in microtube resonators described by a rate equation model

In this section I want to give an in-depth theoretical background to our results presented in Publication 6. Due to the lack of space in Publication 6, in particular, interesting features of the solutions of the rate equations could not be shown there. In the framework of the rate equation model I will show the properties of microtube lasers more detailed. To describe the dynamics in semiconductor lasers the simplest form of rate equations for the charge-carrier density N and the photon density S reads:

$$\dot{N} = -\Gamma S G_0 (N - N_0) - \gamma \frac{N}{\tau_r} - \frac{N}{\tau_{nr}} + P(t) \tag{4.1}$$

$$\dot{S} = \Gamma S G_0 (N - N_0) + \beta\gamma \frac{N}{\tau_r} - \frac{S}{\tau_p}. \tag{4.2}$$

Here, Γ is the optical confinement factor, G_0 the differential gain, N_0 the charge-carrier density at the transparency point, γ the spontaneous emission enhancement factor, τ_r the radiative and τ_{nr} the nonradiative exciton lifetime, $P(t)$ the pump rate, β the ratio between photons emitted into the laser mode and photons emitted into all modes and τ_p the photon lifetime in the cavity. First, I will discuss equation (4.1) and (4.2) in a qualitative way and elucidate the impact of the different parameters on the dynamics of N and S. Later, I will show the solutions of the rate equations corresponding to the measurements in Publication 6.

In the first step the system has to be excited. Electrons and holes are injected into the lasing level with a distinct time-dependent pump rate $P(t)$. In principal, many processes are summarized in the time dependence of $P(t)$, since only the generation rate of charge carriers in the lasing level is described. This term includes how many photons are absorbed by the excitation laser in case of optical pumping and the relaxation dynamics from the excitation level to the laser level. The time dependence of $P(t)$ has a strong impact on the dynamics of N and S. However, especially the relaxation processes are still under discussion. If one is interested in fast response times of the laser, quantum wells as gain material are preferred compared to quantum dots, since quantum dots have a rather large carrier-capture time between 1 and 10 ps [Yua99] that can limit the response of the laser [Luo01, Ell07]. After excitation the charge-carrier density decays with a typical radiative lifetime τ_r and a nonradiative lifetime τ_{nr}. A very prominent nonradiative decay channel is surface recombination. This is a very strong effect in many microcavities containing quantum wells since the quantum well contacts the structured surfaces in lateral direction. It is reported that a passivation of the surface leads to a strong reduction of the lasing threshold [Moh94, Eng07]. Quantum dots, on the contrary, have much

larger surface recombination times. Microtubes have the intrinsic advantage that incorporated quantum wells have nearly no unpassivated surfaces. Thus surface recombination should not play an important role. The loss term by spontaneous radiative decay in equation (4.1) with negative sign appears as generation term in equation (4.2) with a positive sign. The spontaneous emission leads to a buildup of photon density in the laser mode. The term is modified by the β factor that ranges between 0 and 1. The β factor is very important for the dynamics of S. In general, most of the spontaneous photons are emitted isotropically into the surrounding and only few photons are emitted into the laser mode. For macroscopic resonators β is very close to zero. But for microcavities β can reach values very close to 1, which means that nearly all photons are emitted into the laser mode. The reason for this is their small size. The number of modes in microcavities is reduced drastically. In addition very small and high-quality cavities exhibit a large Purcell effect, which means that vacuum fluctuations of the electric field lead to a strong reduction of the spontaneous radiative lifetime and a preferred emission of the photons into the cavity mode. In such cavities γ can reach very high values, e.g. 165 [Eng05]. This already leads to high photon densities in the cavity below the laser threshold and reduces the threshold or leads even to thresholdless lasing.

The most important term for lasing is the first term on the right-hand sides of equations (4.1) and (4.2),

$$\Gamma S G_0 (N - N_0). \tag{4.3}$$

This term describes absorption and stimulated emission in the laser. When N is smaller than N_0, which means that population inversion has not yet reached, the laser level absorbs photons from the cavity indicated by a positive value of the term in equation (4.1) (N increases) and a negative value in equation (4.2) (S decreases). When N exceeds N_0 term (4.3) changes from absorption to stimulated emission, indicated by the change of the sign. Lasing is observed when the loss rate $\frac{S}{\tau_p}$ is compensated by the sum of stimulated and spontaneous emission rate into the laser mode. Usually, in the case of low β lasers, the contribution of the spontaneous emission rate can be neglected and the stimulated emission rate has to overcome the cavity loss rate solely. In this case the laser threshold is reached when the value of term (4.3) exceeds the value of $\frac{S}{\tau_p}$.

In the following I will discuss the impact of Γ, G_0 and N_0 on the laser threshold. Naturally, N_0 should be as small as possible and G_0 and Γ have to be as large as possible. But in general these values cannot be chosen independently from each other, since they are material parameters of the gain material. To achieve a small N_0 in the best case a single quantum dot could be used. But in this case Γ is small if the cavity is too large: Γ is the spatial overlap between the cavity mode and the gain material. Only in very small cavities with strongly confined modes lasing with a

single quantum dot can be achieved [Nom09]. In addition the cavity loss rate has to be small and β has to be high since otherwise a single quantum dot cannot build up a sufficiently high photon density. In larger microcavities an ensemble of quantum dots can be used. But the density of quantum dots is limited and quantum dots have considerably small dipole moments. The latter property is taken into account by the differential gain G_0. It is defined by the cross section of the emitter. Large values of G_0 are obtained for materials with large dipole moments, in which the wave functions of the emitters are widely spread like in quantum wells. In quantum wells one can also achieve very high Γ values since the whole quantum well material can contain excitons in contrast to a layer of dots where the excitons are localized in the quantum dots. The disadvantage is an enlarged N_0 since more charge carriers are needed to achieve population inversion.

Microtubes have the big advantage that they bear a perfect overlap between the gain material and the cavity mode and that the gain material has nearly no contact to the structured surfaces. The disadvantages are that the quality factors, up to now, are not as high as for other microcavities and that they can intrinsically not be fabricated as small as for example photonic crystal cavities. Consequently, microtubes exhibit a smaller Purcell effect than other microcavities. However, there are also disadvantages of microlasers with high Purcell effect. It has been reported that the coherence length of such lasers is smaller than of comparable lasers with smaller Purcell effect [Ate08].

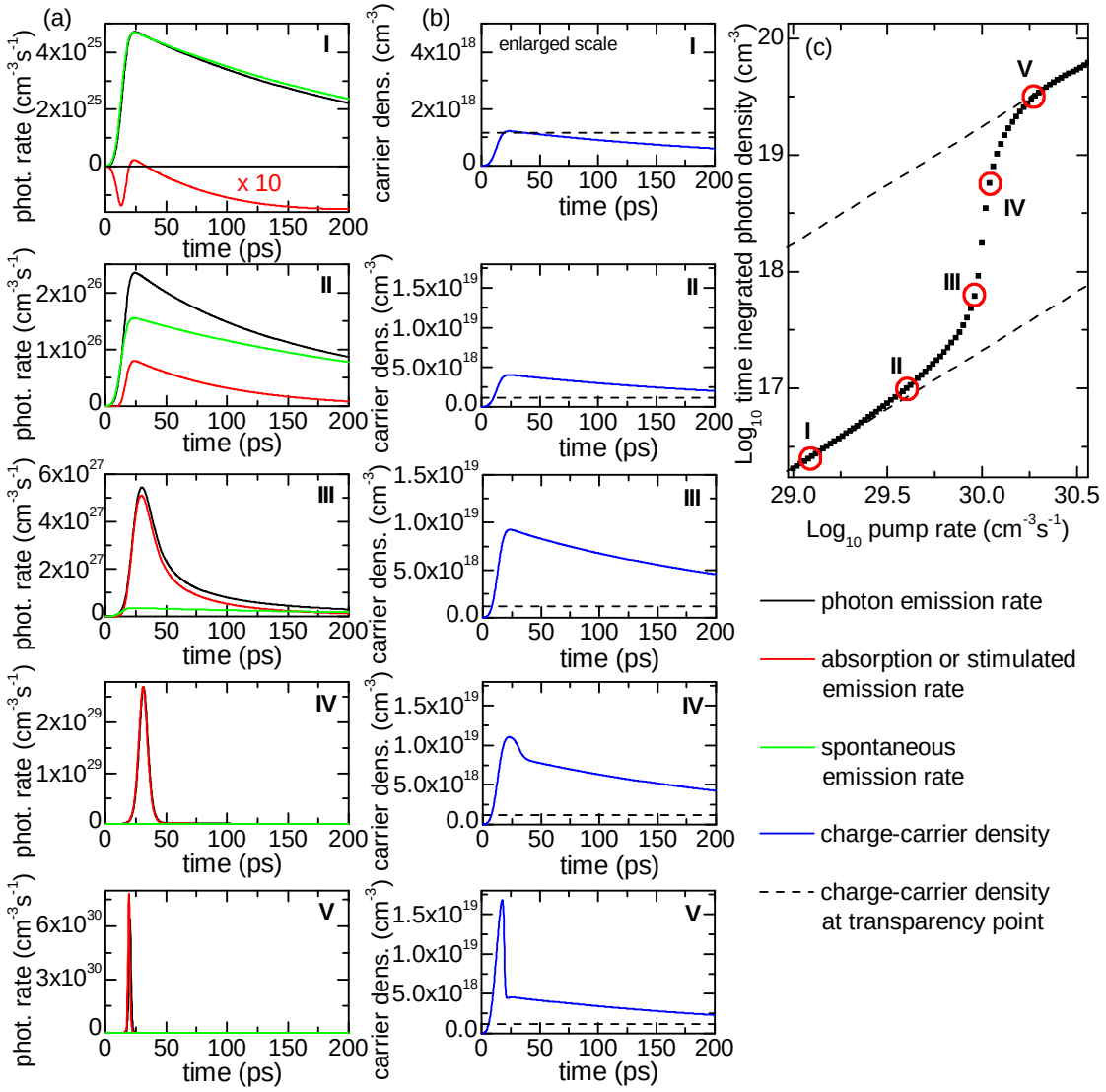

Figure 4.8: Solutions of a rate equation model for the microtube studied in Publication 6. (a) Time evolution of the emitted photon rate (black curve), the spontaneous emission rate (green curve) and absorption and stimulated emission rate (red curve) from the microtube for different pump rates. (b) Corresponding time evolution of the charge-carrier density. (c) Time integrated photon density versus pump rate. The pump rates corresponding to the time evolutions in (a) and (b) are marked and labeled.

In the following, I present the solutions of equation (4.1) and (4.2) that were also partly depicted in Publication 6. Here, I show results for more excitation powers and demonstrate also the contribution of spontaneous and stimulated emission on the emitted light. Figure 4.8(a) depicts the time evolution of the loss rate from the microtube (black curve) as well as the spontaneous emission rate (green curve) and the absorption/stimulated emission rate from the microtube (red curve) for different excitation powers. Figure 4.8(b) shows the time evolution of the charge-carrier density and Fig. 4.8(c) the time integrated photon density in the cavity depending on the the pump rate. The pump rates for which the time evolutions are shown are labeled with I, II, III, IV and V. For pump rate I, the pump pulse $P(t)$ enlarges N very fast followed by an exponential decay of N. Most of the time N is smaller than N_0 indicated by the dashed black line in Fig. 4.8(b). Thus mainly spontaneous processes take part in the decay of N. The time evolution of the photon emission follows the decay of N since the cavity life time is much slower than the spontaneous lifetime. The emitted photons consist almost only of spontaneously emitted photons. At the beginning some photons are absorbed followed by a few stimulated photons when N slightly exceeds N_0 and again absorption for later times, indicated by the changing signs of the red curve. At pump rate II population inversion is reached and N exceeds N_0 considerably quickly. Now, about one third of the emitted light consists already of stimulated photons. Their contribution appears delayed to the contribution of the spontaneous photons. First, spontaneous photons have to be in the cavity to lead to stimulated photons and due to small gain the contribution grows only slowly. In Fig.4.8(c) one observes already a superlinear increase of the time integrated photon density due to the additional stimulated photons. This is indicated by a slope of slightly larger than 1 (dashed line) on the doubly logarithmic scale. For only spontaneous decay the increase would be linear, indicated by the dashed line. The reaching of population inversion before reaching of the threshold is also observed in the experiments in Fig. (2) in Publication 6. A clear decrease of the decay time is observed. But there, the effect is more pronounced since for amplified spontaneous emission (ASE) principally all photons can stimulate excitons to decay not depending on, whether these photons occupy the cavity mode or not. This is not included in the calculations. The difference between ASE and lasing is that all stimulated photons in the case of lasing have the same phase and occupy a coherent state whereas in the case of ASE only pairs of one spontaneous and one stimulated photon have the same phase. At pump rate III the threshold is reached. N clearly exceeds N_0. Roughly 90 % of the photons are stimulated photons and the decay is fastened significantly. The emitted light appears delayed compared to lower pump rates since the photon density needs time to build up by self amplification. In the doubly logarithmic scale in Fig. 4.8(c) one observes slops larger than 1 indicating strongly super linear growth of the photon density with increasing pump rate. For pump rate IV N increases the gain further leading to a fast build up followed by

a fast decay of the photon density in the cavity by the stimulated emission. Now, the fast decay can also be observed in the time evolution of N by a fast drop of N shortly after reaching of the maximum N. The stimulated emission forces more excitons to emit their photons into the cavity mode compared to the spontaneous regime where only the fraction β emits into the cavity mode. For pump rate V the processes become even faster. A high photon density is build up very quickly and drops again very fast. The light is emitted in very short pulses. N decays also very fast even to a lower value than for lower pump rates. With increasing pump rates now the time integrated photon density grows again linear but with a larger slope in a linear plot. For very high pump rates this model can break down, since the laser level cannot be occupied further. The gain saturates and the emission cannot get faster. This might be the case in the experiment in Publication 6.

The calculations show that a considerably high N well above the transparency point is needed to achieve lasing. In experiments under continuous wave excitation in Hamburg we could not observe lasing so far. We observed that the needed high N cannot be generated in Hamburg since, before, heating leads to a breakdown of the photoluminescence. In future the sample design has to be improved. It should be no problem to embed thicker quantum wells inside the microtube. Choosing a thickness of 16 nm instead of the used 4 nm would approximately increase Γ by a factor of 4. The quality factors have also to be improved. The measurements on microtubes with GaAs quantum wells were our first measurements in the spectral range around 800 nm. In all experiments we observed only quality factors up to 1000, in contrast to experiments on microtubes emitting at larger wavelengths. For smaller wavelengths the bilayers might have to be thinner since scattering is more pronounced for shorter wavelengths. It should be no problem to fabricate microtubes with thinner bilayers. Losses that are caused by too thin bilayers can then be balanced by more windings.

Conclusions

This work is a large step in the development of optical microtube resonators. Already the first results on nominally axially unstructured microtubes show that the rolled-up geometry of microtubes with their inside and outside rolling edge can be functionalized to adjust the properties of the eigenmodes in optical microtube resonators in a simple and versatile way. They can be used as a strongly directive output coupler and they can be used for an axial light confinement. The study of spatial pinning at kinks in the rolling edge and the energetical shifting along the microtube axis were important inputs for the development of the theory on three-dimensional light confinement in microtubes as well as for the realization of a controlled axial light confinement.

The subsequent development of microtube bottle resonators was the breakthrough in the fabrication of optical microtube resonators. In these resonators diverse structurings of the microtube geometry along the axis lead to a controlled axial light confinement that drastically changes the eigenmode spectrum compared to unstructured microtubes. Instead of additional modes with small mode spacings that tend to inhomogeneously broaden on the high energy side of each azimuthal mode, single sharp modes are observed. Three different axial structurings were introduced in this work: A modulation of the winding number along the microtube axis, that forms lobes of additional windings in the outside rolling edge, a modulation of the wall thickness of the microtube, formed by a ring of thicker wall thickness between two rings of thinner wall thickness, and a modulation of the radius, where the squeezing of two rings of additional windings lead to smaller radii close to the rings compared to between the rings. All these structurings result in an axial quantization of the modes around the structurings, that has been investigated by micro photoluminescence spectroscopy with spatial resolution along the microtube axis. In these measurements we make the important observation that the axial field distributions resemble the probability density of particle waves confined in an one-dimensional potential. We developed a model that describes this behavior in an intuitive and accurate way as a three-dimensional confinement in a quasi-potential. By adiabatic separation of the circular and the axial mode propagation we demonstrate that

the circular propagation induces a quasi-potential that is introduced in a quasi-Schrödinger equation for the axial propagation. The quasi-potential can simply be determined by the microtube geometry along the axis and a waveguide model.

For microtubes with lobes in the rolling edge we demonstrated experimentally and by calculations that the energies and axial field distributions of the axially confined eigenmodes can be tailored by the shape of the lobe. By numerically solving the quasi-Schrödinger equation for the exact microtube geometry measured in scanning-electron micrographs, we can reproduce the measured mode energies and axial intensity distributions in a nice and accurate way. Comparing these results to the corresponding solutions of particle waves in a one-dimensional potential, we observe a strong analogy: The shape of the lobes is directly reproduced in the shape of the quasi-potential and the solutions of the quasi-Schrödinger equation behave as known from particle waves. Parabolic lobes, for example, lead to an equidistant energy spacing of the the axially confined modes of the same azimuthal mode number. These theoretical and experimental findings enable a wide field of further interesting and useful realizations of microtube bottle resonators. On the one hand we could show that the number of axially confined modes can be reduced to only one axial mode per azimuthal mode. This could be important for lasers to suppress compe-ting modes and lead to a reduction of the laser threshold. One the other hand we presented first results on coupled bottle resonators. Measurements on a microtube with a sinusoidally modulated rolling edge exhibited strong hints on the formation of a photonic crystal. Here, further experiments on different structures should be performed in future. It might be possible that an axial light confinement by the formation of photonic stop bands improves the quality factors.

For microtubes with axial light confinement by a radius modulation we observed also a nice description by our model. We could show that a radius modulation can be induced by squeezing of additional windings but that the effect was only small. Nevertheless, this mechanism has a great potential since a radius modulation confines the light very smoothly. Future experiments that engineer the strain of the microtube by additional well-positioned layers could lead to a stronger radius modulation and thus to a stronger axial light confinement.

For microtubes with a modulated wall thickness represented by two etched rings, we observed that the measured axially confined modes qualitatively follow our theoretical model but that quantitatively deviations appear. Here, the axial mode spacings are larger than found in the calculations. In measurements on those microtubes we find a well-pronounced splitting by broken rotational symmetry that has not been observed in this clarity up to now. We have analyzed the splitting by two-dimensional FDTD simulations and by utilizing our waveguide model and found that it oscillates systematically with the winding number of the microtube.

Interestingly, we observed not only an oscillation of the amount of the mode energy splitting, but also a related redistribution of the loss channels which has direct impact on the quality factors. These findings show that, on the one hand, the control of the splitting by broken rotational symmetry might lead to an increase of the quality factors. On the other hand, it also explains why the splitting was not observed in such a pronounced way in microtubes where the axial confinement is produced by lobes.

Microtube bottle resonators have further unique properties. The very thin walls lead to long-ranging evanescent fields of the resonator modes into the inside of the microtube as well as into the surrounding of the microtube. We demonstrated by filling a solution of chemically synthesized nanocrystals into the microtube that the resonator modes can be excited excellently by emitters that are not embedded into the microtube wall during the growth. This shows a great potential of microtubes as lasers with versatile gain material that cannot be integrated into other types of microcavities. Microtubes can also be used as a component in optofluidic networks, where they can act, e.g., as sensitive sensors. In this fields microtubes should be ideal since they realize flow channels and microcavities in one and the same device. Thus further experiments in this direction are very promising.

Another application for microtube bottle resonators is the use as active laser resonators. We realized a microtube laser with a quantum well as optical gain material. By studying the lasing dynamics by time-resolved photoluminescence spectroscopy we found that microtube lasers exhibit considerable fast turn-on times compared to other microcavity lasers by exciting the quantum well nearly resonantly. In microtubes embedded quantum wells have nearly no contact to structured surfaces which leads to low nonradiative surface recombination rates. So far, the observed threshold power is quite high compared to other types of microcavity lasers. This could be explained by the nearly resonant excitation and the large surface to volume ratio that complicates optical pumping. Electrical pumping should circumvent this problem and is a very interesting future experiment. A strong red shift during the short PL emission is observed which allows conclusions on the charge-carrier dynamics during the lasing process. The dynamical behavior can be qualitatively reproduced by a rate equation model. The theoretical study by the rate equation model suggests to promising improvements of the sample design in future microtube lasers. A thicker quantum well should increase the modal gain by at least a factor of four. Further on microtubes with thinner layers should be fabricated to reduce the scattering losses at the rolling edges. Consequently, further experiments on microtube lasers are very promising since so far we have not reached any fundamental limit to improve the microtube laser.

List of Figures

Bibliography

[Arm03] D. K. Armani, T. J. Kippenberg, S. M. Spillane, and K. J. Vahala. *Ultra-high-Q toroid microcavity on a chip.* Nature **421**, 925–928 (2003).

[Ate08] S. Ates, C. Gies, S. M. Ulrich, J. Wiersig, S. Reitzenstein, A. Löffler, A. Forchel, F. Jahnke, and P. Michler. *Influence of the spontaneous optical emission factor beta on the first-order coherence of a semiconductor microcavity laser.* Phys. Rev. B (Condensed Matter and Materials Physics) **78**, 155319 (2008).

[Bal06] S. Balakrishnan, Y. Gun'ko, Yu. P. Rakovich, J. F. Donegan, T. S. Perova, and R. A. Moore. *Confined optical modes and amplified spontaneous emission from a microtube cavity formed by vacuum assisted filtration.* Appl. Phys. Lett. **89**, 143113 (2006).

[Bay98] M. Bayer, T. Gutbrod, J. P. Reithmaier, A. Forchel, T. L. Reinecke, and P. A. Knipp. *Optical Modes in Photonic Molecules.* Phys. Rev. Lett. **81**, 2582 (1998).

[Bay99] M. Bayer, T. Gutbrod, A. Forchel, T. L. Reinecke, and P. A. Knipp. *Optical Demonstration of a Crystal Band Structure Formation.* Phys. Rev. Lett. **83**, 5374 (1999).

[Bor04] M. Borselli, K. Srinivasan, P. E. Barclay, and O. Painter. *Rayleigh scattering, mode coupling, and optical loss in silicon microdisks.* Appl. Phys. Lett. **85**, 3693–3695 (2004).

[Che03] G. D. Chern, H. E. Tureci, A. Douglas Stone, R. K. Chang, M. Kneissl, and N. M. Johnson. *Unidirectional lasing from InGaN multiple-quantum-well spiral-shaped micropillars.* Appl. Phys. Lett. **83**, 1710–1712 (2003).

[Den02] Ch. Deneke, C. Müller, N.Y. Jin-Phillipp, and O. G. Schmidt. *Diameter Scalability of Rolled-Up In(Ga)As/GaAs Nanotubes.* Semicond. Sci. Technol. **17**, 1278 (2002).

[Die08] K. Dietrich. *Optische Mikroröllchen-Resonatoren mit nasschemisch synthetisierten PbS-Nanokristallen.* Diplomarbeit, Universität Hamburg, 2008.

[Ell07] B. Ellis, I. Fushman, D. Englund, B. Zhang, Y. Yamamoto, and J. Vučković. *Dynamics of quantum dot photonic crystal lasers.* Appl.Phys.Lett. **90**, 151102 (2007).

[Eng05] D. Englund, D. Fattal, E. Waks, G. Solomon, B. Zhang, T. Nakaoka, Y. Arakawa, Y. Yamamoto, and J. Vučković. *Controlling the Spontaneous Emission Rate of Single Quantum Dots in a Two-Dimensional Photonic Crystal.* Phys. Rev. Lett. **95**, 013904 (2005).

[Eng07] D. Englund, H. Altug, and J. Vučković. *Low-threshold surface-passivated photonic crystal nanocavity laser.* Applied Physics Letters **91**, 071124 (2007).

[Gay99] B. Gayral, J. M. Gérard, A. Lemaître, C. Dupuis, L. Manin, and J. L. Pelouard. *High-Q wet-etched GaAs microdisks containing InAs quantum boxes.* Appl. Phys. Lett. **75**, 1908–1910 (1999).

[Gér96] J. M. Gérard, D. Barrier, J. Y. Marzin, R. Kuszelewicz, L. Manin, E. Costard, V. Thierry-Mieg, and T. Rivera. *Quantum boxes as active probes for photonic microstructures: The pillar microcavity case.* Appl. Phys. Lett. **69**, 449 (1996).

[Gér99] J.-M. Gérard and B. Gayral. *Strong Purcell Effect for InAs Quantum Boxes in Three-Dimensional Solid-State Microcavities.* J. Lightwave Technol. **17**, 2089 (1999).

[Gru03] M. Grundmann. *Nanoscroll Formation from Strained Layer Heterostructures.* Appl. Phys. Lett. **83**, 2444 (2003).

[Ham] *http://learn.hamamatsu.com/tutorials/streakcamera/.*

[Hos07] M. Hosoda and T. Shigaki. *Degeneracy breaking of optical resonance modes in rolled-up spiral microtubes.* Appl. Phys. Lett. **90**, 181107 (2007).

[Khi06] G. Khitrova, H. M. Gibbs, M. Kiraz, S. W. Koch, and A. Scherer. *Vacuum Rabi splitting in semiconductors.* Nat. Phys./ **2**, 81 (2006).

[Kip06] T. Kipp, H. Welsch, Ch. Strelow, Ch. Heyn, and D. Heitmann. *Optical Modes in Semiconductor Microtube Ring Resonators.* Phys. Rev. Lett. **96**, 77403 (2006).

[Kne04] M. Kneissl, M. Teepe, N. Miyashita, N. M. Johnson, G. D. Chern, and R. K. Chang. *Current-injection spiral-shaped microcavity disk laser diodes with unidirectional emission.* Appl. Phys. Lett. **84**, 2485–2487 (2004).

[Lev93] A. F. J. Levi, S. L. McCall, S. J. Pearton, and R. A. Logan. *Room Temperature Operation of a Sub-Micron Radius Disk Laser.* Electron. Lett. **29**, 1666 (1993).

[Li09] F. Li, S. Vicknesh, and Z. Mi. *Optical modes in InGaAs/GaAs quantum dot microtube ring resonators at room temperature.* Electron. Lett. **45**, 645–646 (2009).

[Lou01] Roudney Loudon. *The quantum theory of light.* Oxford University Press, Oxford, 2001.

[Lou05] Y. Louyer, D. Meschede, and A. Rauschenbeutel. *Tunable whispering-gallery-mode resonators for cavity quantum electrodynamics.* Phys. Rev. A **72**, 031801(R) (2005).

[Luo01] K. J. Luo, J. Y. Xu, H. Cao, S. H. Chang, S. T. Ho, and G. S. Solomon. *Ultrafast Dynamics of InAs/GaAs Quantum-Dot Microdisk Lasers.* Appl. Phys. Lett. **78**, 3397 (2001).

[Mei08] Y. Mei, G. Huang, A. A. Solovev, E. Bermúdez Ureña, I. Mönch, F. Ding, T. Reindl, R. K. Y. Fu, P. K. Chu, and O. G. Schmidt. *Versatile Approach for Integrative and Functionalized Tubes by Strain Engineering of Nanomembranes on Polymers.* Advanced Materials **21**, 4085–4090 (2008).

[Men05] S. Mendach. *InGaAs-Mikro- und Nanoröhrchen.* Dissertation, Universität Hamburg, 2005.

[Moh94] U. Mohideen, W. S. Hobson, S. J. Pearton, F. Ren, and R. E. Slusher. *GaAs/AIGaAs Microdisk Lasers.* Appl. Phys. Lett. **64**, 1911 (1994).

[Mon07] C. Monat, P. Domachuk, and B. J. Eggleton. *Integrated optofluidics: A new river of light.* Nat. Photon. **1**, 106–114 (2007).

[Nöc97] J. U. Nöckel and A. Douglas Stone. *Ray and wave chaos in asymmetric resonant optical cavities.* Nature **385**, 45–47 (1997).

[Nom09] M. Nomura, N. Kumagai, S. Iwamoto, Y. Ota, and Y. Arakawa. *Photonic crystal nanocavity laser with a single quantum dot gain.* Opt. Express **17**, 15975–15982 (2009).

[Pöl09] M. Pöllinger, D. O'Shea, F. Warken, and A. Rauschenbeutel. *Ultrahigh-Q Tunable Whispering-Gallery-Mode Microresonator*. Phys. Rev. Lett. **103**, 053901 (2009).

[Pai99] O. Painter, R. K. Lee, A. Scherer, A. Yariv, J. D. O´Brien, P. D. Dapkus, and I. Kim. *Two-Dimensional Photonic Band-Gap Defect Mode Laser*. Science **284**, 1819 (1999).

[Pri00] V. Ya. Prinz, V. A. Seleznev, A. K. Gutakovsky, A. V. Chehovskiy, V. V. Preobrazhenskii, M. A. Putyato, and T. A. Gavrilova. *Free-Standing and Overgrown InGaAs/GaAs Nanotubes, Nanohelices and their Arrays*. Physica E **6**, 828 (2000).

[Pur46] E. M. Purcell. *Spontaneous Emission Probabilities at Radio Frequencies*. Phys. Rev. **96**, 861 (1946).

[Reh07] H. Rehberg and C. M. Schultz. *Dreidimensional eingeschlossene optische Moden in Mikroröllchen-Ringresonatoren*. Diplomarbeit, Universtät Hamburg, 2007.

[Rei04] J. P. Reithmaier, G. Sek, A. Löffler, C. Hofmann, S. Kuhn, S. Reitzenstein, L. V. Keldysh, V. D. Kulakovskii, T. L. Reinecke, and A. Forchel. *Strong Coupling in a Single Quantum Dot-Semiconductor Microcavity System*. Nature **432**, 197 (2004).

[Sau09] M. Sauer. *Lasing und Modenaufspaltung in Halbleiter-Mikroröllchen-Resonatoren*. Diplomarbeit, Universität Hamburg, 2009.

[Spi02] S. M. Spillane, T. J. Kippenberg, and K. J. Vahala. *Ultralow-threshold Raman laser using a spherical dielectric microcavity*. Nature **415**, 621–623 (2002).

[Str06] Ch. Strelow. *Photolumineszenzspektroskopie an Mikroröllchen-Ringresonatoren*. Diplomarbeit, Universität Hamburg, 2006.

[Str07] Ch. Strelow, C. M. Schultz, H. Rehberg, H. Welsch, Ch. Heyn, D. Heitmann, and T. Kipp. *Three dimensionally confined optical modes in quantum-well microtube ring resonators*. Phys. Rev. B **76**, 045303 (2007).

[Sum04] M. Sumetsky. *Whispering-gallery-bottle microcavities: the three-dimensional etalon*. Opt. Lett. **29**, 8–10 (2004).

[Th07] S. Tomljenovic-Hanic, C. M. de Sterke, M. J. Steel, B. J. Eggleton, Y. Tanaka, and S. Noda. *High-Q cavities in multilayer photonic crystal slabs*. Opt. Express **15**, 17248–17253 (2007).

[Was99] Z. R. Wasilewski, S. Fafard, and J. P. McCaffrey. *Size and shape engeneering of vertically stacked self-assembled quantum dots.* J. Cryst. Growth **201-202**, 1131 (1999).

[Wie06] J. Wiersig and M. Hentschel. *Unidirectional light emission from high-Q modes in optical microcavities.* Phys. Rev. A (Atomic, Molecular, and Optical Physics) **73**, 031802 (2006).

[Wie08] J. Wiersig and M. Hentschel. *Combining Directional Light Output and Ultralow Loss in Deformed Microdisks.* Phys. Rev. Lett. **100**, 033901 (2008).

[Wil09] F. Wilde. *Unidirectional photoluminescence emission of pierced microdisks.* Dissertation, Universität Hamburg, 2009.

[Yua99] Z. L. Yuan, E. R. A. D. Foo, J. F. Ryan, D. J. Mowbray, M. S. Skolnick, and M. Hopkinson. *Many-body effects in carrier capture and energy relaxation in self-organized InAs/GaAs quantum dots.* Physica B **272**, 12 – 14 (1999).

Publications

T. Kipp, H. Welsch, Ch. Strelow, Ch. Heyn, and D. Heitmann
Optical Modes in Semiconductor Microtube Ring Resonators,
Physical Review Letters **96**, 077403 (2006).

T. Kipp, Ch. Strelow, H. Welsch, Ch. Heyn, and D. Heitmann
Optical Microtube Ring Resonators,
AIP Conf. Proc. **893**, 1127 (2007).

Ch. Strelow, C. M. Schultz, H. Rehberg, H. Welsch, Ch. Heyn, D. Heitmann, and T. Kipp
Three dimensionally confined optical modes in quantum-well microtube ring resonators,
Physical Review B **76**, 045303 (2007).

Ch. Strelow, H. Rehberg, C. M. Schultz, H. Welsch, Ch. Heyn, D. Heitmann, and T. Kipp
Spatial emission characteristics of a semiconductor microtube ring resonator,
Physica E **40**, 1836-1839 (2008).

Ch. Strelow, H. Rehberg, C. M. Schultz, H. Welsch, Ch. Heyn, D. Heitmann, and T. Kipp
Optical Microcavities Formed by Semiconductor Microtubes Using a Bottlelike Geometry,
Physical Review Letters **101**, 127403 (2008).

Ch. Heyn, A. Stemmann, T. Köppen, Ch. Strelow, T. Kipp, M. Grave, S. Mendach, and W. Hansen
Highly uniform and strain-free GaAs quantum dots fabricated by filling of self-assembled nanoholes,
Applied Physics Letters **94**, 183113 (2009).

Ch. Strelow, M. Sauer, S. Fehringer, T. Korn, C. Schüller, A. Stemmann, Ch. Heyn, D. Heitmann, and T. Kipp
Time-Resolved Studies of a Rolled-Up Semiconductor Microtube Laser,
Applied Physics Letters, accepted (2009).

Ch. Strelow, C. M. Schultz, H. Rehberg, M. Sauer, H. Welsch, A. Stemmann, Ch. Heyn, D. Heitmann, and T. Kipp
Light Confinement in Rolled-Up Semiconductor Microtube Bottle Resonators,
to be submitted to Physical Review B (2010).

K. Dietrich, Ch. Strelow, C. Schliehe, Ch. Heyn, A. Stemmann, S. Schwaiger, S. Mendach, A. Mews, H. Weller, D. Heitmann, and T. Kipp
Optical Modes Excited by Evanescent-Wave-Coupled PbS Nanocrystals in Semiconductor Microtube Bottle Resonators,
Nano Letters **10 (2)**, 627–631 (2009).

Conference Contributions

Tailoring Optical Modes in Semiconductor Microtube Bottle Resonators
Ch. Strelow, C. M. Schultz, H. Rehberg, A. Stemmann, H. Welsch, Ch. Heyn, D. Heitmann, and T. Kipp
MSS-14: International Conference on Modulated Semiconductor Structures, Kobe, July 2009
form of contribution: oral presentation

Tailoring the Emission Properties and the Axial Light Confinement in Microtube Resonators
Ch. Strelow, M. Sauer, K. Dietrich, C. M. Schultz, H. Rehberg, Ch. Heyn, D. Heitmann, and T. Kipp
DPG Spring-Meeting in Dresden, March 2009
form of contribution: poster

Optical Microtube Bottle Resonators
Ch. Strelow, C. M. Schultz, H. Rehberg, Ch. Heyn, D. Heitmann, and T. Kipp
DPG Spring-Meeting in Dresden, March 2009
form of contribution: oral presentation

Three-dimensionally Confined Optical Modes in Microtube Bottle Resonators
H. Rehberg, Ch. Strelow, C. M. Schultz, H. Welsch, Ch. Heyn, D. Heitmann, and T. Kipp
DPG Spring-Meeting in Berlin, March 2008
form of contribution: oral presentation by H. Rehberg

Emission Characteristics of Microtube Ring Resonators
Ch. Strelow, H. Rehberg, T. Köppen, C. M. Schultz, H. Welsch, Ch. Heyn, D. Heitmann, and T. Kipp
15th International Winterschool in Bad Hofgastein, February 2008
form of contribution: poster

Microtube Ring Resonators: Three-dimensional confinement of light and preferential emission
Ch. Strelow, H. Rehberg, C. M. Schultz, H. Welsch, Ch. Heyn, D. Heitmann, and T. Kipp
MSS-13: International Conference on Modulated Semiconductor Structures, Genova, July 2007
form of contribution: oral presentation

Localized optical modes in microtube resonators containing InGaAs quantum wells
Ch. Strelow, H. Rehberg, C. M. Schultz, H. Welsch, Ch. Heyn, D. Heitmann, and T. Kipp
DPG Spring-Meeting in Regensburg, March 2007
form of contribution: oral presentation

Properties of Optical Modes in Semiconductor Microtube Resonators
C. M. Schultz, H. Rehberg, Ch. Strelow, H. Welsch, Ch. Heyn, D. Heitmann, and T. Kipp
DPG Spring-Meeting in Regensburg, March 2007
form of contribution: poster

Further Presentations

Optical microcavities in microtubes
Ch. Strelow, C. M. Schultz, H. Rehberg, H. Welsch, Ch. Heyn, D. Heitmann, and T. Kipp
Symposium on Optical Spectroscopy on Microstructured Semiconductors in Hamburg, March 2009
form of contribution: oral presentation

Optische Mikroresonatoren aus aufgerollten Halbleiterschichten
Ch. Strelow, C. M. Schultz, H. Rehberg, H. Welsch, Ch. Heyn, D. Heitmann, and T. Kipp
Lehrstuhlseminar Wegscheider, Regensburg May 2009
form of contribution: oral presentation (invited)

Danksagung

Ich möchte mich herzlich bei allen bedanken, die zum Gelingen dieser Arbeit beigetragen haben und mich in dieser Zeit unterstützt haben.

Besonderer Dank gilt

- Prof. Dr. Detlef Heitmann, für Möglichkeit meine Arbeit in seiner Gruppe anfertigen zu können, für die guten Rahmenbedingungen in seiner Gruppe und die gute Betreuung,
- Prof. Dr. Ulrich Merkt für die Übernahme des Zweitgutachtens meiner Dissertation und die Betreuung im Rahmen des Graduiertenkollegs 1286,
- Prof. Dr. Wolfgang Hansen für die Übernahme des Zweitgutachtens meiner Disputation,
- Dr. Tobias Kipp für die exzellente Betreuung und Athmosphere in seiner Optik Untergruppe, viele anregende und interessante Diskussionen und so manches aufmunternde Wort,
- Dr. Katrin Buth für die hervorragende Koordination des Graduiertenkollegs
- Prof. Dr. Alf Mews für die zeitweilige Freistellung von Tobias Kipp,
- Christoph M. Schultz, Hagen Rehberg, Kay Dietrich und Michael Sauer für eine tolle und sehr produktive Zusamenarbeit an den Mikroröllchen,
- Andrea Stemmann und Holger Welsch für das Probenwachstum,
- Prof. Dr. Christian Schüller für die Möglichkeit in seiner Forschungsgruppe in Regensburg zeitaufgelöste Photolumineszenz Messungen anzufertigen,
- Dr. Tobias Korn für die Durchführung der Messungen in Regensburg
- Dr. Tim Köppen für eine tolle gemeinsame Zeit in der Untergruppe Optik sowie viele und lange Diskussionen während und neben der Arbeit,

- Torben Menke für die gute Zusammenarbeit im Labor,
- Wolfgang Hatje and Klaus Ahrens für die flexible Heliumausgabe auch in Zeiten knappen Heliums,
- Mathias Grave "Bauchladenmann" für die Erschaffung und Pflege des Bauchladens,
- Gernot Stracke, Mathias Grave, Hagen Rehberg, Tim Köppen, Torben Menke und Michael Sauer für die nette Büronachbarschaft,
- der Deutschen Forschungsgemeinschaft für die finanzielle Unterstützung durch den Sonderforschungsbereich 508 und das Graduiertenkolleg GK 1286,
- den Kollegiaten des Graduiertenkollegs 1286 für eine angenehme Athmosphäre bei Veranstaltungen des Graduiertenkollegs,
- den Mitgliedern von Gruppe H und w für ein tolles Arbeitsklima und die gute Zusammenarbeit,
- Petra Israel für das Korrekturlesen meiner Doktorarbeit
- meiner Familie für die permanente Unterstützung und immer einen Ort zum Abschalten und Regenerieren,
- und Steffi für ihre Liebe, ihre Unterstützung in der letzten Zeit und dafür, dass sie einfach nur da war.